Characterization and targeting of ribosome biogenesis in cellular and tissue subtypes of pancreatic ductal adenocarcinoma

Dissertation
for
the doctoral degree of
Dr. rer. nat.

from the Faculty of Biology
University of Duisburg-Essen
Germany

Submitted by
Corinna Münch

Born in Cologne

February 2024

DOI: 10.17185/duepublico/82443
URN: urn:nbn:de:hbz:465-20241002-064802-0

The experiments underlying the present work were conducted at the Bridge Institute of Experimental Tumor Therapy (West German Cancer Center, University Hospital Essen) and the Division of Solid Tumor Translational Oncology (DKTK/DKFZ partner site Essen/Düsseldorf) under supervision of Prof. Dr. Jens T. Siveke and Dr. Marija Trajkovic-Arsic.

1. Examiner: Prof. Dr. Jens T. Siveke

2. Examiner: Prof. Dr. Perihan Nalbant

3. Examiner:

Chair of the Board of Examiners: Prof. Dr. Dr. Jürgen C. Becker

Date of the oral examination: 09.07.2024

In the context of this doctoral work, the following article was submitted for publication:

Münch C., Liffers S.T., Lueong S.S., Althoff K., Kudla M., Jendrossek V., Vega-Rubín-de-Celis S., Trajkovic-Arsic M., and Siveke J.T.

BMH-21-induced inhibition of RNA polymerase I impairs cell viability in pancreatic ductal adenocarcinoma subtypes. In revision.

Table of contents

Summary

Pancreatic ductal adenocarcinoma (PDAC) remains a fatal disease with a five-year overall survival rate of only 12%. This is mainly because the efficacy of existing therapies is strongly restricted by tumor heterogeneity, emphasizing the importance of identifying robust therapeutic targets and applicable combinational treatment approaches. Oncogene-driven cancers often display hyperactivation of ribosome biogenesis (RiBi), allowing the cells to meet their increased demand for protein synthesis and thus maintain their abnormal proliferation rate. The present study investigated the level of RiBi in different PDAC model systems, including conventional PDAC cell lines, primary patient-derived cells (PDC), and a genetically engineered mouse model (CKP), and also analyzed gene expression data from PDAC patients. It was evaluated whether the inhibition of RNA polymerase I (Pol I)-mediated transcription of ribosomal DNA, as the first and rate-limiting step of RiBi, presents a potential treatment strategy for PDAC. High expression levels of multiple RiBi regulators were related to poor survival of PDAC patients, indicating that aggressive tumors may present a stronger dependence on RiBi. Conventional PDAC cell lines showed remarkable differences in the expression of ribosomal proteins (RP) and 45S ribosomal (r)RNA as well as in the nucleolar morphology depending on their molecular characteristics. In turn, pronounced nucleolar heterogeneity was observed within individual PDC populations as well as within endogenous tumors of CKP mice, pointing to RiBi as a highly dynamic process in PDAC. However, despite the observed variations in RP expression, 45S rRNA levels, and nucleolar organization, the RNA Pol I inhibitor BMH-21 effectively reduced cell viability in all investigated conventional PDAC cell lines and PDCs. As expected, BMH-21 treatment decreased the expression of 45S rRNA in PDAC cell lines and consequently caused nucleolar stress, as indicated by the translocation of multiple nucleolar proteins into the nucleoplasm or nuclear spots, respectively. This was followed by the activation of different stress response pathways, including apoptosis, cell cycle arrest, and pro-death autophagy. Additionally, RNA Pol I inhibition induced transcriptional and/or functional alterations in various metabolic pathways, including glycolysis, oxidative phosphorylation, and the tricarboxylic acid cycle. This suggests a potentially targetable connection between RiBi and metabolic reprogramming. Together, the findings of the study support RNA Pol I inhibition as a potential treatment approach in PDAC and open a perspective for future co-targeting strategies.

Zusammenfassung

Das duktale Adenokarzinom des Pankreas (PDAC) hat mit einer Fünfjahresüberlebensrate von nur 12% eine schlechte Prognose, vor allem weil die Heterogenität der Tumore die Wirksamkeit verfügbarer Therapien stark einschränkt. Daher ist die Identifikation robuster Angriffsziele und geeigneter Kombinationstherapien essenziell. Onkogen-gesteuerte Krebsarten weisen häufig eine hohe ribosomale Biogenese (RiBi)-Rate auf, welche es den Zellen erlaubt, ihren erhöhten Bedarf an Proteinbiosynthese zu decken und so ihr schnelles Wachstum aufrechtzuerhalten. Die vorliegende Arbeit untersuchte das RiBi-Level in verschiedenen PDAC-Modellsystemen wie konventionellen PDAC-Zelllinien, aus Patientenproben abgeleiteten Zellen (PDC) sowie einem gentechnisch veränderten Mausmodell (CKP). Zudem wurden Genexpressionsdaten von PDAC-Patienten analysiert. Es wurde untersucht, ob die Inhibition der RNA Polymerase I (Pol I)-vermittelten Transkription ribosomaler DNA, als erster und geschwindigkeits-bestimmender Schritt der RiBi, eine mögliche Behandlungsstrategie für PDAC darstellt. Hohe Expressionslevel einiger RiBi-Faktoren sind mit einer verminderten Überlebensrate von PDAC-Patienten assoziiert, was auf eine stärkere Abhängigkeit aggressiver Tumore von einer entsprechenden RiBi-Aktivität hindeutet. Konventionelle PDAC-Zelllinien zeigten je nach Subtyp deutliche Unterschiede in der Expression ribosomaler Proteine und der 45S ribosomalen (r)RNA sowie in der Morphologie des Nukleolus. Unterdessen wiesen PDC-Populationen sowie endogene CKP-Tumore eine starke nukleolare Heterogenität auf, was darauf hindeutet, dass die RiBi im PDAC einen äußerst dynamischen Prozess darstellt. Trotz der beobachteten Unterschiede in der RiBi reduzierte der RNA Pol I Inhibitor BMH-21 effektiv die Zellviabilität aller getesteten konventionellen Zelllinien und PDCs. Die Behandlung mit BMH-21 führte zu einer verminderten Expression der 45S rRNA in PDAC-Zelllinien sowie zu einer nukleolaren Stressantwort, die sich durch die Translokation nukleolarer Proteine abzeichnete. Infolgedessen kam es zur Aktivierung verschiedener Stress-assoziierter Signalwege (Apoptose, Zellzyklusarrest und Autophagie). Zudem führte die RNA Pol I-Inhibition zu einer transkriptionellen und/oder funktionellen Veränderung metabolischer Signalwege wie der Glykolyse, der oxidativen Phosphorylierung oder des Citratzyklus. Dies spricht für einen Zusammenhang zwischen RiBi und Stoffwechsel, welcher ein mögliches Angriffsziel für neue Behandlungen darstellt. Insgesamt deuten die vorliegenden Ergebnisse darauf hin, dass die Hemmung der RNA Pol I ein vielversprechender Therapieansatz für das PDAC ist und eröffnen zudem eine Perspektive für zukünftige Kombinationstherapien.

1 Introduction

1.1 The human pancreas

1.1.1 Structure and function of the pancreas

The pancreas is a glandular organ, which is located in the upper abdominal cavity behind the stomach and is anatomically subdivided into the pancreatic head, body, and tail (Röder et al., 2016) (Figure 1-1 A). The gland executes both an exocrine and endocrine function, which is reflected in its histological architecture. The exocrine part, which constitutes the majority of pancreatic tissue and consists mostly of acinar and ductal cells, plays an important role in the digestion of nutrients (Shih et al., 2013). Acinar cells account for around 85% of the organ's mass and produce digestive enzymes and zymogens which are secreted into the duodenum via a complex network of pancreatic ducts (Atkinson et al., 2020) (Figure 1-1 B, C). Ductal cells additionally produce fluids and bicarbonate ions, essential for the neutralization of gastric acid in the duodenum (Chandra & Liddle, 2009).

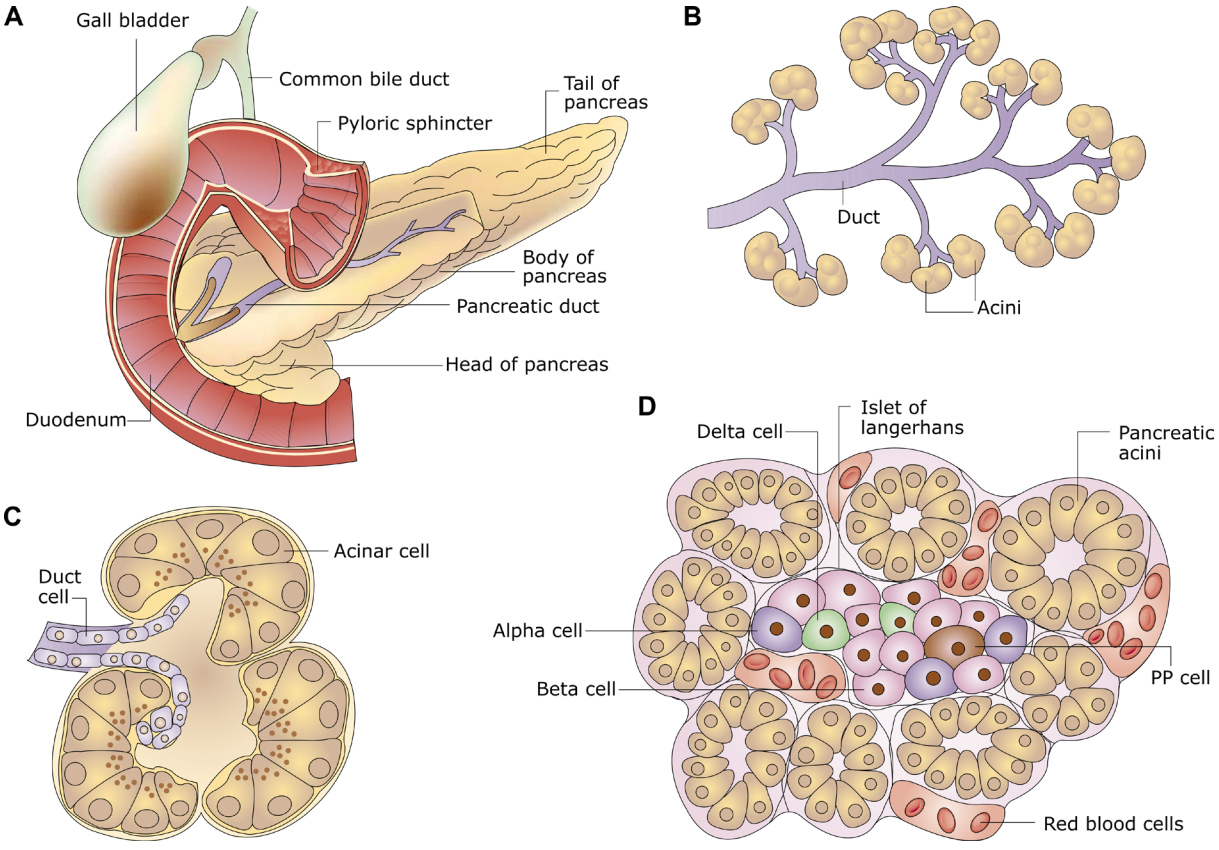

Figure 1-1 Organization of the human pancreas

(A) Schematic overview of the pancreatic anatomy. **(B)** The exocrine part of the pancreas is formed by a complex network of acini and ducts. **(C)** Cross section of a single acinus. **(D)** Pancreatic endocrine cells are organized in the islets of Langerhans, surrounded by a capillary network. Adapted from Bardeesy & DePinho, 2002; reproduced with permission from Springer Nature.

The endocrine cells of the pancreas account for only 1-2% of the organ and produce various hormones (e.g., insulin and glucagon) that are important modulators of glucose homeostasis (Röder et al., 2016). The cells are organized in island-like structures, termed islets of Langerhans, which scatter through the exocrine tissue and are surrounded by a dense capillary network, allowing for the quick release of hormones into the bloodstream (Chandra & Liddle, 2009) (Figure 1-1 D). According to the hormone secreted, five different types of pancreatic endocrine cells can be distinguished, the most prominent being glucagon-secreting α-cells (15-20% of islet cells) and insulin-secreting β-cells (65-80% of islet cells) (Röder et al., 2016). Both the endocrine and exocrine functions of the pancreas are regulated by external stimuli (e.g., food intake) via humoral, hormonal, or neural signaling pathways (Röder et al., 2016). Exocrine secretion is stimulated by the hormones cholecystokinin and secretin which are released by enteroendocrine cells in the duodenum in response to ingested lipids and proteins or a drop in the pH level, respectively (Logsdon, 2004; Karpinska & Czauderna, 2022). On the other hand, the (endocrine) secretion of insulin from β-cells is mainly stimulated by increased glucose levels in the blood (Röder et al., 2016).

1.1.2 Tumors of the pancreas

Neoplastic growth can occur in both endocrine and exocrine structures of the pancreas. Pancreatic neuroendocrine tumors (PanNETs) account for only 2% of all pancreatic neoplasms (Werle et al., 2023). They are primarily grouped into functional and non-functional PanNETs, depending on whether they show excessive hormone production that results in the manifestation of clinical symptoms (Metz & Jensen, 2008). Furthermore, the tumors are categorized according to the produced hormone, for example, into insulinoma or glucagonoma (Klimstra, 2007). Exocrine neoplasms of the pancreas comprise, among others, acinar cell carcinoma and pancreatic ductal adenocarcinoma (PDAC). While acinar cell carcinoma is very rare and accounts for only 1-2% of pancreatic malignancies, PDAC represents the most common type of pancreatic cancer, constituting 90% of all cases (Klimstra, 2007; Orth et al., 2019).

1.2 Pancreatic ductal adenocarcinoma

1.2.1 Epidemiology of PDAC

Pancreatic cancer accounts for only 2.6% of new cancer cases and is ranked as the 14th most common cancer worldwide, with incidence rates being significantly higher in industrial compared to developing countries (Wong et al., 2017; Sung et al., 2021). Pancreatic cancer exhibits a very poor prognostic outcome with a median survival of

10-12 months and a five-year overall survival rate of only 12% (Principe et al., 2021; Siegel et al., 2023). Therefore, pancreatic cancer accounts for almost 5% of all cancer-related deaths worldwide, ranking it as the seventh most common cause of cancer mortality despite its relatively low incidence (Sung et al., 2021). Furthermore, due to a continuous increase in the incidence- and mortality rates over the past decades, pancreatic cancer is predicted to become the second leading cause of cancer-related death in the US by 2030 (Rahib et al., 2014; Grossberg et al., 2020). The increasing incidence can be partly explained by an improved life expectancy, followed by population aging, and a higher occurrence of obesity and diabetes, as these are among the main risk factors for PDAC development (Grossberg et al., 2020). Additional risk factors include lifestyle factors like cigarette smoking and heavy alcohol consumption, but also non-modifiable risk factors like male gender or inherited genetic predisposition (McGuigan et al., 2018). It is estimated that approximately 5-10% of all PDAC patients carry a cancer-promoting pathogenic germline mutation, most often affecting DNA damage repair genes like *BRCA1/2*, *ATM*, or *PALB2* (McGuigan et al., 2018). One of the main reasons for the poor prognosis of PDAC is a delayed diagnosis due to the lack of effective screening methods or reliable biomarkers, and the occurrence of only non-specific symptoms like abdominal pain, fatigue, jaundice, and weight loss (Grossberg et al., 2020; Pereira et al., 2020). Consequently, only 15-20% of PDAC patients present with localized (resectable) disease at the time of diagnosis, while most patients already show locally advanced (30-40%) or metastatic disease (50-60%), respectively (Principe et al., 2021).

1.2.2 PDAC pathogenesis and mutational landscape

PDAC is assumed to arise from the ductal epithelium, undergoing stepwise malignant transformation into invasive cancer through different stages of pre-neoplastic lesions (Bardeesy & DePinho, 2002; Connor & Gallinger, 2022). However, due to recent understandings, pancreatic acinar cells are also considered a potential cell-of-origin for PDAC (Orth et al., 2019; Halbrook et al., 2023). Various stimuli can trigger acinar-to-ductal metaplasia, meaning the differentiation of acinar into ductal-like cells that harbor progenitor-like characteristics (Orth et al., 2019). Initial genetic events, like oncogenic *KRAS* mutations, lead to the formation of precursor lesions, including pancreatic intraepithelial neoplasia (PanINs) and intraductal papillary mucinous neoplasms (IPMNs). Through their sequential progression from low-grade to high-grade lesions, these precursors consecutively acquire genetic alterations, often

affecting oncogenes and tumor suppressor genes (Halbrook et al., 2023) (Figure 1-2). Given that activating mutations of *KRAS* are observed in the majority of PDAC patients (>90%) and already exist in low-grade precursor lesions, they are considered essential for PDAC development and progression (Kanda et al., 2012; Fujikura et al., 2021; Halbrook et al., 2023). Other key alterations include loss of *CDKN2A* in intermediate-grade lesions, as well as loss-of-function mutations in *SMAD4* and *TP53* in high-grade lesions (Waddell et al., 2015; Orth et al., 2019). Additionally, epigenetic reprogramming highly contributes to PDAC carcinogenesis, progression, and metastasis, for example, by modulating the expression of oncogenes and tumor suppressor genes (Iguchi et al., 2016).

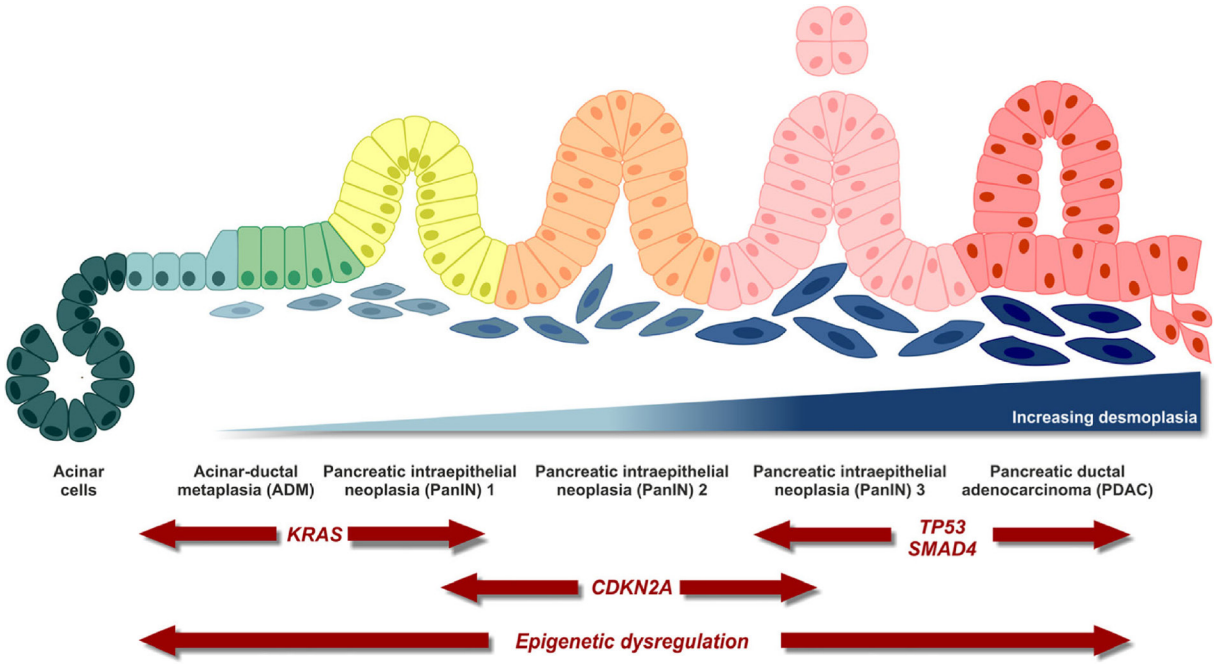

Figure 1-2 Hypothesized gradual development of PDAC

PDAC gradually develops from acinar or ductal cells through different stages of precursor lesions, accompanied by the successive accumulation of genetic alterations in oncogenes and tumor suppressor genes as well as epigenetic dysregulation. Adopted from Orth et al., 2019, Radiation Oncology, distributed under the terms of the Creative Commons Attribution 4.0 International License (https://creativecommons.org/licenses/by/4.0/).

1.2.3 Molecular and metabolic heterogeneity in PDAC

Tumor heterogeneity is one of the main reasons for therapy resistance and poor prognosis associated with PDAC. It is modulated by various cell-intrinsic and -extrinsic factors, including epigenetic and transcriptional regulation as well as interaction with the tumor microenvironment (Espinet et al., 2022). In different transcriptional profiling approaches two major molecular subtypes were identified, namely the quasi-mesenchymal (QM) / squamous / basal-like subtype and the classical / pancreatic

progenitor subtype (Collisson et al., 2011; Moffitt et al., 2015; Bailey et al., 2016; Cancer Genome Atlas Research Network, 2017; Chan-Seng-Yue et al., 2020) (Figure 1-3). Hereafter, the subtypes are referred to as QM and classical, respectively. While the classical subtype is associated with high expression of epithelial-, differentiation-, and adhesion-associated genes, the poorly differentiated QM subtype is characterized by high expression levels of mesenchymal gene sets (Collisson et al., 2011). Importantly, the molecular subtype can also predict the clinical outcome and the treatment efficacy (Collisson et al., 2011; Aung et al., 2018). For PDAC cell lines, Collisson et al. showed that classical cells are, on average, more sensitive to the tyrosine kinase inhibitor erlotinib but less sensitive to the chemotherapeutic agent gemcitabine when compared to QM cell lines (Collisson et al., 2011). Furthermore, in a study from Aung et al., PDAC patients with classical tumors showed prolonged overall survival as well as a better response to the standard-of-care treatment with FOLFIRINOX or with a combination of gemcitabine and nanoparticle albumin-bound (nab-) paclitaxel compared to patients with QM tumors (Aung et al., 2018).

PDAC also presents molecular heterogeneity at an intratumoral level, as subpopulations of QM and classical cells were found to co-exist in primary tumors and metastases of individual patients (Chan-Seng-Yue et al., 2020; Hayashi et al., 2020; Juiz et al., 2020). Current evidence suggests that this intratumor heterogeneity is facilitated both by cancer cell plasticity and clonal evolution, and highly contributes to tumor progression and metastasis (Connor & Gallinger, 2022). Prominent examples of cellular plasticity are the dynamic processes of epithelial-mesenchymal transition (EMT) and mesenchymal-epithelial transition (MET). EMT can be induced by different stimuli, resulting in a variety of transcriptional, morphological, and behavioral changes. These include upregulation of EMT-associated transcription factors (e.g., Zeb1 and Snail) as well as mesenchymal markers (e.g., Vimentin and N-cadherin), with simultaneous downregulation of epithelial markers (e.g., E-cadherin and claudins). Furthermore, cells undergo a shift from an epithelial to a more spindle-like morphology and show an increased invasive capacity (Evan et al., 2022). In PDAC, upregulation of EMT-related genes correlates with the more aggressive QM subtype and is associated with a worse prognosis (Bronsert et al., 2014; Moffitt et al., 2015). Nevertheless, cancer cells can also exist in a hybrid state in which they exhibit both epithelial and mesenchymal features (Aiello et al., 2018; Chan-Seng-Yue et al., 2020).

Metabolic reprogramming is considered a hallmark of cancer, as malignant cells often show alterations in metabolic pathways, allowing them to meet their energetic and biosynthetic needs (DeBerardinis et al., 2008; Hanahan & Weinberg, 2011). Those alterations are mainly driven by dysregulated oncogenes or tumor suppressors, including KRas, MYC, and p53 (DeBerardinis & Chandel, 2016). Additionally, metabolic flexibility allows the cancer cells to adapt to environmental constraints and nutrient limitations, thus maintaining their abnormal growth and proliferation rates (Boroughs & DeBerardinis, 2015). In PDAC, metabolic reprogramming plays a pivotal role as the desmoplastic stroma restricts tumor vascularization, thereby creating especially harsh environmental conditions with limited nutrient and oxygen availability (Encarnacion-Rosado & Kimmelman, 2021; Sherman & Beatty, 2023). Understanding the metabolic dependencies of cancer cells is fundamental in the context of analyzing complex treatment effects as well as developing targeted therapy approaches.

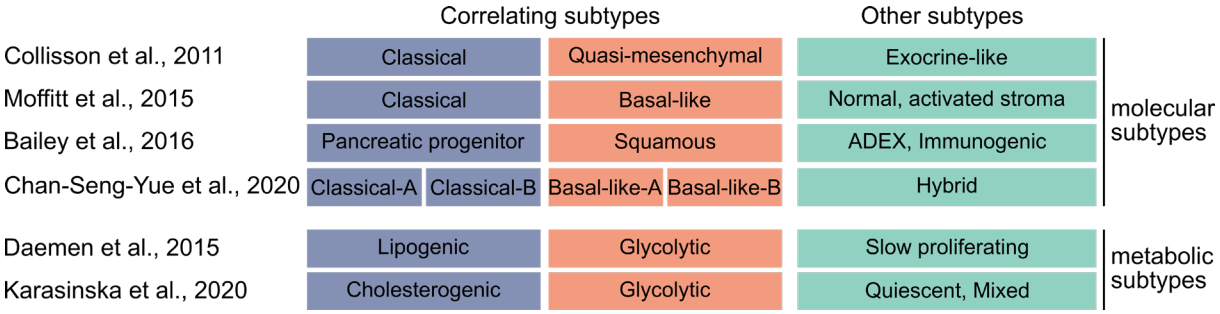

Figure 1-3 Overview of molecular and metabolic subtypes in PDAC

Analysis of transcriptional characteristics identified two main molecular PDAC subtypes, namely the classical / pancreatic progenitor subtype and the quasi-mesenchymal (QM) / basal-like / squamous subtype. Additionally, analysis of transcriptional and metabolic profiles identified two main metabolic subtypes, namely the lipogenic / cholesterogenic and the glycolytic subtype, which transcriptionally align with the classical and the QM subtypes, respectively. ADEX, aberrantly differentiated endocrine exocrine. Adapted from Espiau-Romera et al., 2020.

Metabolite profiling in PDAC cell lines identified three distinct metabolic subtypes, namely the slow proliferating, the glycolytic, and the lipogenic subtypes (Daemen et al., 2015). The observed differences in metabolite levels were further accompanied by alterations in the transcriptional profile, the functional utilization of glucose and glutamine, and the sensitivity toward metabolic inhibitors (Daemen et al., 2015). Similarly, transcriptional analysis of glycolytic and cholesterogenic gene sets in PDAC patient samples identified four different subtypes: glycolytic, mixed, quiescent, and cholesterogenic (Karasinska et al., 2020). This classification provides prognostic value, as the cholesterogenic subtype is associated with prolonged median survival compared to the glycolytic subtype (Karasinska et al., 2020). Additionally, Daemen et

al. as well as Karasinska et al. report a correlation between the identified metabolic subtypes and previously described transcriptional subtypes (Daemen et al., 2015; Espiau-Romera et al., 2020; Karasinska et al., 2020). The glycolytic subtype strongly aligns with the QM transcriptional program while lipogenic / cholesterogenic samples are associated with the classical subtype (Daemen et al., 2015; Karasinska et al., 2020) (Figure 1-3).

1.2.4 PDAC therapy

For PDAC, the selection of an appropriate treatment strategy as well as the therapy efficacy and outcome largely depend on the disease stage and the patient's performance status. Surgical resection, followed by adjuvant chemotherapy, is so far the only potentially curative treatment. However, only 15-20% of all PDAC patients are diagnosed with resectable disease, while the majority already present a locally advanced or metastatic status at the time of diagnosis (Principe et al., 2021). Furthermore, up to 80% of patients undergoing curative resection experience local or distant recurrence, which limits the five-year overall survival after surgery to 25% (Groot et al., 2018; Principe et al., 2021). First-line therapy for patients with unresectable disease is the systemic administration of chemotherapeutic agents like gemcitabine and FOLFIRINOX. Gemcitabine is a deoxycytidine analog that induces cell cycle arrest and cell death via inhibition of DNA replication (Luo et al., 2019). Depending on the patient’s performance status, gemcitabine can be applied as a single drug or in combination with nab-paclitaxel, which inhibits microtubule function during mitosis (Schiff & Horwitz, 1980). The multi-drug regimen FOLFIRINOX comprises 5-Fluorouracil (5-FU), leucovorin, irinotecan, and oxaliplatin, and can be applied to patients with a good performance status (Conroy et al., 2011). Both FOLFIRINOX as well as the combination of gemcitabine and nab-paclitaxel result in prolonged disease-free and overall survival compared to treatment with gemcitabine alone (Conroy et al., 2011; Von Hoff et al., 2013). However, PDAC is characterized by strong intrinsic and acquired chemoresistance, which occurs through various mechanisms that influence drug transport, -metabolism, or -response pathways, eventually impeding treatment efficacy (Sally et al., 2022).

Emerging knowledge about PDAC characteristics and tumor heterogeneity promoted the development of targeted therapies. Approximately 5-10% of all PDAC cases are associated with an inherited genetic predisposition, often involving *BRCA1/2* or *PALB2* mutations that result in homologous repair deficiency (Zhen et al., 2015). Therefore,

respective patients specifically benefit from treatments that induce DNA double-strand breaks, including platin-based chemotherapeutics (e.g., cisplatin) and PARP inhibitors (e.g., Olaparib) (Golan et al., 2019; Halbrook et al., 2023). On the other hand, oncogenic KRAS, a key driver of PDAC development, was long considered undruggable due to the absence of suitable binding sites for pharmacologic compounds. Just recently, two $KRAS^{G12C}$ inhibitors (Adagrasib and Sotorasib) have been developed, which disable the mutated KRAS by covalent binding to the C12 residue (Fell et al., 2020; Lanman et al., 2020). For Sotorasib, clinical studies revealed a partial response in 21% of the patients with advanced PDAC (Strickler et al., 2023), and trials for Adagrasib are currently ongoing (NCT03785249). However, the eligibility of $KRAS^{G12C}$ as a therapeutical target in PDAC is limited by the fact that $KRAS^{G12C}$ accounts for only 1-2% of all PDAC-related KRAS mutations (Luo, 2021). Another KRAS inhibitor, MRTX1133, selectively inhibits $KRAS^{G12D}$, which is the most common KRAS mutation in PDAC and is associated with poor outcome (Qian et al., 2018; Luo, 2021; Wang et al., 2022). Although the inhibitor shows promising effects in pre-clinical studies, its efficacy as well as potential resistance mechanisms remain to be elucidated (Wang et al., 2022).

1.3 Ribosome biogenesis

1.3.1 The human ribosome

The ribosome is a ribonucleoprotein complex that catalyzes the translation of messenger (m)RNA templates into protein sequences. The human 80S ribosome consists of a small (40S) and a large (60S) ribosomal subunit and comprises four ribosomal (r)RNA molecules and ~80 distinct ribosomal proteins (RPs), some of which also occur in tissue-specific paralog forms (Anger et al., 2013; Ferguson et al., 2015; Norris et al., 2021). The 40S small subunit consists of a single rRNA molecule (18S rRNA) and 33 RPs, referred to as RPSs (Dörner et al., 2023). It is part of the translation pre-initiation complex, which binds the mRNA template and scans the base sequence for the start codon AUG (Sonenberg & Hinnebusch, 2009). Furthermore, the small subunit contains the decoding center, facilitating the recognition and binding of the correct transfer (t)RNA via codon-anticodon interaction between mRNA and tRNA (Ramakrishnan, 2002). The 60S large ribosomal subunit consists of three rRNA molecules (5S, 5.8S, and 28S rRNA) and 47 RPs, referred to as RPLs (Dörner et al., 2023). It carries the peptidyl transferase center and catalyzes the formation of peptide bonds, thereby adding amino acids to the emerging polypeptide chain that co-

translationally exits the ribosome through the peptide exit tunnel (Ramakrishnan, 2002; Kramer et al., 2009). Communication between the two subunits, which is important to control structural rearrangements throughout the process of translation, is mediated, for example, by the binding of common ligands (e.g., tRNAs) at respective sites present in both subunits or via intersubunit bridges (Spahn et al., 2001). Different studies indicate that ribosomes exhibit cell type- or context-dependent structural heterogeneity which can relate to differences in rRNA processing or modification, as well as variations in the modification or composition of RPs (Shi et al., 2017; Li & Wang, 2020). This heterogeneity can affect the translational specificity of ribosomes, leading to preferential translation of certain transcripts both in a natural context (e.g., organismal development) as well as in the context of malignant transformation (e.g., cancer) (Bastide & David, 2018; Li & Wang, 2020; Gao & Wang, 2023).

1.3.2 Process and regulation of ribosome biogenesis

RiBi is a highly coordinated cascade-like process that requires the activity of three RNA polymerases (RNA Pol I, -Pol II, and -Pol III) and involves several hundred ribosome biogenesis factors (RBFs), functioning as chaperones as well as modification-, processing-, and remodeling factors (Dörner et al., 2023; Hurt et al., 2023). The process of RiBi largely occurs in the nucleolus, a membrane-less subnuclear structure forming around tandemly arranged clusters of ribosomal (r)DNA which are referred to as nucleolar organizing regions and are located on the five acrocentric chromosomes (Boisvert et al., 2007; Lafontaine et al., 2021). The nucleolus assembles via concentration-dependent liquid-liquid phase separation (LLPS), whereby nascent rRNA functions as a seed for nucleation (Falahati et al., 2016; Lafontaine et al., 2021). Subsequently, interactions between the rRNA and various RBFs, as well as respective protein-protein interactions lead to the formation of different liquid phases (Yao et al., 2019; Lafontaine et al., 2021). This results in a segmentation of the nucleolus into three functionally distinct sub-compartments termed fibrillar center (FC), dense fibrillar component (DFC), and granular component (GC) (Feric et al., 2016). Each of the three compartments is enriched in processing and regulation factors involved in the different steps of RiBi, namely rDNA transcription, pre-rRNA processing, and maturation of pre-ribosomal particles (Lafontaine et al., 2021; Dörner et al., 2023) (Figure 1-4).

RNA Pol I-mediated transcription of rDNA into the early 47S pre-rRNA is the first, rate-limiting step of RiBi and takes place in the FC or at the interface between FC and DFC (Laferte et al., 2006; Boisvert et al., 2007) (Figure 1-4). Transcription initiation requires

the formation of a pre-initiation complex, with the transcription factors UBF-1 and selectivity factor-1 (SL1) cooperatively binding to the rDNA promotor, followed by TIF-IA-mediated recruitment of RNA Pol I (Bell et al., 1988; Miller et al., 2001). The 47S pre-rRNA is a polycistronic molecule that contains the 18S, 5.8S, and 28S rRNAs, flanked by external transcribed spacers (5'ETS, 3'ETS) and internal transcribed spacers (ITS1, ITS2), respectively (Henras et al., 2015). The 5S rRNA, on the other hand, is separately transcribed by RNA Pol III in the nucleoplasm and subsequently imported into the nucleolus (Ciganda & Williams, 2011). Similarly, genes encoding for RPs and RBFs are transcribed by RNA Pol II in the nucleoplasm, the resulting mRNAs are translated at cytoplasmic ribosomes, and the functional proteins are then imported into the nucleolus (Xue & Barna, 2012). The 47S pre-rRNA molecule co-transcriptionally assembles with RBFs and RPs to form the 90S pre-ribosomal particle (Tschochner & Hurt, 2003). Within the DFC, early rRNA processing steps occur (Figure 1-4), which include posttranscriptional modifications such as pseudouridylation or ribose 2′-*O*-methylation (Henras et al., 2008). These specific modifications are facilitated by Dyskerin and Fibrillarin, respectively, both exerting their function as components of small nucleolar ribonucleoprotein complexes (snoRNPs) (Lafontaine et al., 1998; Fatica et al., 2000). Furthermore, the pre-rRNA molecule undergoes endo- and exonucleolytic cleavage at the internal and external transcribed spacers, resulting in the separation of the 90S complex into the small pre-40S and the large pre-60S particles (Tschochner & Hurt, 2003). In the GC, those ribosomal subunit precursors undergo further maturation, including structural remodeling as well as the incorporation of the 5S rRNA into the pre-60S particle (Chaker-Margot & Klinge, 2019; Dörner et al., 2023) (Figure 1-4). This is followed by an independent nuclear export of the pre-mature particles into the cytoplasm where final maturation steps for the functional small 40S and large 60S ribosomal subunits occur (Johnson et al., 2002) (Figure 1-4). Importantly, the multifunctional protein Nucleolin is involved in the regulation of almost every step of RiBi. It not only supports the transcription of rDNA by maintaining the euchromatic state of rDNA (Cong et al., 2012) but also contributes to pre-rRNA processing and ribosome assembly (Bouvet et al., 1998; Ginisty et al., 1998). In addition, due to its ability to shuttle between the nucleus and the cytoplasm, Nucleolin is suggested to also play a role in the nuclear export of ribosomal particles (Ginisty et al., 1999).

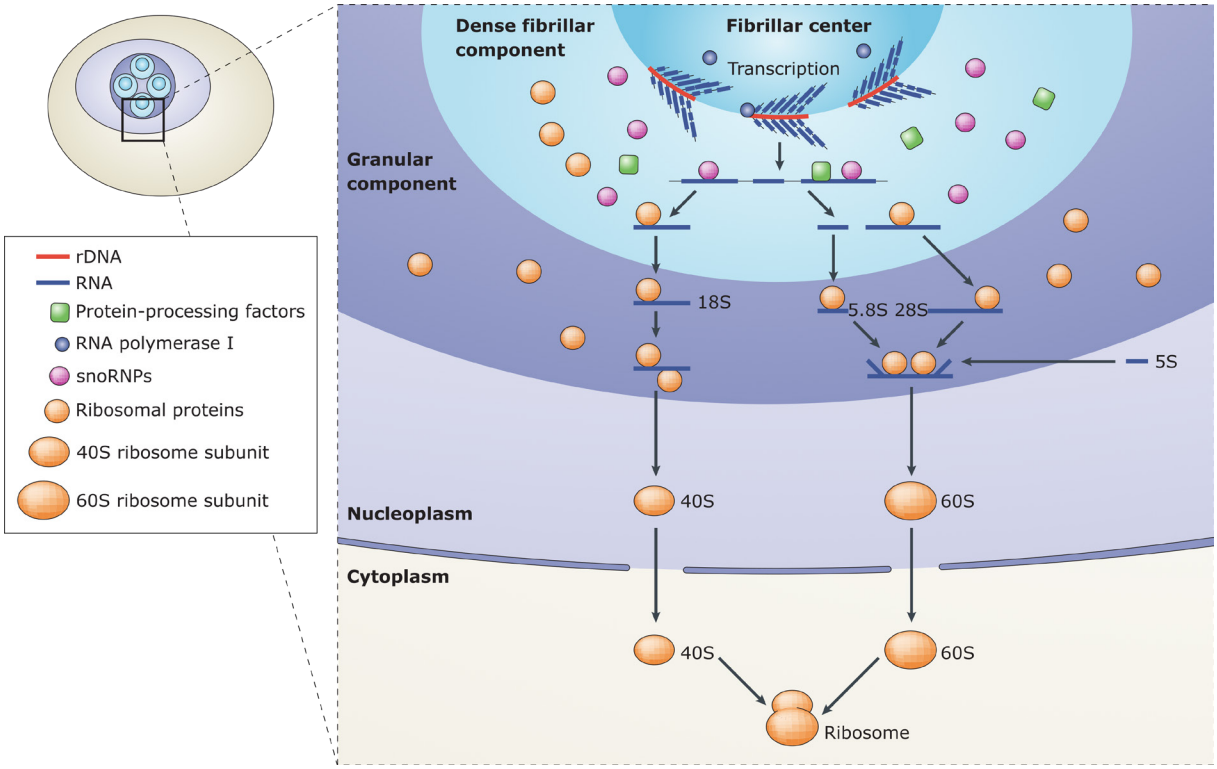

Figure 1-4 Process of ribosome biogenesis

Ribosome biogenesis mainly occurs in the nucleolus, a tripartite subnuclear condensate. Ribosomal (r)RNA is synthesized at the border between the fibrillar center (FC) and dense fibrillar component (DFC) by RNA polymerase I-mediated transcription of ribosomal (r)DNA gene clusters. In the DFC, nascent rRNA molecules undergo early processing steps, mediated by small nucleolar ribonucleoprotein complexes (snoRNPs), and assemble with ribosomal proteins to form pre-ribosomal particles. Further maturation of the pre-ribosomal subunits takes place in the granular component and the cytoplasm, where the small 40S and the large 60S subunits assemble to form the functional 90S ribosome. Adapted from Boisvert et al., 2007; reproduced with permission from Springer Nature.

Expression of the different structural and regulatory components involved in RiBi accounts for the majority of total cellular transcription, considering RiBi one of the most energy-demanding processes in the cell (Warner, 1999). Therefore, the level of RiBi is regulated by various pathways responding to nutrient availability, energy supply, growth factors, or stress signals, and thus dynamically adapts to changes in metabolic- and environmental conditions (Grummt, 2010; Orsolic et al., 2016). Many of those pathways target the 47S rRNA synthesis as the first and rate-limiting step of RiBi, although regulation also occurs at other levels of ribosome production (e.g., RP expression). The level of rDNA transcription is mainly controlled via two different strategies, either by regulating the number of active rRNA genes or by regulating the transcription rate of active gene loci (Grummt, 2010). The (in-)activation of rRNA genes is largely mediated by the transcription factor TTF-I that binds a terminator element (T_0) upstream of the rDNA promotor and interacts with activating or silencing protein complexes to recruit respective histone- and DNA-modifying enzymes (Santoro et al.,

2002; Yuan et al., 2007; Grummt & Langst, 2013). In eukaryotes, about half of the rRNA genes are epigenetically silenced by the repressive nucleolar chromatin remodeling complex (NoRC), therefore appearing in a heterochromatic state which is essential for rDNA stability (Guetg et al., 2010). Epigenetic modulation of rRNA gene activity is mainly considered a long-term regulatory mechanism involved in development and differentiation (Grummt, 2010), although several studies show that the chromatin structure of rDNA loci can also be regulated in an energy-dependent manner (Murayama et al., 2008; Zhou et al., 2009). On the other hand, regulation of the transcription rate at active rRNA gene loci represents a short-term regulatory mechanism, often mediated by the dynamic modulation of basal RNA Pol I transcription factors (Grummt, 2010). Activation of JNK2 or AMPK in response to environmental stressors or low cellular energy levels, respectively, inhibits rRNA synthesis via inactivating phosphorylation of TIF-IA, thereby impairing its interaction with SL1 and RNA Pol I (Mayer et al., 2005; Hoppe et al., 2009). Conversely, upon nutrient or growth factor availability, mTORC1- and MAPK/ERK-signaling promote the activating phosphorylation of UBF-1 and TIF-IA, thereby supporting rDNA transcription initiation and elongation (Stefanovsky et al., 2001; Hannan et al., 2003; Zhao et al., 2003; Mayer et al., 2004). Next to its activating role in 47S rRNA transcription, mTORC1 also positively regulates the RNA Pol III-mediated transcription of 5S rRNA via inactivating phosphorylation of the RNA Pol III repressor MAF1 (Kantidakis et al., 2010; Shor et al., 2010). Additionally, mTORC1 supports RiBi via its positive effect on global protein synthesis, thereby sustaining an adequate supply of RPs and RBFs (Gentilella et al., 2015). Noteworthy, mRNAs of RPs and several translation-related proteins are characterized by a 5' Terminal Oligopyrimidine tract (5' TOP) at their 5′ m^7G cap transcriptional start site, which puts the translation of respective mRNAs under the control of mTORC1 (Levy et al., 1991; Jefferies et al., 1997).

1.3.3 Role of ribosome biogenesis in cancer

An increase in the nucleolar size and number has been identified in various cancer types, considering hyperactivation of RiBi a hallmark of highly proliferative malignant cells (Pianese, 1896; Derenzini et al., 2009). An elevated level of RiBi not only supports the abnormal proliferation of cancer cells by providing an adequate translation capacity, but also acts as a key driver in cancer initiation, progression, and metastasis (Orsolic et al., 2016; Elhamamsy et al., 2022). Multiple oncogenes and tumor suppressors are well-described to modulate RiBi and protein synthesis via different

mechanisms (Ruggero & Pandolfi, 2003; Pelletier et al., 2018) (Figure 1-5). Gain-of-function mutations in *KRAS* and the resulting constitutive activation of the RAS/RAF/MEK/ERK pathway promote RNA Pol I-dependent transcription through ERK-mediated phosphorylation of TIF-IA and Nucleolin (Zhao et al., 2003; Azman et al., 2023). Furthermore, MYC promotes the transcriptional activity of all three RNA polymerases, thereby supporting the expression of rRNAs, RPs, and RBFs for ribosome production (van Riggelen et al., 2010). On the other hand, loss-of-function mutations in the tumor suppressor gene *TP53* contribute to increased activity of the RNA Pol I machinery by abrogating the inhibitory effect of p53 on the interaction between UBF-1 and SL1 (Zhai & Comai, 2000).

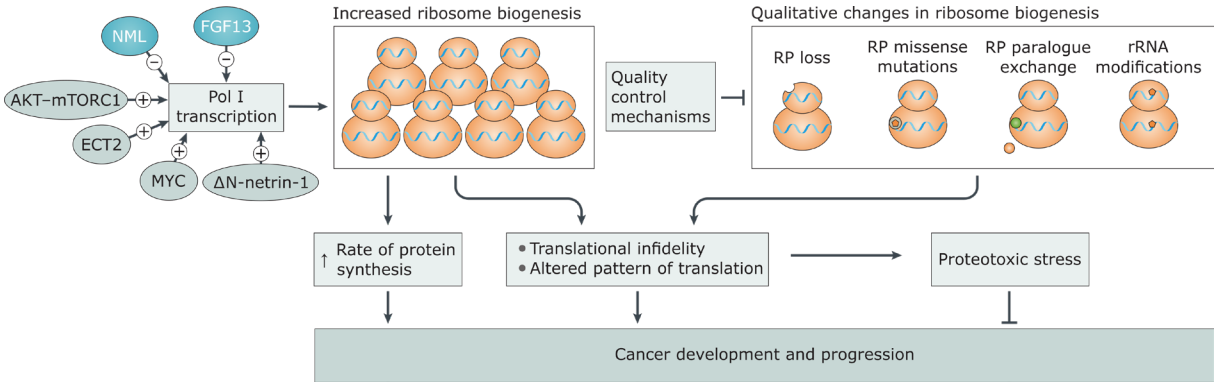

Figure 1-5 Ribosome biogenesis in cancer

Hyperactivity of RNA Pol I transcription, caused by dysregulation of oncogenic- and tumor-suppressive pathways, results in an increased level of RiBi, consequently promoting cancer development and progression by enhancing the rate of protein synthesis and affecting the translational quality. Similarly, qualitative changes in RiBi, due to aberrant modification or composition of rRNAs and RPs, can also result in translational infidelity or altered translational patterns, thereby contributing to cancer initiation and progression. Adopted from Pelletier et al., 2018; reproduced with permission from Springer Nature.

The resulting increase in ribosome concentration not only provides increased levels of protein synthesis but also leads to translational reprogramming and infidelity (Orsolic et al., 2016). The translation of protooncogenes is often modulated by *cis*-regulatory elements in the mRNA, which limit their ribosome affinity and thus their translation rate to maintain cellular homeostasis (Ruggero, 2013). An increased ribosome concentration may eliminate the competitive regulation by mRNAs with higher ribosome affinity, resulting in an elevated translation of oncogenic mRNAs that promotes cancer development and progression (Orsolic et al., 2016). Furthermore, mutations in RPs or aberrant modifications of rRNA molecules drive ribosome heterogeneity and the emergence of “onco-ribosomes”, which execute a preferential translation of oncogenes and pro-survival genes, thereby promoting malignant

transformation (Bastide & David, 2018; Elhamamsy et al., 2022). In breast- and colorectal cancer cell lines, loss of p53 is associated with an increased expression of Fibrillarin, entailing an elevated level of ribose 2′-*O*-methylation of rRNA molecules (Marcel et al., 2013). This interferes with translational fidelity and results in enhanced internal ribosome entry site (IRES)-dependent translation of distinct oncogenic mRNAs (Marcel et al., 2013; Pelletier et al., 2018).

1.3.4 Inhibition of ribosome biogenesis

Given that hyperactive RiBi is a key element for driving malignant transformation and for maintaining the abnormal proliferation rate of cancer cells, the inhibition of RiBi is considered an applicable approach for cancer treatment (Pelletier et al., 2018). Different chemotherapeutic agents interfere with rDNA transcription (e.g., Oxaliplatin, Actinomycin D) or rRNA processing (e.g., 5-FU), suggesting that their anticancer effect is at least partially due to inhibition of RiBi (Burger et al., 2010). However, given that most of the classic chemotherapeutics function as DNA/RNA intercalators and therefore cause substantial side effects, recent studies aim to more specifically inhibit RiBi by targeting RNA Pol I activity. Multiple small-molecule inhibitors have been identified to impede RNA Pol I-mediated rRNA synthesis, thereby causing restriction of cell viability and proliferation in different cancer model systems. CX-5461 inhibits the initiation of rDNA transcription by hampering the interaction between SL1 and the rDNA promotor, which is pivotal for the pre-initiation complex formation (Drygin et al., 2011). CX-3543, on the other hand, inhibits rDNA transcription elongation by disrupting the Nucleolin-mediated stabilization of G-quadruplexes (G4), i.e. guanine-rich secondary DNA structures that prevent renaturation of the rDNA template (Drygin et al., 2009). Another small-molecule inhibitor, BMH-21, intercalates into the GC-rich regions of rDNA gene clusters, thereby hindering RNA Pol I activity at the levels of transcription initiation, promotor escape, and elongation (Peltonen et al., 2014; Jacobs et al., 2022).

Inhibition of rDNA transcription results in decreased levels of nascent 47S pre-rRNA and subsequently in a quantitative imbalance between ribosomal components. This imbalance promotes a redistribution of RPs and RBFs from the nucleolus into the nucleoplasm, thus, disintegrating the nucleolar structure (Boulon et al., 2010; Yang et al., 2018). Such changes in nucleolar morphology and function are summarized as “ribosomal stress” or “nucleolar stress”, which is associated with various downstream response pathways, often activated in a p53-dependent manner (Yang et al., 2018). A well-described p53-dependent mechanism is the impaired ribosome biogenesis

checkpoint (IRBC): Upon RNA Pol I inhibition, the disequilibrium between 47S rRNA and other ribosomal components triggers the formation of the IRBC-complex, comprising 5S rRNA as well as RPL5 and RPL11. This complex binds the E3 ubiquitin ligase HDM2, thereby preventing the ubiquitylation and proteasomal degradation of p53. The following accumulation of p53 promotes, among others, cell cycle arrest and apoptosis (Bursac et al., 2012; Donati et al., 2013). However, given that more than 70% of all PDAC cases present with loss of p53 function (Waddell et al., 2015), it should be noted that inhibition of RNA Pol I can activate stress response pathways also in the absence of functional p53 (James et al., 2014). Some of these mechanisms are triggered by RPs which, in their free form, can exert various extra-ribosomal functions like regulation of oncogene expression or induction of apoptosis, without prior activation of p53 (Russo & Russo, 2017). Specifically, for the small molecule inhibitor BMH-21, Peltonen et al. showed that cell growth is effectively repressed in both p53 mutant and wild-type cell lines of the NCI-60 cancer cell line panel (Peltonen et al., 2014).

1.4 Aim of the study

Hyperactivation of RiBi is considered a hallmark of various cancers as it increases the translational capacity, thereby supplying the cancer cells' increased demand for protein synthesis. An emerging strategy for targeting RiBi is the selective inhibition of RNA Pol I-mediated transcription of rDNA genes as the first and rate-limiting step of RiBi. CX-5461, developed as one of the first RNA Pol I-specific inhibitors, was already shown to restrict the viability of different PDAC cell lines. Nevertheless, one of the main reasons for the limited efficacy of various PDAC treatment approaches is the strong inter- and intratumoral heterogeneity, promoting therapy resistance and tumor recurrence.

Therefore, the present study aimed to further characterize the suitability of RNA Pol I inhibition as a treatment strategy for PDAC, considering potential differences in the level of RiBi activity between tumors or intratumoral subpopulations of cancer cells, as well as the interaction between RiBi and other cellular pathways. The investigation involved different PDAC model systems, namely conventional PDAC cell lines, primary patient-derived cells (PDCs), and a genetically engineered PDAC mouse model. Additionally, publicly available transcription data of 204 PDAC patients were included in the analysis. The level of RiBi is mainly influenced by the availability of required building blocks, including rRNAs and RPs. Furthermore, the nucleolar morphology, meaning the size and number of nucleoli per cell, is considered a reliable parameter for the level of RNA Pol I activity in different cancer types. Therefore, transcriptional analysis of RPs and rRNA precursors as well as nucleolar staining were performed to determine the level of RiBi in different PDAC samples and estimate the associated heterogeneity.

Inhibition of rRNA synthesis results in a disequilibrium between ribosomal components and consequently in a disintegration of the nucleolar structure, including the translocation of nucleolar proteins into the nucleoplasm. Some of these proteins are described to exert extra-ribosomal functions associated with different stress response pathways. In this study, the effect of the selective RNA Pol I inhibitor BMH-21 on the viability of PDAC cell lines was investigated, focusing on the role of the nucleolar stress response and respective downstream pathways (e.g. apoptosis, cell cycle regulation, autophagy) for the anticancer effect of BMH-21 in PDAC cells. Moreover, the effect of RiBi inhibition was analyzed in the context of cellular metabolism, aiming to identify potential candidates for combinational treatment approaches.

2 Materials and methods

2.1 Cell culture

2.1.1 Cultivation of conventional PDAC cell lines

The eight conventional PDAC cell lines used in this study (Table 2-1) were obtained from the American Type Culture Collection and regularly authenticated by single nucleotide polymorphism (SNP)-profiling (Multiplexion, Heidelberg, Germany). Cells were grown in DMEM with glucose levels adapted to human plasma-like conditions; the term Low Glucose DMEM is used hereafter. For preparation, glutamine-supplemented DMEM (#11966025, Thermo Fisher Scientific, Waltham, MA, USA) and DMEM without additives (#A1443001, Thermo Fisher Scientific) were mixed at a 1:1 ratio, thereby achieving a final L-glutamine concentration of 2 mM. Additionally, the medium was supplemented with 5 mM D-glucose (#A2494001, Thermo Fisher Scientific), 5% v/v fetal bovine serum (FBS, #10500-064, Thermo Fisher Scientific), and 1% v/v penicillin/streptomycin (#15140122, Thermo Fisher Scientific). Cells were cultivated at 37 °C and 5% CO_2 in a humidified atmosphere, provided with fresh medium every 2-3 days, and passaged at a confluency of 70-80%. Enzymatic detachment during passaging was achieved using 0.05% or 0.25% Trypsin/EDTA (#25300096 / #25200056, Thermo Fisher Scientific). All cell lines were monthly tested for mycoplasma contamination.

Table 2-1 Conventional PDAC cell lines

Cell line	*Research Resource Identifier*	*Molecular subtype*
HPAC	CVCL_3517	Classical
HPAF-II	CVCL_0313	Classical
HuP-T4	CVCL_1300	Classical
PaTu 8988s	CVCL_1846	Classical
KP-4	CVCL_1338	QM
MIA PaCa-2	CVCL_0428	QM
PaTu 8988t	CVCL_1847	QM
PSN1	CVCL_1644	QM

2.1.2 Cultivation of primary patient-derived cells

The patient-derived cells (PDC) used in this study (Table 2-2) were previously isolated from patient-derived xenografts (PDX) and, based on their transcriptional profile, assigned to the QM or classical PDAC subtype, respectively (Karakaya, 2020; Heid et al., 2022). PDCs were grown in a 1:1 mixture of Low Glucose RPMI and Keratinocyte medium. Low Glucose RPMI was prepared from glutamine-containing RPMI 1640 (#11879020, Thermo Fisher Scientific) by adding 4 mM D-glucose, 10% v/v FBS, and 1% v/v penicillin/ streptomycin. Keratinocyte medium was prepared from Keratinocyte serum-free medium (#17005075, Thermo Fisher Scientific) by adding 50 µg/mL Bovine pituitary extract (BPE), 5 ng/mL recombinant human epidermal growth factor (hEGF), 2% v/v FBS, and 1% v/v Antibiotic-Antimycotic (#15240-062, Thermo Fisher Scientific). Nutrient concentrations in the final medium were the following: 5 mM D-glucose, 4.5 mM L-glutamine, 0.26 mM sodium pyruvate, 6% v/v FBS, 0.5% v/v penicillin/ streptomycin, and 0.5% v/v Antibiotic-Antimycotic. Cells were cultivated and passaged as described for the conventional cell lines and equally tested for mycoplasma contamination once a month.

Table 2-2 Primary patient-derived cells

Cell line	*Molecular subtype*
PDC2	Classical
PDC4	Classical
PDC5	Classical
PDC6	Classical
PDC8	Classical
PDC11	Classical
PDC1	QM
PDC3	QM
PDC7	QM
PDC9	QM
PDC10	QM

2.1.3 siRNA transfection

For silencing of *POLR1A* gene expression, cells were transfected with Silencer Select small interfering (si)RNA (#4392420, Thermo Fisher Scientific) directed against human *POLR1A* (siRNA IDs: s405 (termed siRNA #1) and s223666 (termed siRNA #2)). Silencer Select Negative Control #1 (#4390843, Thermo Fisher Scientific) was used as control. The indicated siRNAs were diluted in Opti-MEM reduced serum medium (#31985047, Thermo Fisher Scientific) and cells were transfected at a final concentration of 10 nM using HiPerfect transfection reagent (#301705, Qiagen, Hilden, Germany). Cells were analyzed 72 h after transfection.

2.2 Cell viability assays

2.2.1 CellTiter-Glo® luminescent cell viability assay

Cell culture plates were equilibrated at room temperature (RT) for approximately 30 min before the measurement. CellTiter-Glo® reagent (#G7573, Promega, Mannheim, Germany), diluted 1:2 or 1:4 in phosphate-buffered saline (PBS, #14190169, Thermo Fisher Scientific), was added to the cells at a 1:1 ratio and plates were shaken to achieve cell lysis. The reaction mixture was further incubated for 5-10 min at RT in the dark. The intensity of the luminescent signal was recorded by the Spark 10M microplate reader (Tecan, Männedorf, Switzerland) with the respective SparkControl software (version 1.2, Tecan).

2.2.2 Proliferation assay

Cells were seeded to white 96-well microplates (#3917, Corning, Corning, NY, USA) at a density of 2,000 cells/well and cultivated for up to 5 days. Each measurement was performed on an individual cell culture plate. Cells were provided with fresh medium every 48 h and cell viability was determined by CellTiter-Glo® luminescent cell viability assay at intervals of 24 h. A detailed description of the measurement procedure is given in 2.2.1. The increase in cell viability was calculated relative to the luminescent signal measured 24 h after cell seeding (t = 0).

2.2.3 Dose-response analysis

Dose-response analyses were performed in a 96-well format. Desired concentrations of BMH-21 (#S7718, Selleckchem, Houston, TX, USA) or CX-5461 (#S2684, Selleckchem) were printed to white microplates (#3917, Corning) using the D300 digital dispenser (Tecan) and the corresponding D300eControl Software (version 3.3.3, Tecan). The inhibitor concentrations were applied in technical

triplicates, and dimethyl sulfoxide (DMSO)-treated cells were used as control. All wells were normalized to the highest DMSO volume and plates were stored at -80 °C until further processing. Plates were equilibrated at RT for approximately 1 h before cell seeding. Cells were automatically seeded to the inhibitor-containing microplates by the reagent dispenser Multidrop Combi (Thermo Fisher Scientific) and incubated for 72 h under normal growth conditions. Cell viability was measured using the CellTiter-Glo® luminescent cell viability assay as described in 2.2.1. Data analysis and calculation of the absolute IC_{50} were performed using the R Software with the drc package (Ritz et al., 2015).

2.2.4 Drug interaction studies

For drug interaction studies between BMH-21 and the autophagy inhibitor 3-Methyladenine (3-MA; #189490, Sigma-Aldrich, St. Louis, MO, USA) or the mTOR inhibitor Rapamycin (#S1039, Selleckchem), respective printing layouts were designed using the synergy wizard of the D300eControl Software. The DMSO-based inhibitors BMH-21 and Rapamycin as well as pure DMSO for normalization were automatically printed to the microplates as described before, while the water-based 3-MA and pure water for normalization were added manually. The inhibitor concentrations were applied in technical duplicates, and DMSO/water-treated cells were used as control. All wells were normalized to the highest volume of DMSO/water. Cells were automatically seeded to the inhibitor-containing microplates and incubated for 72 h as described before. Cell viability was measured using the CellTiter-Glo® luminescent cell viability assay as described in 2.2.1. Data analysis was performed using the SynergyFinder web application (version 3.0, synergyfinder.fimm.fi) (Ianevski et al., 2022) with the Bliss/Loewe consensus synergy scoring method. Synergy scores were interpreted as suggested by the SyngeryFinder user documentation: synergy score < -10 = antagonism; synergy score from -10 to 10 = additive effect; synergy score > 10 = synergism.

2.2.5 Crystal violet staining

For determination of cell viability by crystal violet staining, cells were fixed with ice-cold methanol for 10 min on ice and subsequently stained with crystal violet solution (#C0775, Sigma-Aldrich) (0.1% in 25% methanol) for 30 min at RT. The excessive staining solution was removed by rinsing the cells with water, and the plates were air-dried overnight. Crystal-violet stained cells were imaged using the GelCount colony counter (Oxford Optronix, Abingdon, UK) with the respective GelCount software

(version 1.2.4.2, Oxford Optronix). Cell confluency was measured using the NyONE automated cell imager (Synentec, Elmshorn, Germany) with the respective NyONE Reader software (version 1.5.8267, Synentec).

2.3 Gene expression analysis

2.3.1 Quantitative real-time polymerase chain reaction

RNA was isolated with the Maxwell RSC Automated Nucleic Acid Purification System (Promega) and the corresponding Maxwell RSC simplyRNA Cells Kit (#AS1390, Promega) according to the manufacturer's manual. RNA concentrations were measured using the NanoDrop 2000c spectrophotometer (Thermo Fisher Scientific) with the respective NanoDrop 2000 software (version 1.6.198, Thermo Fisher Scientific). PrimeScript™ reverse transcriptase (#RR036A, TaKaRa, Kusatsu, Japan) was used for cDNA synthesis with an input of 1 µg total RNA, and the resulting cDNA was diluted at a ratio of 1:5 with nuclease-free water. For quantitative real-time polymerase chain reaction (qRT-PCR), the GoTaq qPCR Master Mix (#A6002, Promega) or a 2× EvaGreen qPCR master mix, prepared from the PrimeTaq DNA-polymerase Kit (#1801, Primetech ALC, Minsk, Belarus), EvaGreen dye (#31019, Linaris, Dossenheim, Germany), and dNTPs (#R0192, Thermo Fisher Scientific), was used. All primers used in this study (Table 2-3) were designed with NCBI Primer-BLAST (Ye et al., 2012), if not stated otherwise, and purchased from Eurofins Genomics (Ebersberg, Germany). Samples were measured in triplicates with 4 µL cDNA, 0.3 µM primers, and 10 µL master mix in a total reaction volume of 20 µL. Measurements were performed using the qPCR platform LightCycler 480 (Roche, Basel, Switzerland) and the respective LightCycler 480 Software (version 1.5.1.62, Roche). PCR conditions were the following: 5 min at 95 °C followed by 45 cycles with 95 °C for 15 s, 59 °C for 20 s, and 72 °C for 20 s. Gene expression was analyzed via relative quantification using the $2^{-\Delta\Delta CT}$-method (Livak & Schmittgen, 2001), with *GUSB* as the reference gene.

Table 2-3 Primer sequences

Target gene	*Primer sequence (5' – 3')*	*Reference*
45S rRNA (5'ETS)	Fwd: CAGGTGTTTCCTCGTACCG	(Metge et al., 2021)
	Rvs: GCTACCATAACGGAGGCAGA	
45S rRNA (ITS1)	Fwd: CTCGCCAAATCGACCTCGTA	
	Rvs: GCAAGTGCGTTCGAAGTGTC	

Target gene	*Primer sequence (5' – 3')*	*Reference*
CDH1	Fwd: CGCATTGCCACATACACTCT	
	Rvs: TTGGCTGAGGATGGTGTAAG	
GUSB	Fwd: TGCAGGTGATGGAAGAAGTG	
	Rvs: TTGCTCACAAAGGTCACAGG	
POLR1A	Fwd: CTGAGCCCCTGGGAATTGAG	
	Rvs: CTTCCACAGGGCAGAAAGGT	
UBTF	Fwd: AAACCACCGAATCACACATGG	
	Rvs: TCTGTCAATGTACGGAACTTCCT	
VIM	Fwd: AATGGCTCGTCACCTTCGTGAAT	
	Rvs: CAGATTAGTTTCCCTCAGGTTCAG	
ZEB1	Fwd: TTACACCTTTGCATACAGAACCC	
	Rvs: TTTACGATTACACCCAGACTGC	

The primer product of the 45S rRNA (ITS1) primers reaches from the ITS1 region into the 5.8S region.

2.3.2 RNA sequencing and Illumina bead array

Analysis of ribosome biogenesis-associated genes in conventional PDAC cell lines and PDCs was performed based on previously published data (Karakaya, 2020; Heid et al., 2022). For gene expression analysis of HPAF-II cells with and without BMH-21 treatment, the cells were seeded to 10 cm dishes. After 24 h, the medium was replaced with Low Glucose DMEM supplemented with 0.5 µM BMH-21 or the respective volume of DMSO, and cells were cultivated for 72 h in total. After 48 h, the cells were supplied with fresh medium containing BMH-21 or DMSO. RNA was isolated as described above and 3'mRNA sequencing was performed at Life & Brain GmbH (Bonn, Germany). The analysis of RNA sequencing data was performed by Dr. Sven T. Liffers (Bridge Institute of Experimental Tumor Therapy and Division of Solid Tumor Translational Oncology (DKTK/DKFZ partner site Essen/Düsseldorf), West German Cancer Center, University Hospital Essen, Germany), who also kindly provided the following method section. FASTQ reads were aligned to the human reference genome (GRCh38) using the STAR aligner v. 2.7 (Dobin et al., 2013) with the gene annotation file (GCA_000001405.28) from the Ensembl database. Differential gene expression was estimated using the packages DESeq2 v. 1.33 (Love et al., 2014) and sva v. 3.40

(Leek et al., 2012) in the RStudio v. 1.4 (RStudio Team, 2022) environment for R v.4.1. Lowly expressed genes were filtered in a group-wise manner with at least one count/500,000 transcripts. After data was batch corrected using the Combat_seq function from the sva-package, differential genes were estimated by comparing BMH-21 treated cells with the DMSO control group.

2.3.3 STRING analysis

STRING analysis was performed using the Cytoscape software (version 3.10.1) with the stringApp (version 2.0.1), the yFiles layout algorithms app (version 1.1.3, yWorks GmbH, Tübingen, Germany), and further integrated analysis tools (Shannon et al., 2003; Assenov et al., 2008; Morris et al., 2014; Doncheva et al., 2019; Raudvere et al., 2019). A molecular network based on differential gene expression data was created using the STRING: protein query data source with confidence (score) cut-off = 0.4 and without displaying additional interactors. All genes used for the analysis fulfilled the following criteria: |log2-fold change| > 1.5 and $p_{adjusted} < 0.05$. The analysis was limited to the largest subnetwork and functional enrichment analysis was performed using the GO biological process, the KEGG pathways, and the REACTOME pathways databases. For better visualization, overlaps between multiple nodes were removed using the yFiles remove overlaps algorithm.

2.3.4 Hierarchical clustering

Heatmaps were generated using the R Software with the gplots and the dendextend packages (Galili, 2015; Warnes et al., 2022). Unsupervised hierarchical clustering analysis was based on a complete linkage method with Euclidean distance.

2.3.5 Gene set enrichment analysis

Gene set enrichment analysis (GSEA) was performed based on normalized expression values using the GSEA software (version 4.3.2, UC San Diego and Broad Institute) (Mootha et al., 2003; Subramanian et al., 2005). The permutation type Gene Set was used with the number of permutations being set to 1000. A pathway was considered significantly enriched with |NES| > 1.5 and FDR < 0.05.

2.3.6 Survival analysis

Gene expression data used for the analysis of patient overall survival were obtained from the human protein atlas (proteinatlas.org) (Uhlen et al., 2017). FPKM cut-off values were defined as suggested by proteinatlas.org. Kaplan-Meier plots were

generated using R software with the survminer (Kassambara et al., 2021) and survival (Therneau, 2022) packages.

2.4 Protein related assays

2.4.1 Western blot

Cell lysis was achieved with RIPA buffer (#9806, Cell Signaling Technology, Danvers, MA, USA) containing protease- (#4693124001, Merck, Darmstadt, Germany) and phosphatase inhibitors (#4906837001, Merck). The BCA Protein Assay Kit (#23225, Thermo Fisher Scientific) was used according to the manufacturer's instructions to determine the protein concentration of the lysates. Protein samples were separated on 6-12% polyacrylamide gels and subsequently transferred to nitrocellulose membranes (#1704270, BIO-RAD Laboratories, Hercules, CA, USA) via the semi-dry blot transfer system Trans-Blot Turbo (BIO-RAD Laboratories). The membrane was blocked with 5% w/v skim milk powder (#70166, Sigma-Aldrich) or 5% w/v bovine serum albumin (BSA, #8076, Carl Roth, Karlsruhe, Germany), resolved in Tris-buffered saline (TBS) containing 0.1% v/v Tween 20 (#9127, Carl Roth), for 1 h at RT. Primary antibodies (Table 2-4) were diluted in antibody diluent comprising 5% w/v BSA resolved in 0.1% Tween/TBS and applied at 4 °C overnight. Incubation with anti-rabbit (#111-035-003, Jackson ImmunoResearch, West Grove, PA, USA; 1:25,000) or anti-mouse (#115-035-003, Jackson ImmunoResearch; 1:10,000) secondary antibody, diluted in antibody diluent, was performed for 1 h at RT. SuperSignal West Dura Extended Duration Substrate (#34076, Thermo Fisher Scientific) was used for signal detection. Actin was used as the housekeeper to verify equal protein loading.

Table 2-4 Primary antibodies for western blot

Target protein	*Supplier*	*Catalog number*	*Research Resource Identifier*	*Dilution*
β-Actin	Abcam	ab8227	AB_2305186	1:10,000
Fibrillarin	Novus Biologicals	NB300-269	AB_2100980	1:2,000
Nucleolin	Cell Signaling Technology	14574	AB_2798519	1:2,000/ 1:4,000
RPA194	Santa Cruz Biotechnology	sc-48385	AB_671403	1:200

Target protein	*Supplier*	*Catalog number*	*Research Resource Identifier*	*Dilution*
UBF-1	Santa Cruz Biotechnology	sc-13125	AB_671403	1:200
cleaved PARP	Cell Signaling Technology	9544	AB_2160724	1:1,000
cleaved Caspase 3	Cell Signaling Technology	9664	AB_2070042	1:1,000
LC3B	Sigma-Aldrich	L7543	AB_796155	1:1,000
p62	Cell Signaling Technology	5114	AB_10624872	1:1,000
E-cadherin	Cell Signaling Technology	3195	AB_2291471	1:1,000
Vimentin	Novus Biologicals	NBP1-92687	AB_11017879	1:10,000
4E-BP1	Cell Signaling Technology	9452	AB_331692	1:1,000
Phospho-4E-BP1	Cell Signaling Technology	2855	AB_560835	1:1,000
p70 S6 Kinase	Cell Signaling Technology	2708	AB_390722	1:1,000
Phospho-p70 S6 Kinase	Cell Signaling Technology	9234	AB_2269803	1:1,000

2.4.2 Immunofluorescence

For immunofluorescent (IF) staining of cultivated cell lines, the cells were grown in µ-slide 8 well chambers (#80826, ibidi) upon respective culturing conditions. Cells were fixed with 4% paraformaldehyde (PFA)/PBS (#sc-281692, Santa Cruz Biotechnology) for 15 min at RT, permeabilized using 0.2% Triton X-100 (#3051, Carl Roth)/PBS for 10 min at RT, and blocked in 3% BSA (#05479, Sigma-Aldrich)/PBS for 30 min at RT. Primary antibodies (Table 2-5) were diluted in SignalStain Antibody Diluent (#8112, Cell Signaling Technology) and applied at 4 °C overnight. Cells were incubated with

mouse-specific secondary antibody (#SA5-10173, Thermo Fisher Scientific; 1:400), diluted in 1% BSA/PBS, for 1 h at RT. Counterstaining was performed by applying DAPI (#D1306, Thermo Fisher Scientific) at a concentration of 1 µg/mL for 5 min at RT. For IF staining of Nucleolin, an adapted protocol was used. Cells were cultivated in 8 well culture slides (#354108, Corning). Fixation was performed using 4% PFA/PBS as described before. For blocking, cells were incubated with 10% normal goat serum (NGS, #G9023, Sigma-Aldrich) in PBS with 0.05% Triton X-100 (PBS-T), for 1 h at RT. The primary antibody (Table 2-5) was diluted in 1% NGS/PBS-T and applied for 1 h at RT. The rabbit-specific secondary antibody (#SA5-10033/#35553, Thermo Fisher Scientific; 1:400), diluted in 1% NGS/PBS-T was applied as described before. Between each step, cells were washed three times with PBS for 5 min each. After mechanical removal of the chamber, slides were mounted using Vectashield Antifade Mounting Medium with DAPI (#H-1200, Vector Laboratories; Burlingame, CA, USA). IF stainings were imaged using the fluorescent microscope Axio Observer.Z1 (Zeiss, Oberkochen, Germany). If necessary, the signal intensity was uniformly adjusted for better visualization of the structures shown. However, quantification of the nuclear signal intensity was performed based on the original images using the ZEN software (version 3.0, blue edition, Zeiss).

For IF staining of formalin-fixed, paraffin-embedded (FFPE) tissue, the sections were first deparaffinized with xylene and a decreasing ethanol row using the AutoStainer XL (Leica Biosystems, Wetzlar, Germany). For epitope retrieval, slides were heated to 110 °C for 15 min in a decloaking chamber (Biocare Medical, Pacheco, CA, USA), covered with citrate- (#H 3300, Vector Laboratories, Burlingame, CA, USA) or Tris-based (#H-3301, Vector Laboratories) antigen unmasking solution. Slides were blocked with 10% NGS in TBS with 0.1% v/v Triton X-100 for 1 h at RT. Primary antibodies (Table 2-5) were diluted in antibody diluent, comprising 1% NGS in TBS with 0.1% v/v Triton X-100, and applied for 1 h at RT. Sections were covered with rabbit- (#35553, Thermo Fisher Scientific) or mouse-specific (#SA5-10173, Thermo Fisher Scientific) secondary antibody, diluted in antibody diluent at a ratio of 1:400, and incubated for 1 h at RT. Between each step, slides were washed in TBS containing 0.1% v/v Triton X-100 for 5 min each and rinsed with TBS. Slides were mounted using Fluoromount-G with DAPI (#00-4959-52, Thermo Fisher Scientific). IF stainings were imaged using the fluorescent microscope Axio Observer.Z1 (Zeiss, Oberkochen, Germany).

Table 2-5 Primary antibodies for immunofluorescence

Target protein	*Supplier*	*Catalog number*	*Research Resource Identifier*	*Dilution*
Fibrillarin	Novus Biologicals	NB300-269	AB_2100980	1:100
Nucleolin	Cell Signaling Technology	14574	AB_2798519	1:300/ 1:500
RPA194	Santa Cruz Biotechnology	sc-48385	AB_671403	1:250
UBF-1	Santa Cruz Biotechnology	sc-13125	AB_671403	1:50
pan-Cytokeratin	Abcam	ab6401	AB_305450	1:200

2.4.3 Immunohistochemistry

Immunohistochemistry (IHC) was performed on FFPE sections. Before staining, deparaffinization of the sections as well as epitope retrieval were performed as described above. Endogenous peroxidase activity was inhibited by incubation with 3% hydrogen peroxide solution for 15 min at RT. Slides were blocked with ready-to-use blocking solution (#ZYT-ZUC007-100, Zytomed, Berlin, Germany) for 5 min at RT. Primary antibodies (Table 2-6), diluted in SignalStain Antibody Diluent, were applied at 4 °C overnight. Sections were covered with horseradish peroxidase (HRP) one-step polymer (#zuc053-100, Zytomed) and incubated for 30 min at RT. Between each step, slides were washed in TBS containing 0.1% v/v Triton X-100 for 5 min each and rinsed with TBS. Staining was developed using the Liquid DAB+ Substrate Chromogen System (#K3468, Agilent Technologies, Santa Clara, CA, USA) and slides were counterstained with Hematoxylin solution (#105174, Sigma-Aldrich). Sections were dehydrated with an increasing ethanol row and xylene. Subsequently, slides were mounted with pertex mounting medium (#41-4010-00, MEDITE, Orlando, FL, USA) and air-dried at RT overnight. Slide imaging was performed using the Zeiss Axio Scan.Z1 (Zeiss).

Table 2-6 Primary antibodies for immunohistochemistry

Target protein	*Supplier*	*Catalog number*	*Research Resource Identifier*	*Dilution*
Fibrillarin	Novus Biologicals	NB300-269	AB_2100980	1:100/ 1:200
Nucleolin	Cell Signaling Technology	14574	AB_2798519	1:1,000
RPA194	Santa Cruz Biotechnology	sc-48385	AB_671403	1:200

2.4.4 GFP-LC3 assay

The GFP-LC3 assay was performed and quantified by Dr. Silvia Vega-Rubín-de-Celis and Matthias Kudla (Institute of Cell Biology (Cancer Research), University Hospital Essen, Germany), and the following method section was kindly provided by Dr. Silvia Vega-Rubín-de-Celis. Cells were seeded to 24-well black imaging plates (#0030741021, Eppendorf, Hamburg, Germany) at a density of 10,000 cells/well and transfected with a pBabe-GFP-LC3 plasmid (Vega-Rubin-de-Celis et al., 2018) using the Mirus LT1 reagent (#MIR2300, Mirus, Madison, WI, USA) according to manufacturer's instructions. After 24 h, the medium was replaced with fresh Low Glucose DMEM supplemented with BMH-21 at the indicated concentrations, 0.25 µM Torin 1 (#4247, Tocris Bioscience, Bristol, UK), or DMSO as control. The cells were further cultivated for the indicated time periods, and subsequently fixed in 4% PFA/PBS (Will et al., 2022). Three hours prior to fixation, Bafilomycin A1 (#HY-100558, MedChemExpress, Monmouth Junction, NJ, USA) was added to respective cells at a concentration of 100 nM. Autophagosome numbers were counted in a Zeiss AxioCam MRm microscope (Zeiss).

2.4.5 Autophagy LC3 HiBiT reporter assay

The LC3 HiBiT reporter assay was performed by Dr. Silvia Vega-Rubín-de-Celis, who also kindly provided the following method section. Stable cell lines expressing the HiBiT-LC3 reporter (#GA255A, Promega) were generated by transient transfection of Hup-T4 and PSN1 cells and further selection with 250 µg/ml of G418 (#10131035, Thermo Fisher Scientific), as described before (Hegedus et al., 2022). Cells were seeded into white 96-well plates (#sc-204449, Santa Cruz Biotechnology) at a density

of 5,000 cells/well. The next day, the media was replaced with fresh Low Glucose DMEM containing BMH-21 at the indicated concentrations, 0.25 µM Torin 1, or DMSO as control. The cells were further cultivated for the indicated time periods before HiBiT luminescence was measured as previously described (Will et al., 2022). Treatment with 100 nM Bafilomycin A1 for 3 h was used as an additional control.

2.5 Metabolic assays

2.5.1 Seahorse metabolic flux analysis

Using the Seahorse XF96 metabolic flux analyzer (Agilent Technologies), the influence of BMH-21 on metabolic processes was investigated. Cells were pretreated with BMH-21 (HPAF-II: 0.5 µM, PSN1: 0.17 µM) or the respective volume of DMSO for 48 h. Then, the pretreated cells were trypsinized and seeded into an XF96 cell culture microplate, treated with BMH-21 or DMSO, and further incubated for 24 h. An XFe96 sensor cartridge was hydrated with 200 µL Seahorse XF Calibrant Solution per well and kept in a non-CO2 incubator at 37 °C overnight. XF96 cell culture microplates, XFe96 sensor cartridges, and the Seahorse XF Calibrant Solution are part of the Seahorse XFe96 FluxPak (#102416-100, Agilent Technologies). In addition, the heater of the Seahorse analyzer was set to 37 °C to establish a stable temperature overnight. Before the assay, cells were washed once with Seahorse XF DMEM assay medium (#103575-100, Agilent Technologies) containing 5 mM glucose (#103577-100, Agilent Technologies), 2 mM glutamine (#103579-100, Agilent Technologies), and BMH-21 or DMSO, respectively. Cells were incubated in a non-CO_2 incubator for 45 min and calibration of the hydrated sensor cartridge was performed. Cells were washed again with the assay medium containing BMH-21 or DMSO, and provided with a final volume of 180 µL/well before starting baseline measurements of the oxygen consumption rate (OCR) and the extracellular acidification rate (ECAR).

To ensure comparability between the treatment conditions, absolute OCR and ECAR values were normalized to the DNA content. Following the assay, cells were fixed with 4% PFA/PBS and stained with DAPI nucleic acid stain (#D1306, Thermo Fisher Scientific) at a concentration of 2.5 µg/mL in PBS for 10 min at RT. The resulting fluorescent signal was measured using the Spark 10M Microplate Reader (excitation wavelength: 385 nm, emission wavelength: 461 nm). Values of five technical replicates per condition were averaged. Relative fluorescent units (RFU) with a scale factor of 10,000 were used as normalization units.

2.5.2 Isocitrate dehydrogenase activity assay

Cells were pretreated with BMH-21 (HPAF-II: 0.5 µM, PSN1: 0.17 µM) or the respective volume of DMSO for 72 h. After 48 h, cells were supplied with fresh medium containing BMH-21 or DMSO, respectively. The activity of isocitrate dehydrogenase (IDH) was measured using the IDH Activity Assay Kit (#MAK062, Sigma-Aldrich) according to the manufacturer's manual. In brief, cells were homogenized in ice-cold IDH Assay Buffer at a concentration of 1×10^6 cells / 200 µL and centrifuged at 13,000×g for 10 min. Determined as the optimal sample amount in a pilot experiment, 30 µL (HPAF-II) or 50 µL (PSN1) of the supernatant was used as input for the assay. Only NAD^+ was added to the reaction mix, limiting the measurement to the activity of the NAD^+-dependent IDH3. Using the Spark 10M microplate reader, optical density at 450 nm was measured in kinetic mode over a period of 20 min at 5 min intervals.

2.6 Cell cycle analysis

Cell cycle analysis was performed based on propidium iodide staining after 72 h of treatment without occasional medium exchange. Cells were enzymatically detached using 0.05% Trypsin/EDTA and fixed with 70% ethanol for 2 h on ice or at 4 °C for at least 16 h. Fixed cells were rehydrated and stained with DNA staining solution comprising 0.1% Triton X-100, 0.5 mg/mL RNase A (#1007885, Qiagen), and 0.06 mg/mL propidium iodide (#P3566, Thermo Fisher Scientific) for 30 min at RT. Measurements were performed using the BD FACSCelesta™ Multicolor Flow Cytometer (BD, Franklin Lakes, NJ, USA) and the respective FACSDiva™ Software (version 8.0.1.1, BD). Data analysis was performed using the FlowJo™ Software (version 10.8.1, BD).

2.7 Animal handling

Animal experiments and tissue preparation were organized and conducted by Dr. Kristina Althoff, Dr. Marija Trajkovic-Arsic, Rui Fang, Konstantinos Savvatakis, and Vuk Dinovic (Bridge Institute of Experimental Tumor Therapy and Division of Solid Tumor Translational Oncology (DKTK/DKFZ partner site Essen/Düsseldorf), West German Cancer Center, University Hospital Essen, Germany). Animal experiment applications were prepared by Dr. Kristina Althoff, who also kindly provided the following method section. Animal experiments were approved by the appropriate national authorities. Animal care protocols were as prescribed in the national laws and regulations as well as the European Federation of Animal Science Associations (FELASA; http://www.felasa.eu). Orthotopic and subcutaneous transplantations were

conducted by Rui Fang and Dr. Marija Trajkovic-Arsic, respectively. For orthotopic transplantation, a suspension of human PDAC cells was transplanted orthotopically into the pancreas of immunosuppressed NMRI nude mice under ultrasound image guidance. For subcutaneous transplantation, a suspension of human PDAC cells was transplanted subcutaneously into the flank of immunosuppressed NMRI nude mice. At the endpoint, tumors and organs were collected and fixed in 4% PFA/PBS. Further tissue preparation was performed by Konstantinos Savvatakis and Vuk Dinovic. After fixation, the tissue was dehydrated and embedded in paraffin, and subsequently sectioned at 3 µm thickness. Tissue sections were then further processed by IF and IHC as described in 2.4.2 and 2.4.3, respectively.

2.8 Data analysis and visualization

Data- and statistical analysis were performed using GraphPad PRISM (version 9), R Software (version 4.2.1), and R Studio (version 2022.07.0+548) (R Core Team, 2022; RStudio Team, 2022). In addition to analysis-specific packages stated in the respective sections, the tidyverse package, the RColorBrewer package, and the ggpattern package were used for general data analysis and graphical representation (Wickham et al., 2019; FC et al., 2022; Neuwirth, 2022).

Shapiro-Wilk test was used to test for the normality of data and the F- or Levene test was used to assess the equality of variances. The appropriate test for statistical analysis was selected accordingly. Mann-Whitney-U test was used to compare the RP expression levels between PDAC- and normal pancreatic tissue samples, as well as the nuclear intensity of nucleolar markers in BMH-21-treated and control cells. Kruskal-Wallis test with Dunn's multiple comparison test was used for statistical analysis of the GFP-LC3B assay. The chi-square test with Bonferroni post-hoc analysis was used to compare the cell cycle distribution of cells with and without BMH-21 treatment. For all other experiments, p-values were calculated by Student's t-test (unpaired, two-sided) or by One-way ANOVA with Bonferroni's multiple comparison test. In the case of fold change data, statistical tests were applied on log2-transformed ratios. Differences were considered statistically significant with p-values < 0.05.

Figures were arranged using the Inkscape software and illustrations were prepared using building blocks from Servier Medical Art. Servier Medical Art (Servier, Suresnes, France) is licensed under a Creative Commons Attribution 3.0 Unported License (https://creativecommons.org/licenses/by/3.0/).

3 Results

3.1 Ribosome biogenesis in PDAC

3.1.1 PDAC patients exhibit differences in ribosomal gene expression

The expression of ~90 RPs and emerging paralogs (Guimaraes & Zavolan, 2016) was analyzed in PDAC patient samples (n = 204) and normal pancreatic tissue (n = 41) based on previously published Illumina bead chip array data (E-MTAB-1791). The comparison of the median RP expression levels revealed no overall difference between the two groups (Figure 3-1 A). Nevertheless, hierarchical cluster analysis resulted in a nearly complete separation of PDAC- and normal pancreatic tissue samples and unveiled a complex and heterogeneous expression pattern of RPs in PDAC (Figure 3-1 B). For a large number of RPs (e.g., RPL34, RPL32), generally increased expression levels were detected in normal- compared to PDAC tissue samples. On the other hand, individual RPs, including RPL10L and RPL39L, exhibited higher expression in a subgroup of tumor samples compared to normal pancreatic tissue (Figure 3-1 B and Annexed Figure 1). However, high variation in the expression of RP-encoding genes was found not only between PDAC- and normal tissue but also between different tumor samples. Next to PDAC samples that presented with a generally increased or decreased RP expression, others exhibited deregulation of only individual RPs in the global comparison (Figure 3-1 B). These findings indicate that RPs may play a complex role in the context of PDAC tumorigenesis.

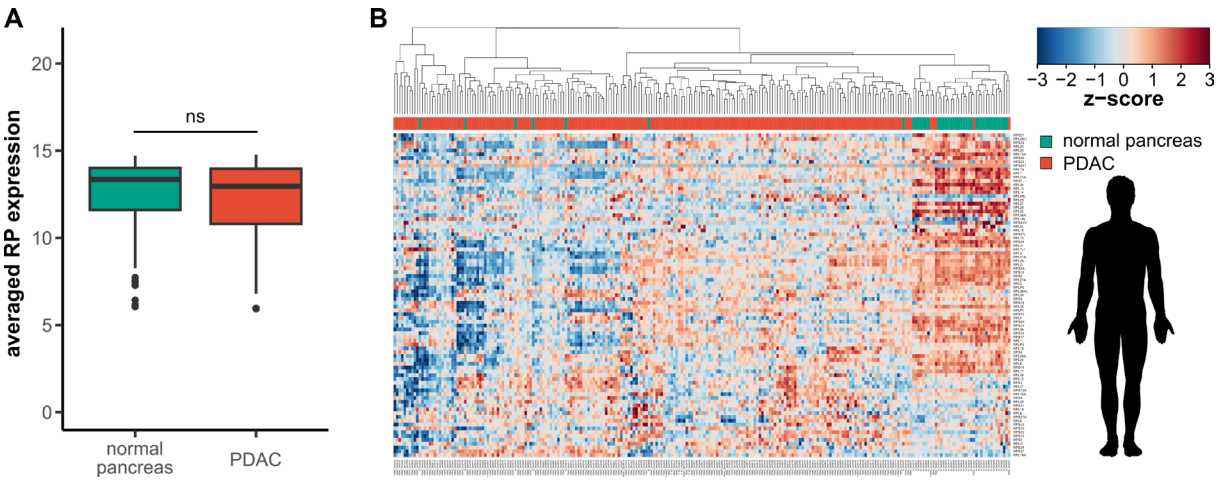

Figure 3-1 Ribosomal proteins are heterogeneously expressed in PDAC samples and normal pancreatic tissue

Expression analysis for ~90 ribosomal protein-encoding genes in PDAC patient samples (n = 204) and normal pancreatic tissue (n = 41) based on Illumina bead chip array data (E-MTAB-1791). **(A)** Boxplots presenting the median RP expression in normal pancreatic tissue (green) and PDAC samples (red). ns not significant. **(B)** Hierarchical cluster analysis strongly separated PDAC- from normal pancreas samples.

MYC oncogene, which is frequently overexpressed in PDAC (Schneider et al., 2021), was described to promote RiBi by upregulating the transcriptional activity of RNA polymerases as well as the translational capacity of the cell, thereby contributing to a favorable supply with rRNAs, RPs, and RBFs (van Riggelen et al., 2010). PDAC patient samples were grouped according to their *MYC* expression level, with the cut-off values being defined as the average log2-expression ± one standard deviation. In this way, 38 PDAC patient samples were classified as MYC^{high} and 30 samples as MYC^{low}, respectively. Subsequent gene set enrichment analysis (GSEA) showed significant enrichment of gene sets associated with rRNA processing and -modification, ribosomal subunit maturation, and translational processes in MYC^{high} samples (Figure 3-2 and Annexed Table 1). These findings point to a correlation between high levels of *MYC* expression and an increased RiBi activity in PDAC.

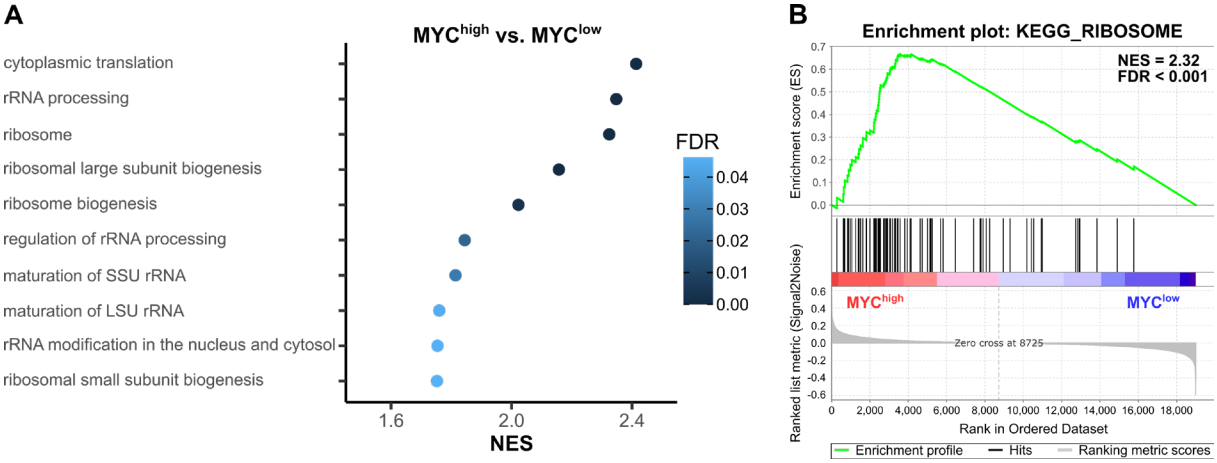

Figure 3-2 MYC expression influences the transcription of ribosome biogenesis- and translation-associated gene sets

Gene set enrichment analysis for PDAC patient samples (MYC^{high} vs. MYC^{low}). Samples were classified based on *MYC* expression with mean ± SD being used as cut-off values. **(A)** Normalized enrichment scores (NES) and false discovery rates (FDR) are presented for a selection of ribosome biogenesis- and translation-associated pathways enriched in MYC^{high} samples. **(B)** Enrichment plot of one exemplary gene set (KEGG_RIBOSOME) found to be enriched in MYC^{high} samples.

Furthermore, publicly available TCGA datasets were used to evaluate whether the expression of nucleolar proteins, involved in different steps of RiBi, is related to the survival of pancreatic cancer patients. The transcription factors UBF-1 (*UBTF*) and TIF-IA (*RRN3*), together with the RNA Pol I catalytic subunit RPA194 (*POLR1A*), are essential for the synthesis of 47S pre-rRNA. Fibrillarin (*FBL*) and Nucleophosmin (*NPM1*) are involved in rRNA modification and ribosome assembly, respectively, while Nucleolin (*NCL*) plays a role in rDNA transcription as well as rRNA processing (Dörner et al., 2023). The analysis revealed differences in the prognostic impact between the

investigated genes. Higher expression levels of *FBL*, *NCL*, *NPM1*, and *RRN3* were associated with significantly reduced overall survival in PDAC patients. In contrast, high expression levels of *UBTF* and *POLR1A* were linked with better prognosis (Figure 3-3).

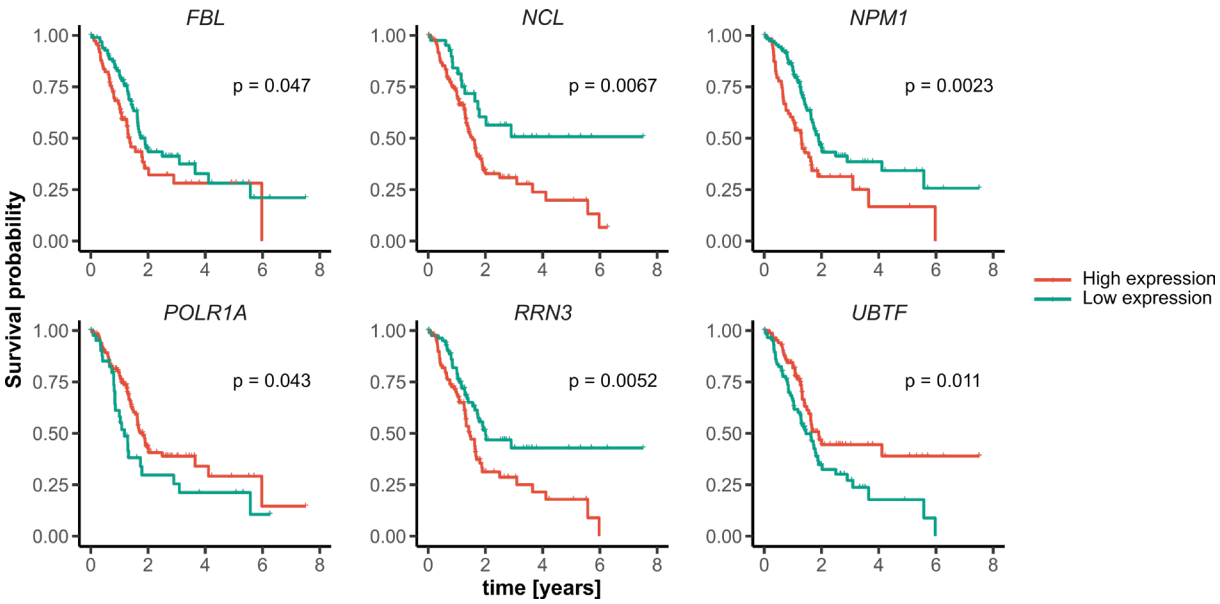

Figure 3-3 Gene expression of individual ribosome biogenesis regulators is associated with poor survival in PDAC

Kaplan-Meier plots presenting the overall survival of PDAC patients grouped by gene expression level for different RiBi regulators: *FBL* (n^{high} = 76, n^{low} = 100), *NCL* (n^{high} = 134, n^{low} = 42), *NPM1* (n^{high} = 65, n^{low} = 111), *POLR1A* (n^{high} = 133, n^{low} = 43), *RRN3* (n^{high} = 92, n^{low} = 84), *UBTF* (n^{high} = 86, n^{low} = 90). Data and FPKM cut-off values were obtained from www.proteinatlas.org.

3.1.2 PDAC cells show variation in ribosome biogenesis activity

Based on the transcriptional profile, conventional human PDAC cell lines (n = 8) were previously assigned to the two main molecular PDAC subtypes, namely the classical (HuP-T4, HPAC, HPAF-II, PaTu 8988s) or the QM subtype (KP-4, PaTu 8988t, PSN1, MIA PaCa-2) (Collisson et al., 2011; Daemen et al., 2015). While classical cell lines are characterized by high expression levels of epithelial genes like E-cadherin (*CDH1*), QM cells show strong expression of mesenchymal genes, for example, Vimentin (*VIM*) (Figure 3-4 A). High levels of Vimentin and E-cadherin expression in QM and classical cell lines, respectively, have previously been validated by qPCR analysis (Heid et al., 2022). To compare the level of RiBi in these cell lines, the expression of RP-encoding genes was analyzed via hierarchical clustering using previously obtained RNA sequencing data (Karakaya, 2020; Heid et al., 2022). The analysis revealed a clear separation into two clusters, whereby QM cell lines presented higher expression of RP genes while lower expression levels were observed in cell lines of the classical subtype

(Figure 3-4 B). A similar result was observed in GSEA comparing QM and classical cells. The QM subtype showed significant enrichment of gene sets associated with the three main steps of RiBi, namely rDNA transcription, rRNA modification, and ribosome assembly (Figure 3-4 C and Annexed Table 2).

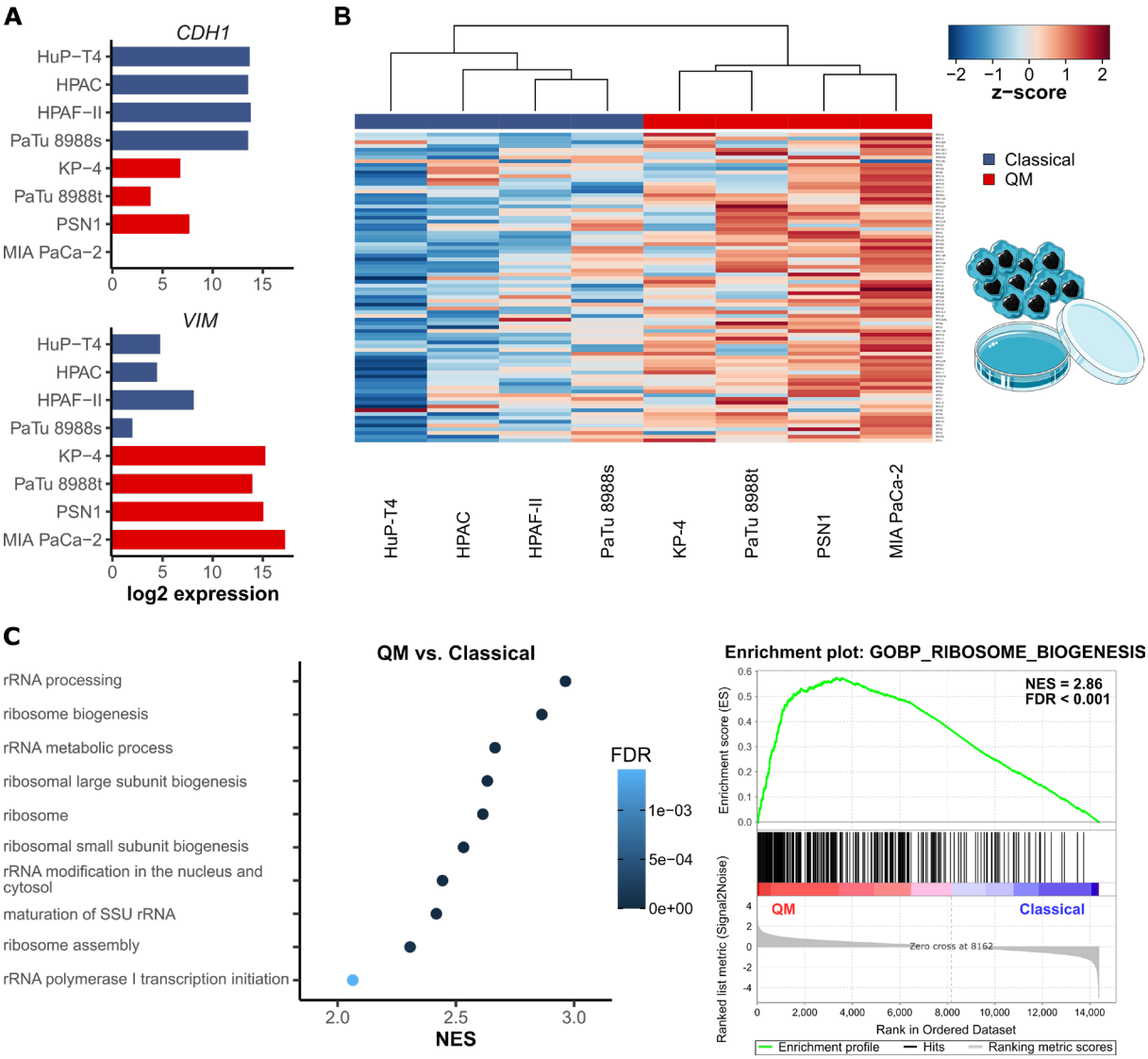

Figure 3-4 PDAC cell lines show subtype-specific differences in the expression of ribosome biogenesis-associated genes

(A) Expression levels (RNA sequencing) for E-cadherin (*CDH1*) and Vimentin (*VIM*) in classical (blue) and QM (red) PDAC cell lines. **(B)** Hierarchical cluster analysis for ~90 ribosomal protein-encoding genes in PDAC cell lines based on RNA sequencing data. **(C)** Gene set enrichment analysis for PDAC cell lines (QM vs. Classical). Left: Normalized enrichment scores (NES) and false discovery rates (FDR) are presented for ribosome biogenesis-related gene sets enriched in the QM subtype. Right: Enrichment plot of one exemplary gene set (GOBP_RIBOSOME_BIOGENESIS) found to be enriched in QM PDAC cell lines.

Given that various gene sets related to RNA Pol I-mediated transcription were enriched in the QM subtype, the level of rRNA synthesis in PDAC cell lines was evaluated via qPCR for the 5'ETS and ITS1 regions of the nascent 45S pre-rRNA (Figure 3-5 A).

ETS and ITS regions are present in the pre-rRNA molecule and removed via exo- and endonucleolytic cleavage in early processing steps. Therefore, their expression is used as a parameter for nascent rRNA synthesis and RNA Pol I activity. For both the 5'ETS and the ITS1 region, relative expression levels were significantly higher in QM compared to classical cells, with the QM cell line PSN1 presenting the highest expression (Figure 3-5 B). Taken together, this indicates a higher RiBi activity in QM compared to classical PDAC cell lines.

Furthermore, hyperactivation of RiBi is tightly related to abnormal cell growth and proliferation observed in cancer, as upregulation of ribosome production supports the cells' increased demand for protein synthesis. Therefore, to estimate the proliferation of different PDAC cell lines, the increase in cell viability over time was followed by CellTiter-Glo® assay. Proliferation rates were generally higher in QM compared to classical cells, with the fastest increase in cell viability being detected in QM PSN1 cells and the slowest in classical HPAF-II cells (Figure 3-5 C). These observations suggest a link between high levels of RiBi and an increased proliferative capacity in PDAC.

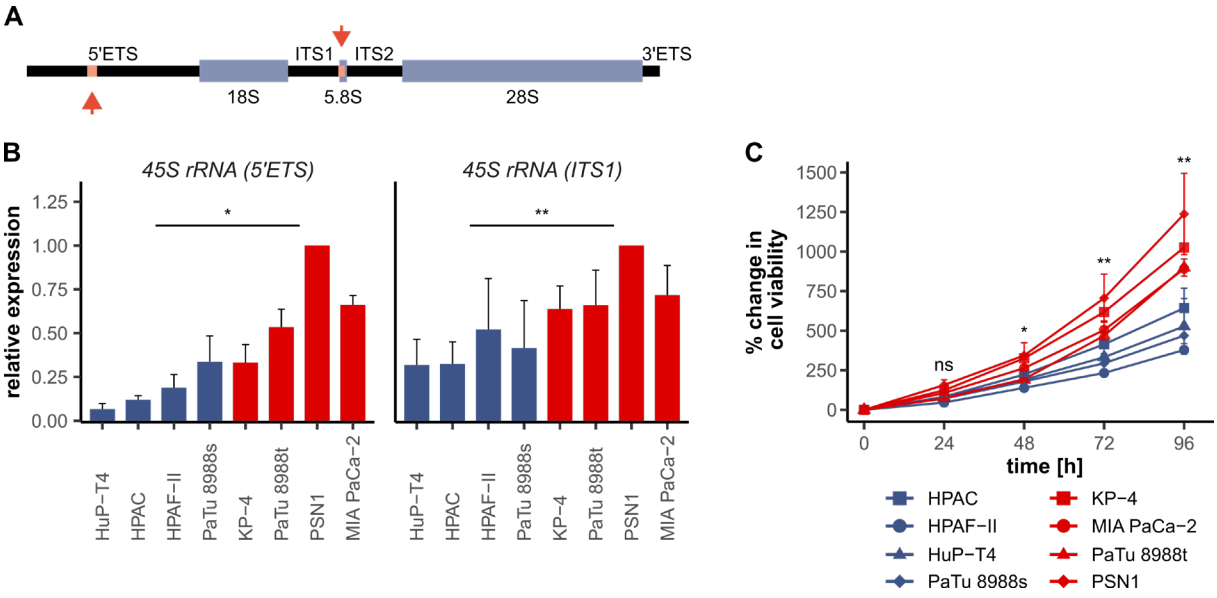

Figure 3-5 Subtype-dependent variation in the RNA polymerase I activity is present in PDAC cell lines

(A, B) qPCR analysis for the expression of 45S rRNA in conventional PDAC cell lines. **(A)** Schematic representation of the 45S rRNA structure with primer binding sites (red arrows) in the 5'ETS and ITS1 region. **(B)** Expression levels, normalized to *GUSB*, are presented relative to the expression levels in PSN1 cells as mean + SD of three independent experiments. **(C)** Relative increase in cell viability for PDAC cell lines over a 96 h period. Data presented as mean ± SD of two independent experiments. ns not significant, * $p < 0.05$, ** $p < 0.01$.

The nucleolus strongly adapts its morphology according to changes in the level of ribosome production and especially rDNA transcription (Derenzini et al., 2009). Therefore, the nucleolar organization in QM and classical PDAC cell lines was compared by IF for four nucleolar marker proteins, namely Fibrillarin, RPA194, Nucleolin, and UBF-1. According to their role in the different steps of RiBi, the proteins are located in distinct nucleolar subcompartments. While RPA194 and UBF-1 play a role in rDNA transcription and are therefore enriched in the FC, Fibrillarin is associated with early rRNA modification in the DFC, and Nucleolin is mainly involved in rRNA processing and ribosome assembly in the DFC and the GC (Biggiogera et al., 1990; Raska et al., 2006; Boisvert et al., 2007). Staining with all four markers revealed a pronounced difference in the nucleolar organization between the two molecular subtypes. While in classical cell lines with lower RNA Pol I activity, a more scattered/dispersed nucleolar pattern was observed, QM cell lines with comparatively higher levels of rRNA expression mainly presented compact macronucleoli (Figure 3-6).

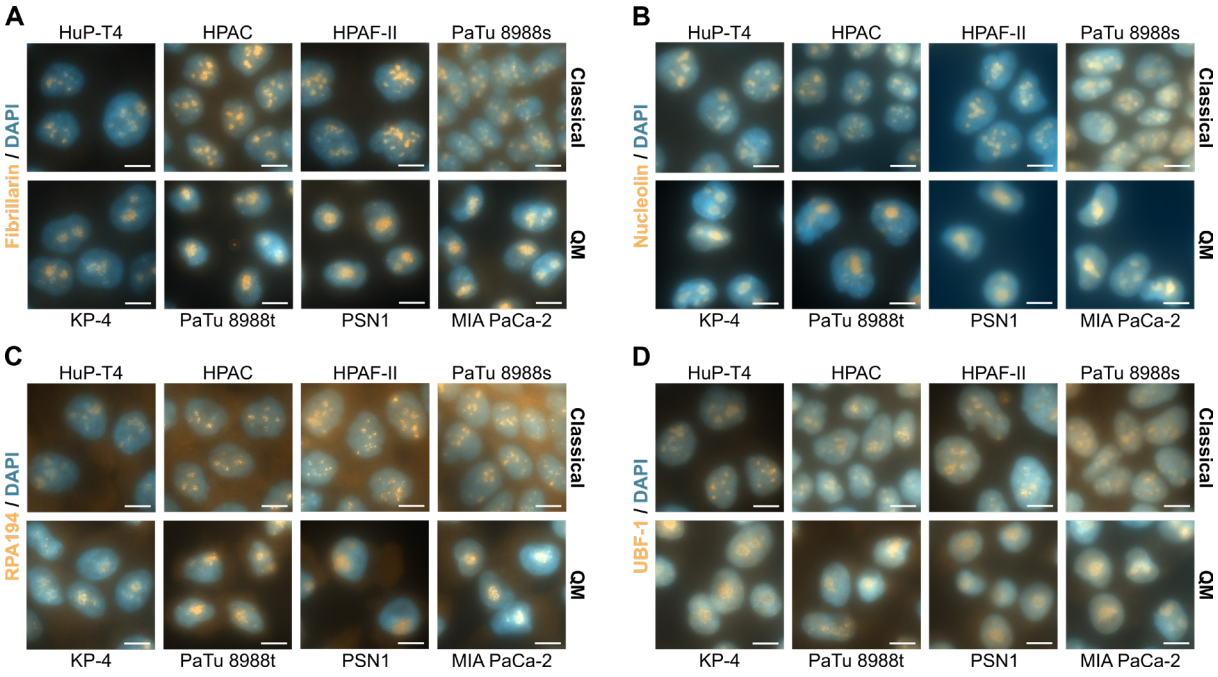

Figure 3-6 Variation in the level of ribosome biogenesis is reflected in the nucleolar structure

Immunofluorescence for the nucleolar markers Fibrillarin **(A)**, Nucleolin **(B)**, RPA194 **(C)**, and UBF-1 **(D)** in conventional PDAC cell lines showing more compact macronucleoli in QM cells and a rather scattered nucleolar pattern in classical cell lines. Scale bar = 10 µm.

Additionally, the nucleolar appearance of the respective cells in subcutaneous and orthotopic xenografts was evaluated via IHC. Staining for Fibrillarin, Nucleolin, and RPA194 on tumor sections from subcutaneous xenografts showed mainly large

compact nucleoli in QM PSN1 tumors, but a more scattered nucleolar pattern in classical HPAF-II tumors (Figure 3-7 A). Similarly, Fibrillarin staining on orthotopic xenografts revealed mostly prominent macronucleoli in QM tumors of PaTu 8988t and PSN1 cells but a rather dispersed nucleolar pattern in classical tumors of HPAC and HPAF-II cells (Figure 3-7 B). This demonstrates that the subtype-specific nucleolar morphology of PDAC cell lines is maintained in an *in vivo* setting.

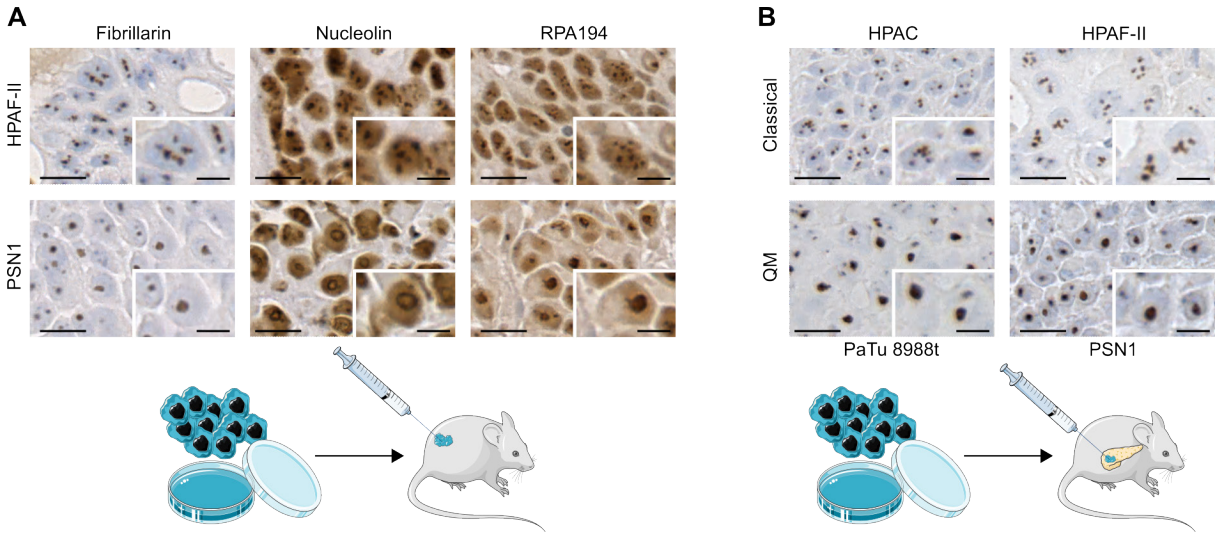

Figure 3-7 Subtype-specific nucleolar organization of PDAC cell lines is maintained *in vivo*

(A) Immunohistochemistry (IHC) for Fibrillarin, Nucleolin, and RPA194 on FFPE sections of HPAF-II and PSN1 tumors (subcutaneously injected xenografts). Scale bar = 20 µm (detail = 10 µm). **(B)** IHC for Fibrillarin on FFPE sections of HPAC, HPAF-II, PaTu 8988t, and PSN1 tumors (orthotopically injected xenografts). Scale bar = 20 µm (detail = 10 µm).

Similarly, analyses of RP gene expression, RNA Pol I activity, and the nucleolar organization were performed for PDCs (n = 11), which were transcriptionally characterized as classical (PDC2, PDC4, PDC5, PDC6, PDC8, PDC11) or QM (PDC1, PDC3, PDC7, PDC9, PDC10) in previous studies (Karakaya, 2020; Heid et al., 2022). For RPs, a heterogeneous expression pattern was observed between different PDCs that was independent of the molecular subtype. Moreover, individual RPs were up- or downregulated in the respective PDCs (Figure 3-8 A), again suggesting that the deregulation of RP gene expression is highly dynamic in PDAC. PDCs further displayed a rather uniform RNA Pol I activity (Figure 3-8 B) and similar proliferation rates (Figure 3-8 C). Interestingly, although PDC3 showed a substantially lower proliferation rate, its RiBi activity was still comparable to other primary cells when considering the expression levels of RP genes and 45S rRNA (Figure 3-8 A-C). Furthermore, in contrast to conventional cell lines, PDCs did not exhibit a predominant

nucleolar organization in the respective cell lines, be it a scattered or compact morphology. Instead, IF staining for all four tested nucleolar markers (Fibrillarin, Nucleolin, RPA194, and UBF-1) revealed the presence of both structure types, i.e. dispersed nucleoli as well as compact macronucleoli, in individual cells of the same cell line.

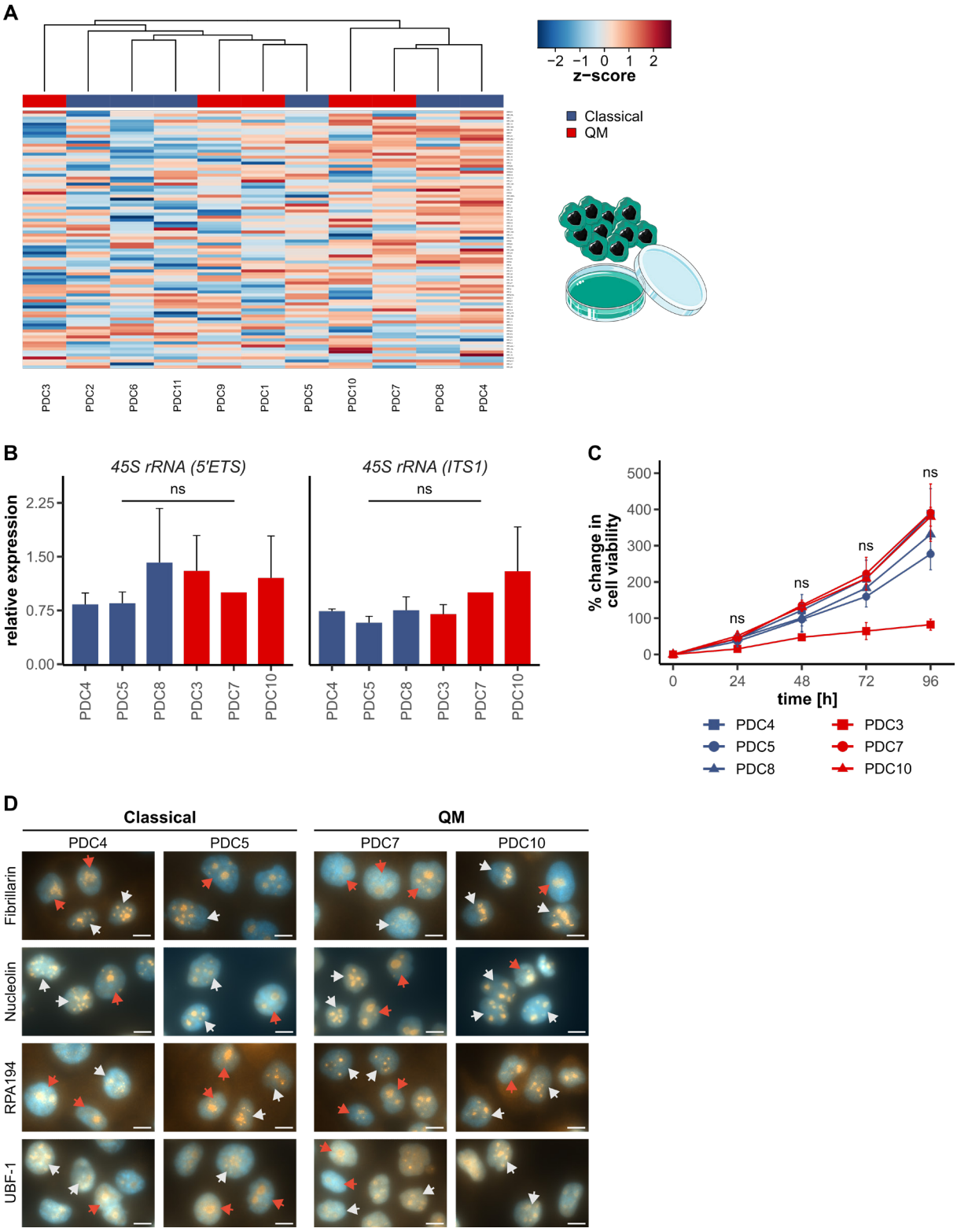

Figure 3-8 Continued

Figure 3-8 Patient-derived cells do not present subtype-dependent differences in RNA polymerase I activity or nucleolar organization

(A) Hierarchical cluster analysis for ~90 ribosomal protein-encoding genes in primary patient-derived cells (PDC) based on Illumina microarray data. **(B)** qPCR analysis for the expression of 45S rRNA in PDCs. Expression levels of the 5'ETS and ITS1 regions, normalized to *GUSB*, are presented relative to the expression levels in PDC7 cells as mean + SD of three independent experiments. **(C)** Relative increase in cell viability for PDCs over a 96 h period. Data presented as mean ± SD of two independent experiments. ns not significant. **(D)** Immunofluorescence for the nucleolar markers Fibrillarin, Nucleolin, RPA194, and UBF-1 in PDCs showing heterogeneity in the nucleolar morphology with compact nucleoli (red arrows) and scattered nucleoli (white arrows) present within one cell line. Scale bar = 10 µm.

3.1.3 Nucleolar heterogeneity is present in murine PDAC samples

To further investigate the nucleolar organization in an *in vivo* context, IHC staining for the nucleolar marker proteins was performed on tumor tissue of a genetically engineered PDAC mouse model (*Ptf1a*$^{wt/Cre}$ *Kras*$^{wt/LSL\text{-}G12D}$ *Trp53*$^{lox/lox}$, termed CKP hereafter). CKP mice carry a pancreas-specific heterozygous *Kras*^{G12D} mutation together with a homozygous deletion of *Trp53*, resulting in spontaneous PDAC development (Bardeesy et al., 2006; Mazur et al., 2015). IHC for the nucleolar markers Fibrillarin and Nucleolin revealed region-dependent differences in the nucleolar morphology, with compact and scattered nucleoli being present in different cancer cell populations throughout the tumor tissue (Figure 3-9 A). To validate the heterogeneous nucleolar morphology specifically in cancer cells, co-IF for Nucleolin and pan-Cytokeratin (pan-CK) was performed, the latter being considered a marker for tumor cells (Cheung et al., 2022). Among pan-CK-positive cancer cells, both those with a more scattered and those with a more compact nucleolar pattern were observed, respectively (Figure 3-9 B). These findings validate that heterogeneity in the size and the number of nucleoli is indeed present in different populations of tumor cells.

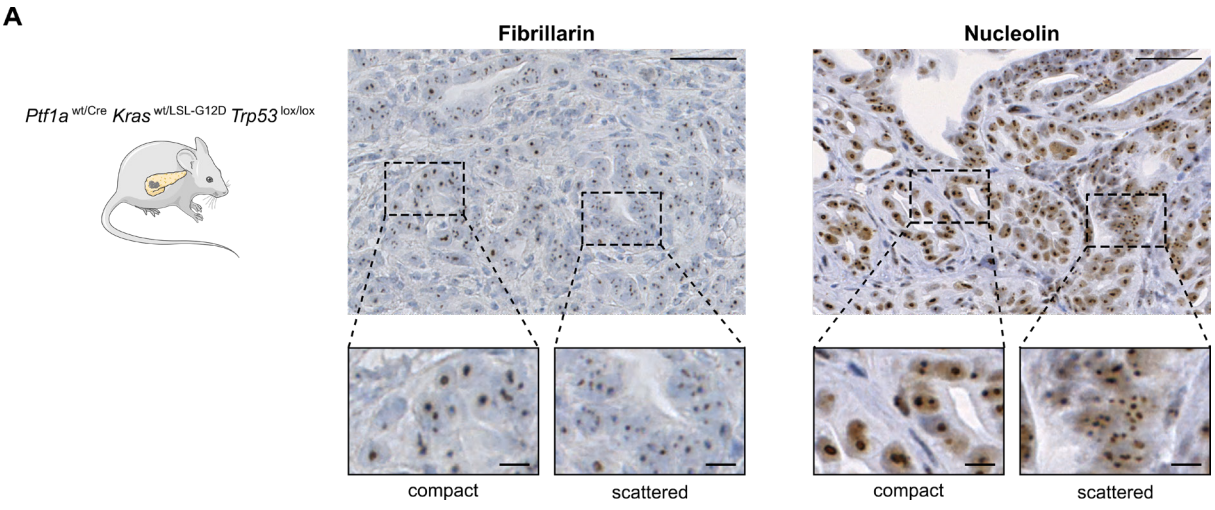

Figure 3-9 Continued

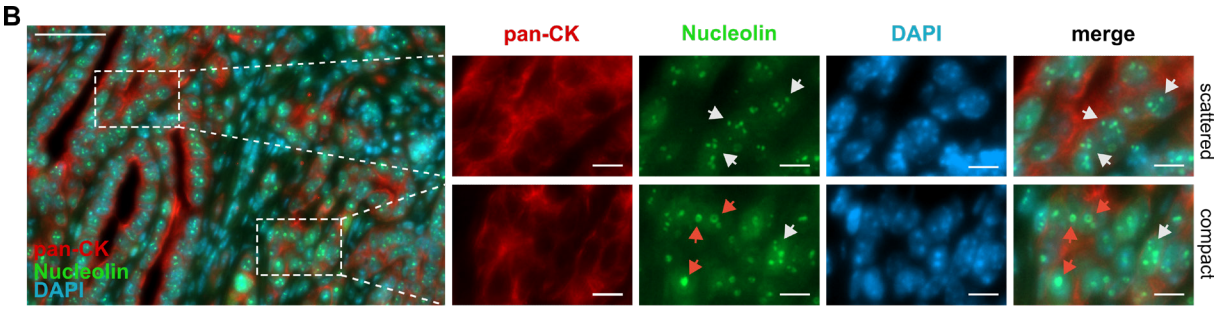

Figure 3-9 Tumors of a genetically engineered PDAC mouse model are characterized by intratumoral heterogeneity in the nucleolar organization

FFPE tissue sections were derived from tumors of a genetically engineered PDAC mouse model (*Ptf1a* $^{wt/Cre}$ *Kras* $^{wt/LSL-G12D}$ *Trp53* $^{lox/lox}$; CKP). **(A)** Immunohistochemistry for Fibrillarin and Nucleolin. Scale bar = 50 µm (detail = 10 µm). **(B)** Immunofluorescence for Nucleolin (green) and pan-CK (red) with DAPI-counterstaining (blue). Scale bar = 50 µm (detail = 10 µm). Heterogeneity in the nucleolar organization was detectable, with compact nucleoli (red arrows) and scattered nucleoli (white arrows) being present in pan-CK-positive tumor cells.

3.2 Antitumor effects of ribosome biogenesis inhibition

3.2.1 RNA polymerase I inhibition decreases cell viability in PDAC cells

Analysis of RP encoding genes, rRNA synthesis, and the nucleolar appearance in PDAC cell lines and PDCs revealed substantial differences between individual cell lines, pointing to varying levels of RiBi activity. Therefore, the effect of RNA Pol I inhibition on cell viability was determined for the described cell lines and PDCs, and potential correlations between the level of RiBi and the treatment response were evaluated.

Conventional PDAC cell lines and PDCs were treated with the small-molecule inhibitor BMH-21, which inhibits RNA Pol I-mediated transcription by intercalating into the GC-rich regions of rDNA gene clusters (Peltonen et al., 2010; Peltonen et al., 2014). BMH-21 effectively reduced the cell viability of nearly all tested cell lines with half maximal inhibitory concentrations (IC_{50}) in the nano- or low micromolar range (Figure 3-10). Conventional cell lines showed a subtype-dependent difference in the response toward BMH-21 with QM cell lines presenting stronger treatment responses compared to classical cell lines (Figure 3-10 A and B). Specifically, PSN1 cells exhibited the strongest sensitivity toward BMH-21 treatment with an IC_{50} of 0.46 µM (Figure 3-10 A). Compared to conventional PDAC cell lines, PDCs in general showed a slightly lower sensitivity toward BMH-21. Notably, the primary cell line PDC3 exhibited some degree of treatment resistance with an IC_{50} of 11.52 µM (Figure 3-10 C). For PDCs, no correlation between the molecular subtype and the treatment efficiency was observed (Figure 3-10 D).

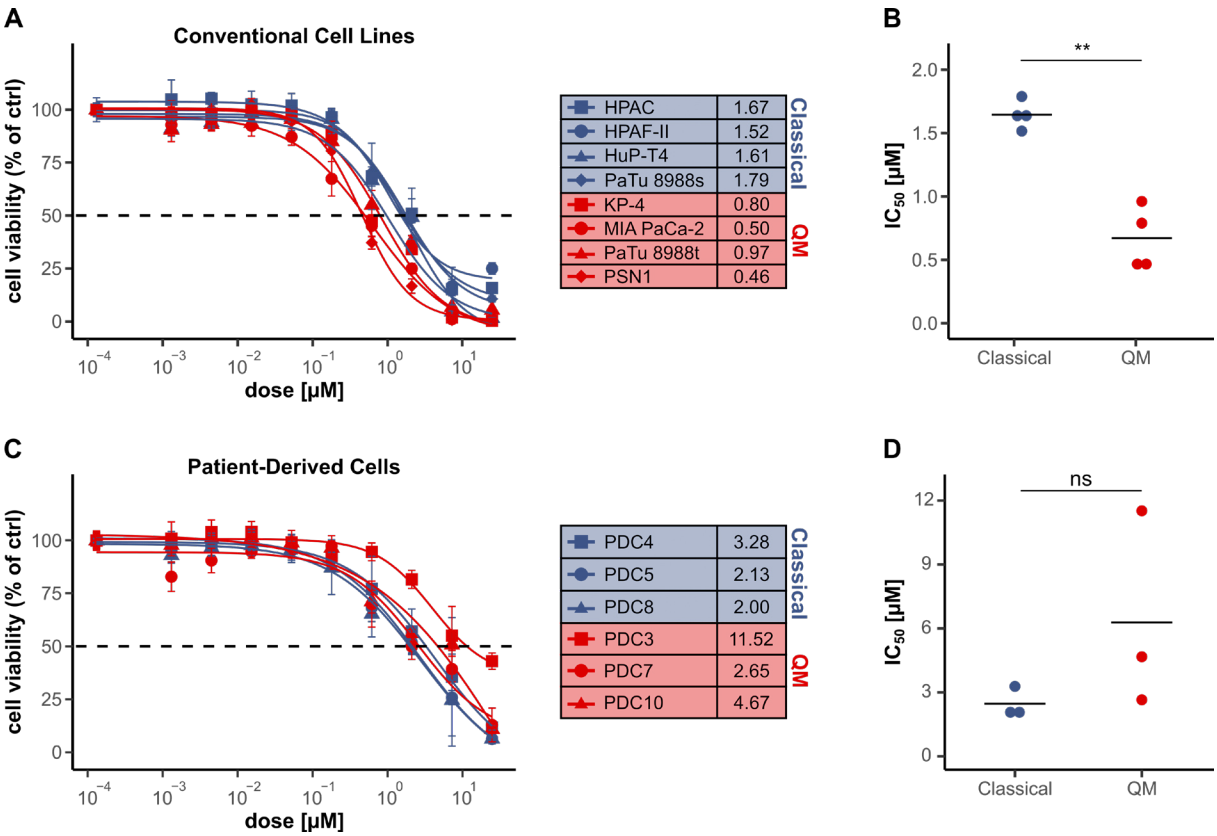

Figure 3-10 BMH-21 treatment reduces cell viability in PDAC cells

Dose-response analysis for conventional PDAC cell lines and primary patient-derived cells (PDCs) treated with BMH-21 (1 nM – 25 µM) for 72 h. **(A, C)** Dose-response curves and absolute IC_{50} values for conventional cell lines **(A)** and PDCs **(C)**. Cell viability was normalized to untreated control cells and is presented as mean ± SD of two independent experiments. **(B, D)** Dot plots for the absolute IC_{50} values of conventional cell lines **(B)** and PDCs **(D)** grouped by the molecular subtype. ns not significant, ** $p < 0.01$.

Another first-in-class inhibitor, CX-5461, was described to impair RNA Pol I activity by interfering with the transcription factor binding of SL1 to the rDNA promotor, thereby preventing the interaction with RNA Pol I and the initiation of rDNA transcription (Drygin et al., 2011). Similar to the effects observed for BMH-21, treatment with CX-5461 also caused a dose-dependent decrease in the cell viability of all PDAC cell lines tested (Figure 3-11). Again, the treatment sensitivity largely correlated with the level of RiBi activity observed for the respective cell lines. MIA PaCa-2 and PSN1 cells, both associated with the QM subtype, showed the strongest response toward CX-5461 with an IC_{50} of ~0.2 µM, while the classical cell line HPAF-II showed the lowest sensitivity with an IC_{50} of 4.14 µM (Figure 3-11). Importantly, given that it is still a subject of discussion whether inhibition of RNA Pol I activity is the primary mechanism of CX-5461-mediated cytotoxicity (Xu et al., 2017; Bruno et al., 2020), the present work focuses on the small-molecule inhibitor BMH-21 to evaluate the consequences of specifically targeting RiBi in PDAC.

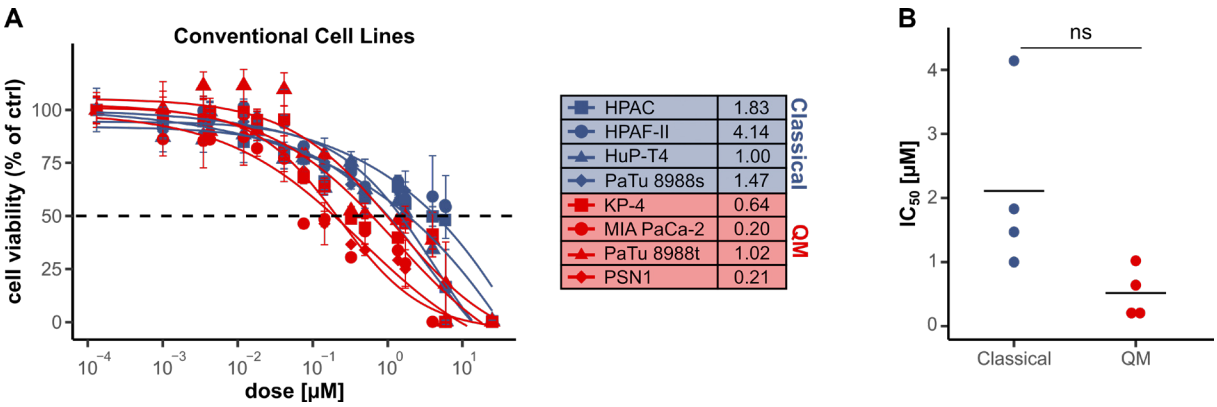

Figure 3-11 CX-5461 treatment reduces cell viability in PDAC cells

Dose-response analysis for conventional PDAC cell lines treated with CX-5461 (1 nM – 25 µM) for 72 h. **(A)** Dose-response curves and absolute IC_{50} values for conventional cell lines. Cell viability was normalized to untreated control cells and is presented as mean ± SD of three independent experiments. **(B)** Dot plots for the absolute IC_{50} values of conventional cell lines grouped by the molecular subtype. ns not significant.

Furthermore, siRNA-mediated knockdown of *POLR1A* (RPA194) was performed for classical HPAF-II and QM PSN1 cells, aiming to inhibit the activity of RNA Pol I by targeting its catalytic subunit. Initially, knockdown efficiency was validated by qPCR and western blot analysis, revealing a downregulation of the relative *POLR1A* mRNA level as well as a decreased RPA194 protein abundance in both cell lines (Figure 3-12 A and B). Notably, the knockdown efficiency was higher in PSN1 compared to HPAF-II cells, potentially because the epithelial-like character of HPAF-II cells and the resulting formation of cell clusters impede the uptake of transfection complexes. HPAF-II cells showed an unexpected fluctuation in the expression of 45S rRNA (5'ETS and ITS1 region) upon *POLR1A* knockdown (Figure 3-12 C), suggesting that the detected downregulation of RPA194 is not sufficient to effectively decrease RNA Pol I activity in this cell line. In PSN1 cells, only treatment with siRNA#1 but not siRNA#2 resulted in a significant downregulation of 45S rRNA (Figure 3-12 C), although the knockdown efficiency was comparable as shown at the level of mRNA and protein (Figure 3-12 A and B).

Additionally, the effect of *POLR1A* knockdown on cell viability was analyzed by comparing the cell confluency of siRNA-transfected and respective control cells. Neither for HPAF-II nor PSN1 cells, cell confluency considerably decreased upon knockdown of *POLR1A* (Figure 3-12 D and E). Taken together, these findings implicate that the pharmacologic inhibition of the rDNA transcription process, but not the partial knockdown of the RNA Pol I catalytic subunit can effectively hamper the synthesis of 45S pre-rRNA in the tested PDAC cells.

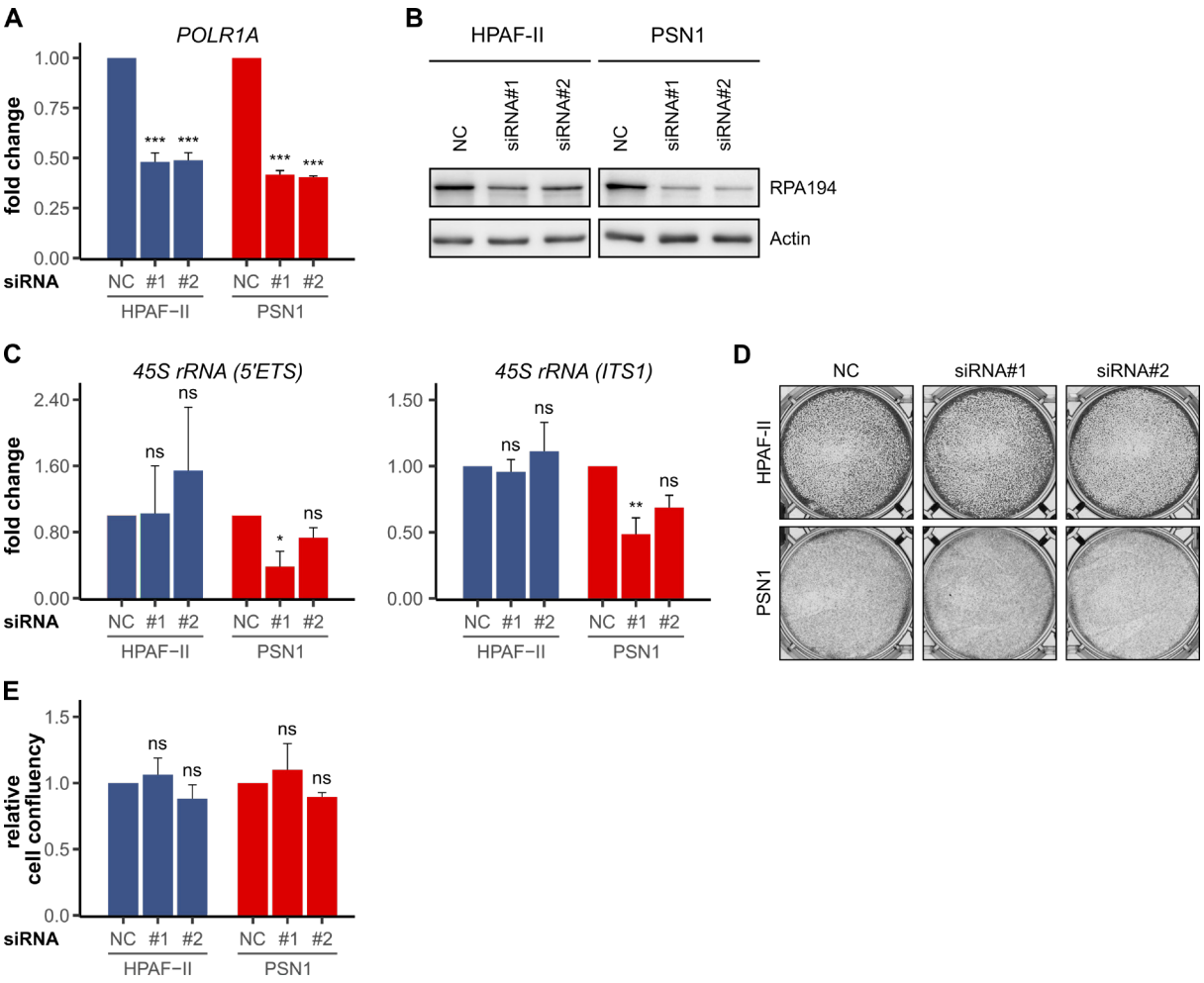

Figure 3-12 Knockdown of POLR1A partially inhibits RNA polymerase I activity

Analysis of HPAF-II and PSN1 cells transfected with 10 nM siRNA against *POLR1A* (RPA194) or negative control (NC) siRNA, cultivated for 72 h after transfection. **(A, B)** Validation of an effective knockdown via qPCR and western blot. **(A)** qPCR for *POLR1A*. Expression levels are presented as fold change data normalized to *GUSB* and relative to control cells as mean + SD of three independent experiments. **(B)** Western blot for RPA194. Exemplary images of one representative experiment (n = 2). **(C)** qPCR analysis for the expression of 45S rRNA (5'ETS and ITS1). Expression levels are presented as fold change data normalized to *GUSB* and relative to control cells as mean + SD of three independent experiments. **(D, E)** Crystal violet staining of HPAF-II and PSN1 cells 72 h after transfection. **(D)** Exemplary images of one representative experiment (n = 3). **(E)** Cell confluency of crystal violet-stained cells is presented relative to control cells as mean + SD of three independent experiments. ns not significant, * $p < 0.05$, ** $p < 0.01$, *** $p < 0.001$.

3.2.2 BMH-21 causes 45S rRNA downregulation and nucleolar disruption

The effect of BMH-21 on the RNA Pol I activity of PDAC cells was evaluated by analyzing changes in the 45S rRNA (5'ETS and ITS1) expression via qPCR for HPAF-II and PSN1 cells. HPAF-II cells were chosen as a representative of the classical PDAC subtype with comparatively lower RiBi activity and a scattered nucleolar pattern, while PSN1 cells represent the QM subtype with higher RiBi activity and a compact nucleolar morphology (Figure 3-4 – Figure 3-6). Notably, due to the observed differences in the sensitivity toward BMH-21, treatment concentrations for subsequent

experiments were defined based on the cell line-specific IC_{50}. Independent of the cells' basal RNA Pol I activity or the nucleolar organization, treatment with BMH-21 at sub-IC_{50} concentrations induced a strong dose-dependent decrease in the expression of 45S rRNA (5'ETS) in both cell lines (Figure 3-13 A). Similarly, HPAF-II cells exposed to defined doses of BMH-21 for different time periods showed progressive reduction of 45S rRNA (ITS1) expression with increasing treatment dose and -duration (Figure 3-13 B). Thus, BMH-21 treatment results in a dose- and time-dependent inhibition of RNA Pol I activity in PDAC cell lines.

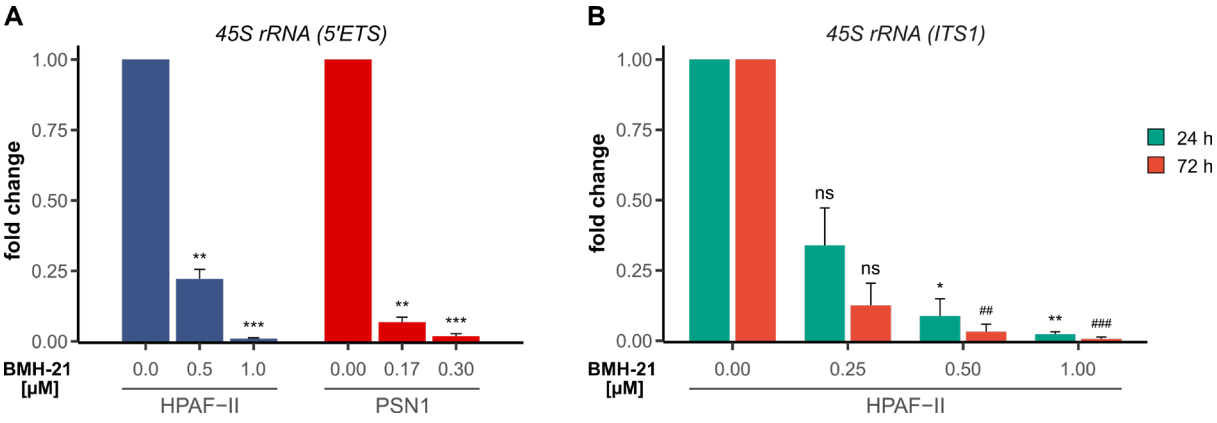

Figure 3-13 BMH-21 inhibits rDNA transcription in a time- and dose-dependent manner

qPCR analysis for 45S rRNA in HPAF-II and PSN1 cells. *GUSB* was used as the housekeeper gene for normalization. **(A)** 5'ETS expression in HPAF-II and PSN1 cells after treatment with BMH-21 at indicated concentrations for 48 h. Fold change + SD of three independent experiments. ** $p < 0.01$, *** $p < 0.001$. **(B)** ITS1 expression in HPAF-II cells after treatment with 0.25 – 1 µM BMH-21 for 24 or 72 h. Fold change + SD of two independent experiments. * $p < 0.05$ and ** $p < 0.01$ for comparison to control cells (24 h). ## $p < 0.01$ and ### $p < 0.001$ for comparison to control cells (72 h).

Furthermore, RNA sequencing was performed for HPAF-II cells treated with 0.5 µM BMH-21 for 72 h and respective control cells. GSEA comparing treated vs. control samples revealed that RNA Pol I inhibition leads to significant downregulation of various gene sets associated with RiBi sub-processes, including rRNA transcription and -processing as well as biogenesis of ribosomal subunits (Figure 3-14 A and B and Annexed Table 3). In particular, transcriptional downregulation of multiple RPs was observed upon treatment (Figure 3-14 C). Additionally, BMH-21 also reduced the expression of translation-associated gene sets (e.g., tRNA processing and translation initiation) as well as target genes of MYC (Figure 3-14 A and B and Annexed Table 3), which acts as a central node in the regulation of RiBi and translation. Together, this suggests a regulatory connection between the level of rRNA synthesis and the transcription of various components involved in the RiBi- and translational machinery, although the exact mechanism of this connection remains to be elucidated.

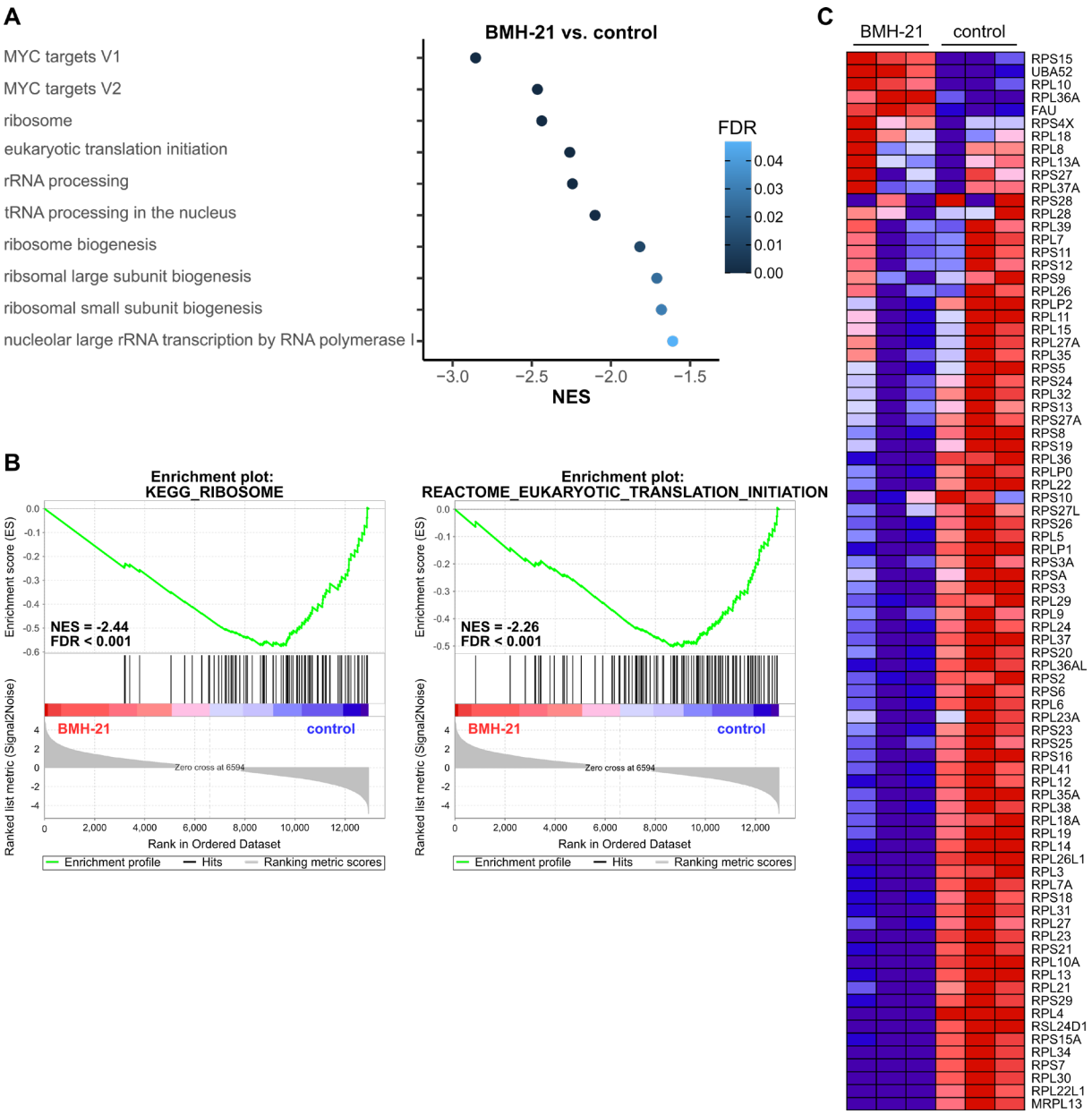

Figure 3-14 BMH-21 treatment results in transcriptional downregulation of ribosome biogenesis- and translation-associated gene sets

Gene set enrichment analysis (GSEA) for HPAF-II cells (BMH-21 vs. control). **(A)** Normalized enrichment scores (NES) and false discovery rates (FDR) are presented for ribosome biogenesis-, translation-, and MYC-associated gene sets significantly downregulated in BMH-21-treated cells. **(B)** Enrichment plot of two exemplary gene sets (KEGG_RIBOSOME, REACTOME_EUKARYOTIC_TRANSLATION_INITIATION) downregulated upon BMH-21 treatment. **(C)** GSEA-derived heatmap for the KEGG_RIBOSOME gene set, displaying a downregulation of several ribosomal proteins in response to BMH-21.

The nucleolus is considered a sensor for various cellular stresses and an impaired rRNA synthesis was previously associated with loss of nucleolar integrity (Boulon et al., 2010). Therefore, the effect of BMH-21 on the nucleolar structure in HPAF-II and PSN1 cells was investigated by evaluating the expression and localization of individual nucleolar marker proteins via IF staining, western blot, and qPCR. For Fibrillarin and

Nucleolin, the overall nuclear intensity and total protein level remained mostly unaltered upon BMH-21 treatment, with only a slight increase in the intensity of Fibrillarin being detected in HPAF-II cells (Figure 3-15 A and B). However, IF staining revealed BMH-21-induced alterations in the protein localization and distribution of both markers, with Fibrillarin accumulating in nuclear spots and Nucleolin translocating into the nucleoplasm (Figure 3-15 A). Staining for RPA194 and UBF-1, on the other hand, showed a significantly reduced nuclear intensity upon treatment, with only isolated nuclear spots remaining after treatment (Figure 3-15 A). This was in line with western blot analysis presenting downregulation of the total protein level for RPA194 and, upon treatment with higher concentrations of BMH-21, also for UBF-1 (Figure 3-15 B). Simultaneously, the relative mRNA levels of *POLR1A* were slightly upregulated in BMH-21-treated HPAF-II cells and nearly unaffected in PSN1 cells (Figure 3-15 C), indicating that the reduced RPA194 protein level was not caused by an impaired transcription but potentially by protein degradation as previously described (Peltonen et al., 2014). For *UBTF*, however, BMH-21 treatment induced a slight decrease in the mRNA level (Figure 3-15 C), suggesting that transcriptional deregulation may be partially responsible for the reduced abundance of UBF-1 protein. Collectively, inhibition of RNA Pol I transcription by BMH-21 caused alterations in the expression and spatial organization of various nucleolar proteins, consequently resulting in the dispersion of the nucleolar structure. This points to a BMH-21-mediated activation of the nucleolar stress response in PDAC cell lines.

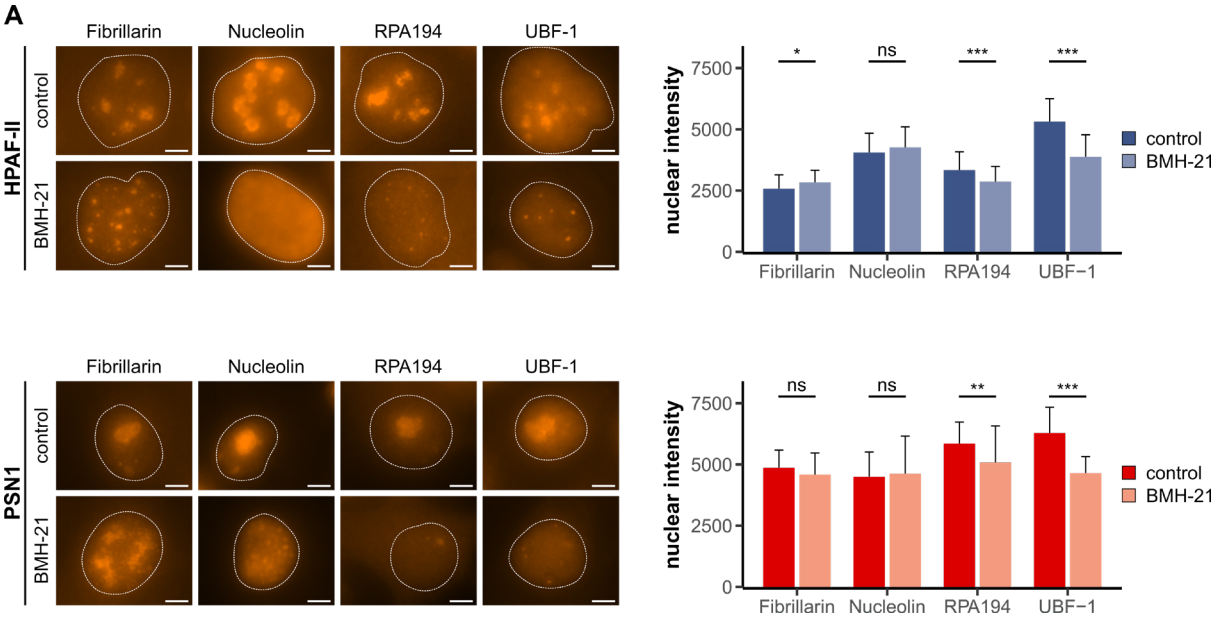

Figure 3-15 Continued

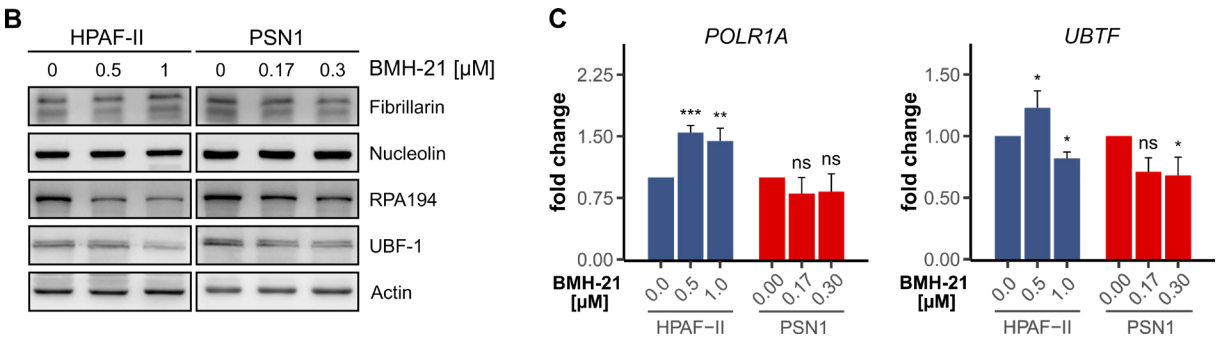

Figure 3-15 Inhibition of RNA polymerase I causes nucleolar disruption

(A) IF for nucleolar markers (Fibrillarin, Nucleolin, RPA194, and UBF-1) in HPAF-II and PSN1 cells incubated with 0.5 µM (HPAF-II) or 0.17 µM (PSN1) BMH-21 for 72 h. Left: Exemplary images of HPAF-II and PSN1 cells with and without BMH-21 treatment. Scale bar = 5 µm. Right: Quantification of the nuclear intensity in treated and control cells. Mean + SD of 50 evaluated cells per condition. **(B, C)** Western blot and qPCR analysis for nucleolar marker expression in HPAF-II and PSN1 cells treated with BMH-21 at indicated concentrations for 48 h. **(B)** Western blot analysis for Fibrillarin, Nucleolin, RPA194, and UBF-1. Exemplary images of one representative experiment (n = 3). **(C)** qPCR analysis for *POLR1A* (RPA194) and *UBTF* (UBF-1). Expression levels are presented as fold change data normalized to *GUSB* and relative to untreated control cells as mean + SD of three independent experiments. ns not significant, * $p < 0.05$, ** $p < 0.01$, *** $p < 0.001$.

3.2.3 BMH-21 treatment induces various stress response pathways

An impaired rRNA synthesis and the resulting nucleolar segregation were shown to cause an activation of various cellular stress response pathways that can interfere with cell proliferation and survival (Boulon et al., 2010). Apoptosis and cell cycle arrest were analyzed as two potential mechanisms contributing to the restriction of cell viability detected in BMH-21-treated PDAC cell lines. Western blot analysis for the cleaved protein forms of caspase 3 and poly-ADP ribose polymerase I (PARP) showed an increased abundance of both markers in response to BMH-21 (Figure 3-16 A), indicative of a treatment-mediated induction of apoptotic cell death. Notably, the observed upregulation of apoptotic markers was more pronounced in PSN1 compared to HPAF-II cells (Figure 3-16 A).

Furthermore, RNA sequencing data of BMH-21-treated HPAF-II cells and respective control cells pointed to a correlation between an impaired RNA Pol I activity and alterations in cell cycle regulation. STRING analysis for the top 150 genes significantly downregulated upon treatment revealed a considerable involvement of respective genes in the regulation of cell cycle progression (Figure 3-16 B and Annexed Table 4). Concomitantly, GSEA unveiled a BMH-21-induced downregulation of gene sets associated with various processes involved in cell cycle regulation, including the E2F pathway, cell cycle phase transition, and checkpoint signaling (Figure 3-16 C and Annexed Table 3).

To functionally validate the effect of RNA Pol I inhibition on cell cycle progression, flow cytometric analysis of propidium iodide-stained cells was performed. For HPAF-II and PSN1 cells, significant changes in the cell cycle phase distribution were detected in response to BMH-21. In particular, the proportion of cells in the G2/M phase was markedly increased in treated cells, with a stronger treatment effect being present in PSN1 cells (Figure 3-16 D). Taken together, these findings identified apoptotic cell death and cell cycle deregulation, specifically G2/M arrest, as two mechanisms contributing to the decrease in cell viability observed upon RNA Pol I inhibition.

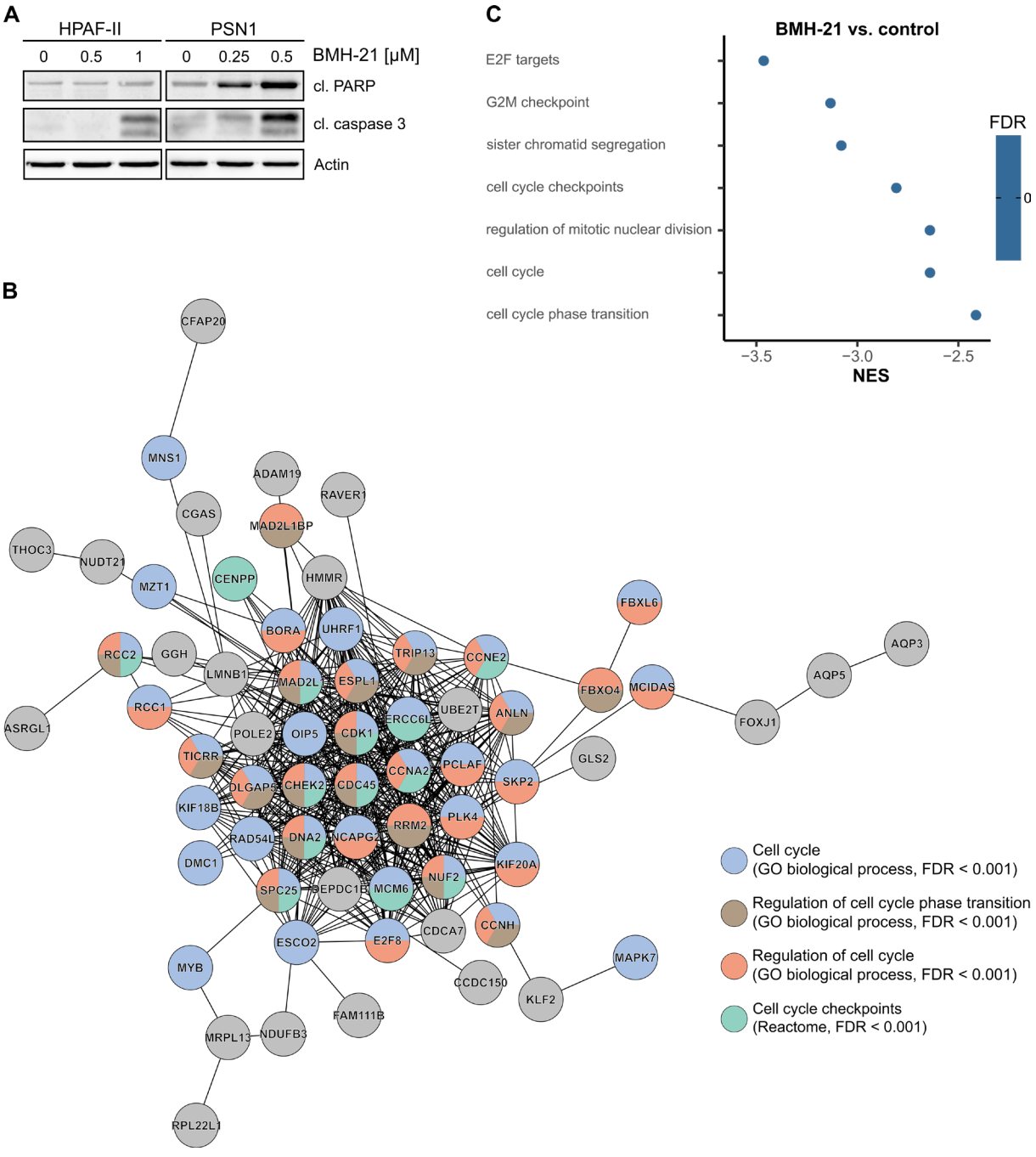

Figure 3-16 Continued

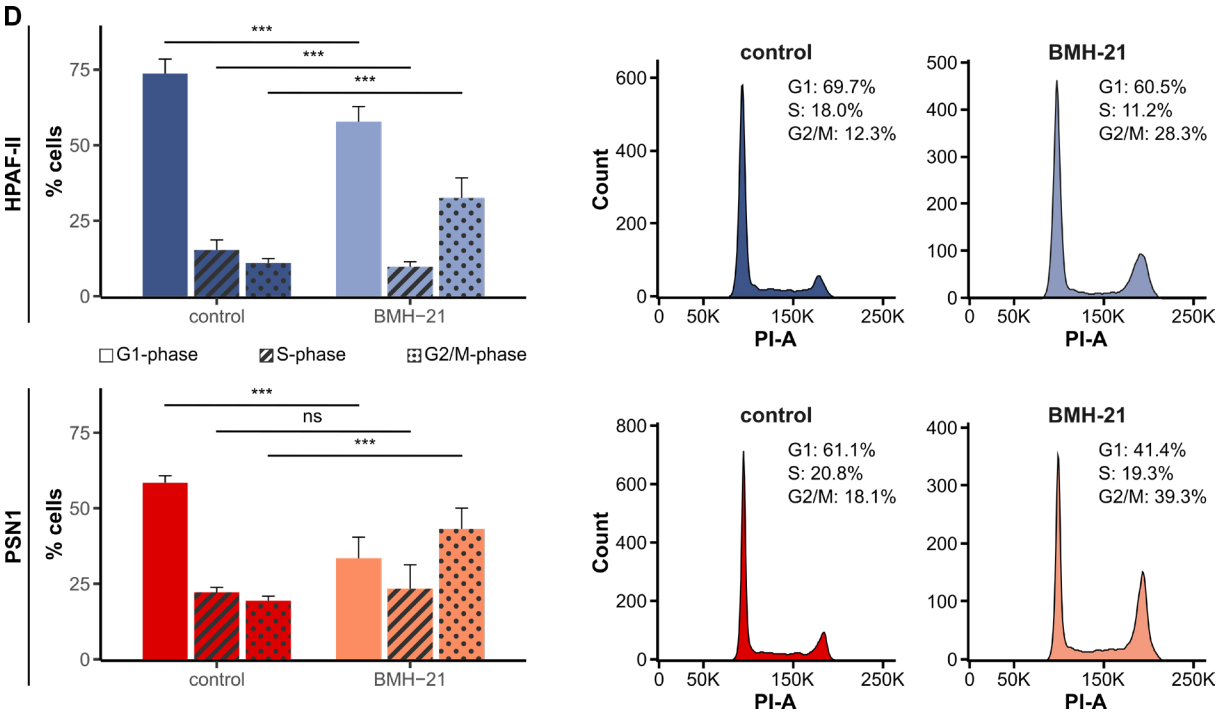

Figure 3-16 BMH-21 treatment leads to induction of apoptotic cell death and cell cycle arrest

(A) Western blot analysis for the apoptotic markers cleaved caspase-3 and cleaved PARP in HPAF-II and PSN1 cells treated with indicated concentrations of BMH-21 for 48 h. Exemplary images of one representative experiment (n = 2). **(B)** STRING analysis for the top 150 genes, downregulated in BMH-21-treated HPAF-II cells, showed a strong association with cell cycle regulation. **(C)** Gene set enrichment analysis of HPAF-II cells (BMH-21 vs. control). Normalized enrichment scores (NES) and false discovery rates (FDR) are presented for cell cycle-related gene sets downregulated in BMH-21-treated cells. **(D)** Flow cytometric analysis of propidium iodide-stained HPAF-II and PSN1 cells after treatment with 0.5 µM (HPAF-II) or 0.17 µM (PSN1) BMH-21 for 72 h. Left: Bar plots showing the percentage of cells in the respective cell cycle phases. Mean + SD of three independent experiments. Right: Exemplary histograms of one representative experiment (n = 3). ns not significant, *** $p < 0.001$.

In addition to its role in apoptosis and cell cycle arrest, nucleolar stress is further associated with the induction of autophagy (Pfister, 2019). Therefore, it was assessed whether BMH-21 treatment promotes autophagy in PDAC cell lines. To evaluate changes in autophagosome formation and the autophagic flux, LC3B I-to-LC3B II conversion and p62 levels were analyzed by western blot for classical HuP-T4 cells (scattered nucleolus) and QM PSN1 cells (compact nucleolus). Both cell lines showed a BMH-21-mediated increase in the LC3B II level as well as further LC3B II accumulation upon treatment with the lysosomal inhibitor Bafilomycin A1 (Figure 3-17 A), pointing to an upregulation of autophagosome formation in response to RNA Pol I inhibition. Additionally, BMH-21 treatment led to a downregulation of the autophagosome cargo receptor p62 in PSN1 cells, which was rescued by Bafilomycin A1 (Figure 3-17 A). These observations suggest that BMH-21 causes an

increase in the autophagic flux, although the downregulation of p62 was not detectable in HuP-T4 cells (Figure 3-17 A).

Treatment-induced alterations in autophagosome formation were further analyzed using a GFP-LC3 reporter assay. The assay allows following the autophagy-associated recruitment of LC3B to autophagosomal membranes, indicated by the appearance of GFP-LC3 puncta. HuP-T4 and PSN1 cells, expressing a GFP-LC3 reporter protein, were cultivated with or without BMH-21 and the number of GFP-LC3 puncta per cell was quantified. HuP-T4 cells showed a BMH-21-mediated increase in the number of GFP-LC3 puncta per cell that was further enhanced by Bafilomycin A1 (Figure 3-17 B), again indicating that RiBi inhibition causes an upregulation of autophagosome formation. In PSN1 cells, however, the number of GFP-LC3 puncta did not change upon treatment (Figure 3-17 B), although a substantial increase in the LC3B II levels, indicative of autophagosome formation, was observed in response to BMH-21 (Figure 3-17 A). Furthermore, a luminescent HiBiT-LC3 reporter assay was performed to quantify changes in the total LC3 levels as a parameter for lysosomal degradation and the autophagic flux. Both HuP-T4 and PSN1 cells showed a decrease in the luminescent signal in response to BMH-21, comparable to the signal reduction triggered by the mTOR-inhibitor Torin 1, a well-known autophagy inducer (Figure 3-17 C). This demonstrates that the treatment with BMH-21 causes an upregulation of lysosomal LC3 degradation and consequently an increase in the autophagic flux. Collectively, the results of all three performed assays support the idea that RNA Pol I inhibition promotes autophagy induction in PDAC cells.

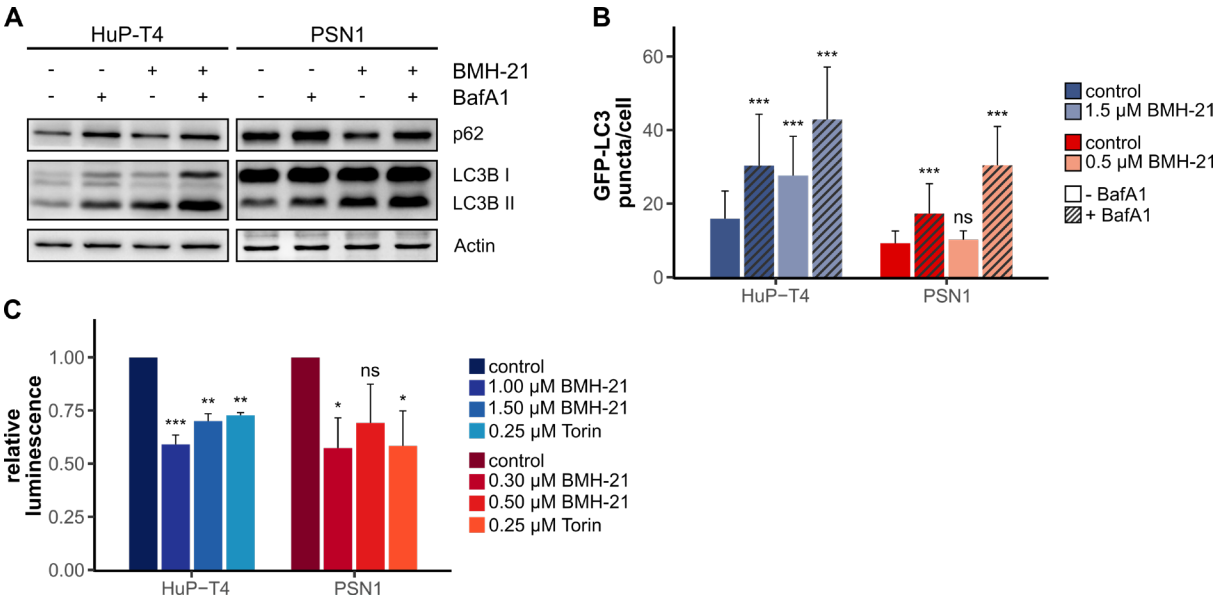

Figure 3-17 Continued

Figure 3-17 Ribosome biogenesis inhibition causes autophagy induction in PDAC cells

(A) Western blot analysis for the autophagy marker p62 and LC3B in HuP-T4 and PSN1 cells treated with 1.5 µM (HuP-T4) or 0.5 µM (PSN1) BMH-21 for 48 h. The autophagy inhibitor Bafilomycin A1 (BafA1) was applied to the medium 6 h before harvesting. Exemplary images of one representative experiment (n = 3). **(B)** GFP-LC3 assay for quantitative analysis of autophagosome formation. Number of GFP-LC3 puncta in HuP-T4 and PSN1 cells after 48 h treatment with BMH-21 at indicated concentrations presented as mean + SD of 25-50 evaluated cells per condition. Data are representative of three independent experiments. **(C)** LC3 HiBiT reporter assay for HuP-T4 and PSN1 cells incubated with BMH-21 at indicated concentrations for 48 h. The intensity of the luminescence signal was normalized to untreated control cells. Mean + SD of two (HuP-T4) or three (PSN1) independent experiments. ns not significant, * $p < 0.05$, ** $p < 0.01$, *** $p < 0.001$. The GFP-LC3 assay and the LC3 HiBiT reporter assay were kindly conducted by Silvia Vega-Rubín-de-Celis and Matthias Kudla.

Nevertheless, it is still insufficiently understood whether the induction of autophagy in response to RNA Pol I inhibition has a positive or negative effect on cell viability (Pfister, 2019). To further investigate the functional role of autophagy in the response of PDAC cells toward BMH-21, the viability of BMH-21-treated HuP-T4 and PSN1 cells was evaluated in the presence and absence of the phosphoinositide 3-kinase (PI3K) inhibitor 3-Methyladenine (3-MA). Inhibition of PI3K via 3-MA hinders autophagy by blocking the class III PI3K complex activity that is essential for autophagosome formation (Petiot et al., 2000). In both cell lines, treatment with BMH-21 in combination with 3-MA resulted in a moderate reduction (up to 10%) of the fraction affected, compared to treatment with respective concentrations of BMH-21 alone (Figure 3-18). Consequently, a global antagonistic relation between the compounds was detected in HuP-T4 cells (synergy score: -15.22) as well as in PSN1 cells (synergy score: -16.32) (Figure 3-18). Thus, 3-MA-mediated inhibition of autophagy partially reduced the inhibitory effect of BMH-21 on cell survival, suggesting that autophagy induction triggers a pro-death effect upon impaired RNA Pol I activity in PDAC.

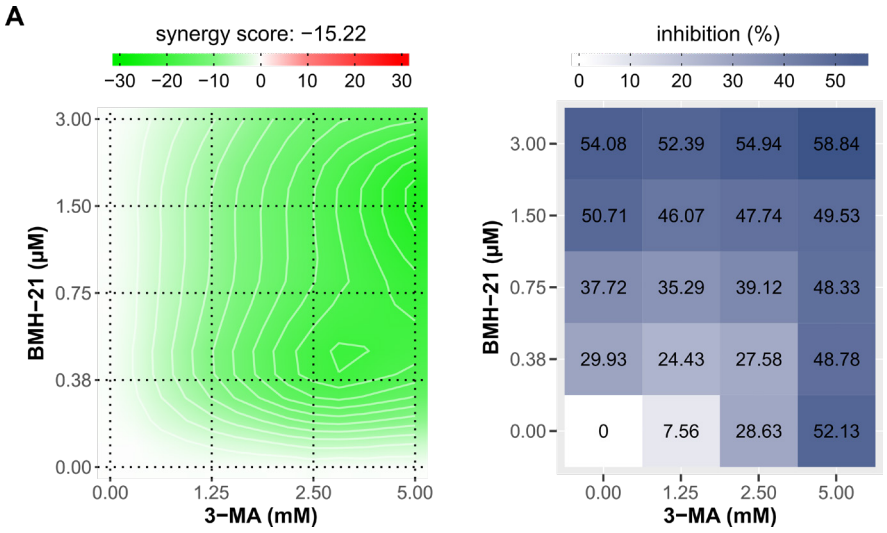

Figure 3-18 Continued

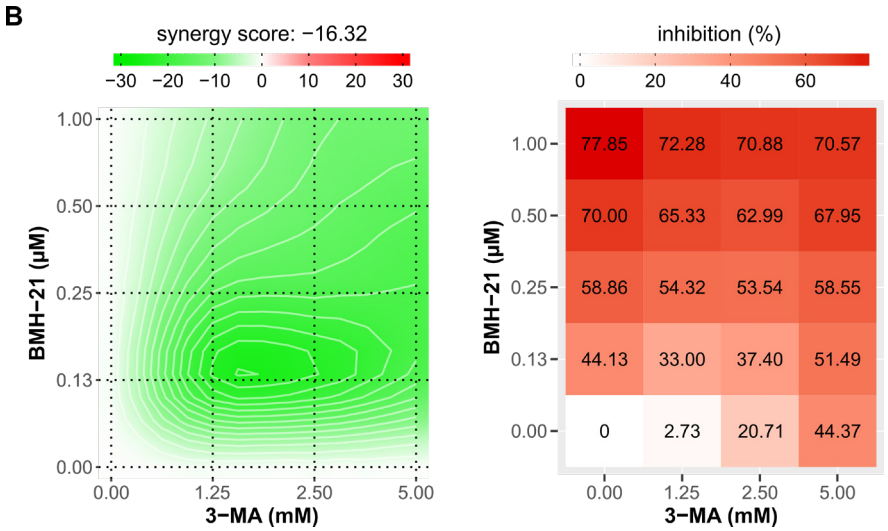

Figure 3-18 BMH-21-induced autophagy has a pro-death effect

Multi-drug analysis for classical HuP-T4 **(A)** and QM PSN1 **(B)** cells treated with BMH-21 and 3-MA at the indicated concentrations for 72 h. The status of drug interaction was analyzed using the SynergyFinder web application (version 3.0, synergyfinder.fimm.fi) with the Bliss/Loewe consensus synergy scoring method. Synergy score (2D synergy plot) and fraction affected (heat map) are shown for one representative experiment (n = 3). Synergy score: < -10 = antagonism, -10 to 10 = additive effect, > 10 = synergism.

3.3 Functional consequences of targeting ribosome biogenesis

3.3.1 BMH-21 treatment influences the phenotypic state of PDAC cells

Prior studies identified an upregulation of rRNA synthesis during EMT in breast cancer and demonstrated that inhibition of RiBi can reverse or overcome various cancer-promoting effects of EMT, including cancer cell de-differentiation, metastasis, and chemoresistance (Prakash et al., 2019; Ban et al., 2023).

Intriguingly, GSEA for HPAF-II cells showed significant enrichment of the HALLMARK “EMT” gene set in BMH-21-treated cells compared to control cells (Figure 3-19 A). This was further validated by analyzing the expression of the mesenchymal marker Vimentin (*VIM*), the EMT-associated transcription factor zinc finger E-box-binding homeobox 1 (*ZEB1*), and the epithelial marker E-cadherin (*CDH1*) via qPCR and/or western blot. For HPAF-II cells, a dose-dependent increase in the mRNA level was observed for both *VIM* and *ZEB1* (Figure 3-19 B), further supporting the idea that BMH-21 treatment induces a transcriptional EMT program in this cell line. PSN1 cells, on the other hand, did not show any significant change in the expression of *VIM* or *ZEB1* (Figure 3-19 B), potentially because this cell line already presents a mesenchymal-like phenotype along with comparatively high basal expression levels of EMT transcription factors and mesenchymal markers. Interestingly, both cell lines also showed a slightly increased mRNA expression of the epithelial marker gene *CDH1*,

especially at higher doses of BMH-21 (Figure 3-19 B). Correlating with the observed changes in gene expression, western blot analysis revealed a dose-dependent increase in the abundance of Vimentin in HPAF-II but not in PSN1 cells. The protein level of E-cadherin, however, was nearly unaffected in both cell lines upon BMH-21 treatment (Figure 3-19 C).

Alterations in the phenotypic cell state were further reflected in the cellular morphology. Under basal conditions, classical HPAF-II cells are characterized by an epithelial-like phenotype with close cell-cell interactions and the formation of island-like structures. Treatment with BMH-21 initially resulted in a less tightly packed cellular organization and, at higher treatment concentrations, in the formation of cell protrusions (Figure 3-19 D). Although for QM PSN1 cells no increase in the EMT marker expression was detectable, RNA Pol I inhibition enhanced the more spindle-like cellular morphology (Figure 3-19 D). Collectively, the findings indicate that RNA Pol I inhibition influences the phenotypic plasticity of PDAC cells and, especially in classical HPAF-II cells, causes a shift toward a more mesenchymal cell state.

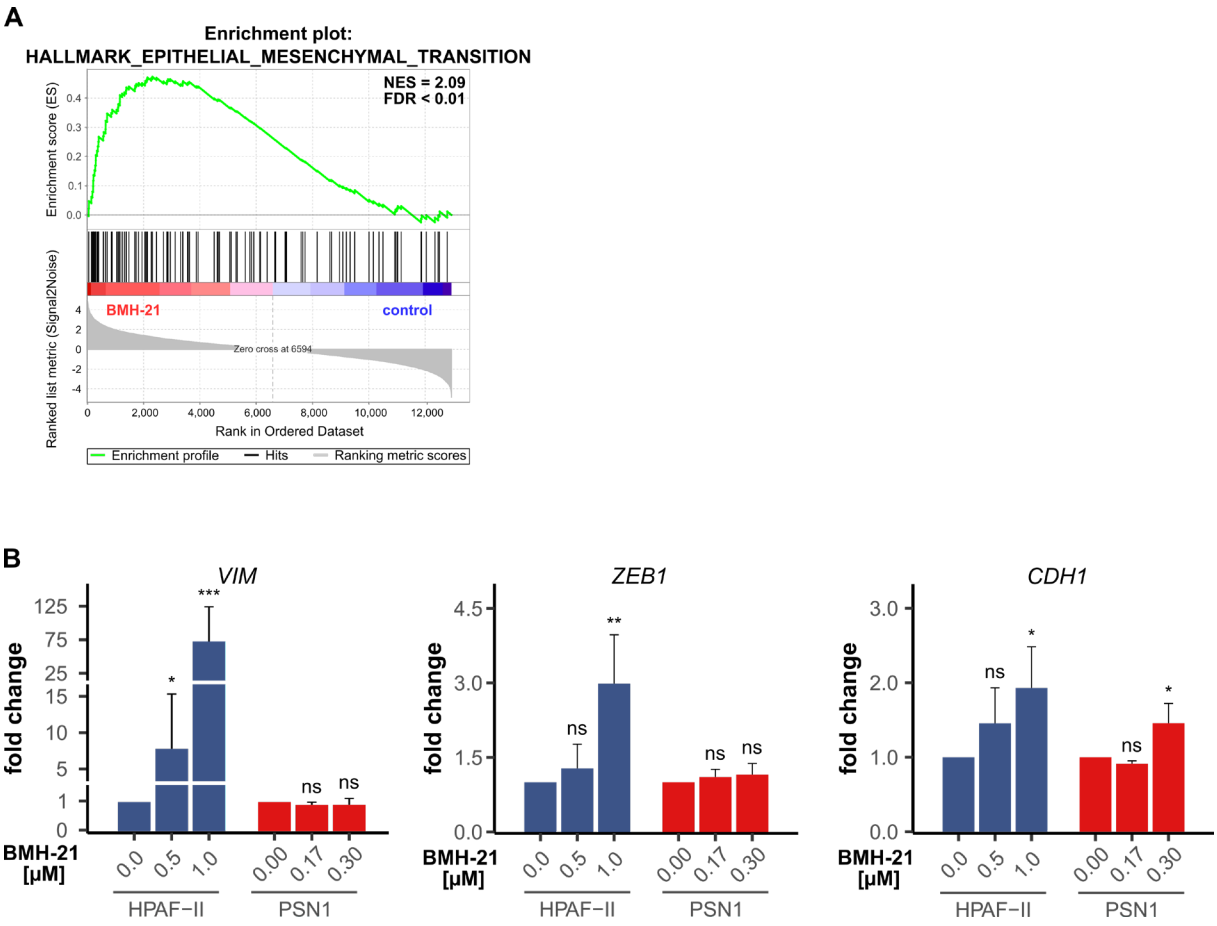

Figure 3-19 Continued

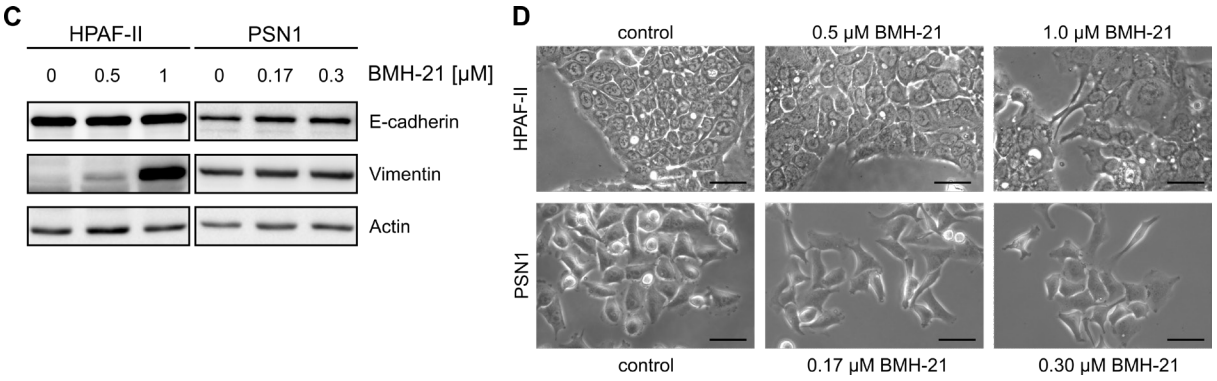

Figure 3-19 BMH-21 treatment leads to an upregulation of EMT-associated markers

(A) Gene set enrichment analysis of HPAF-II cells (BMH-21 vs. control). Enrichment plot of the HALLMARK_EPITHELIAL_MESENCHYMAL_TRANSITION gene set significantly enriched in BMH-21-treated HPAF-II cells. **(B, C)** qPCR and western blot analysis for markers of epithelial-mesenchymal transition in HPAF-II and PSN1 cells treated with BMH-21 at indicated concentrations for 48 h. **(B)** qPCR analysis for *VIM* (Vimentin), *ZEB1* (Zinc finger e-box binding homeobox 1), and *CDH1* (E-cadherin). Expression levels are presented as fold change data normalized to *GUSB* and relative to untreated control cells as mean + SD of three independent experiments. ns not significant, * $p < 0.05$, ** $p < 0.01$, *** $p < 0.001$. **(C)** Western blot analysis for Vimentin and E-cadherin. Exemplary images of one representative experiment (n = 3). **(D)** Bright-field images of HPAF-II and PSN1 cells treated with BMH-21 at indicated concentrations for 48 h.

3.3.2 Ribosome biogenesis is closely linked to mTORC1 signaling

The PI3K-AKT-mTOR pathway is one of the most important signaling networks in PDAC and strongly links RiBi and protein synthesis (Gentilella et al., 2015). Addressing this interconnection by combining RiBi- and translation-targeting approaches was previously shown to improve the treatment effect in Myc-driven B-cell lymphoma (Devlin et al., 2016; Kusnadi et al., 2020).

The influence of RNA Pol I inhibition on mTORC1 signaling was assessed by determining the phosphorylation status of RP S6 kinase 1 (p70-S6K) and protein initiation factor 4E-binding protein 1 (4E-BP1), two main downstream targets of mTORC1. In both HPAF-II and PSN1 cells, an increase in the phosphorylation of the two substrates was observed in response to BMH-21 (Figure 3-20 A), pointing to a treatment-induced upregulation of mTORC1 activity. Based on these results, it can be hypothesized that an elevated mTORC1 signaling may function as a compensatory mechanism in response to RNA Pol I inhibition in PDAC cells. Therefore, the interplay between BMH-21 and the mTORC1 inhibitor Rapamycin was addressed in a combinational treatment. While in HPAF-II cells, the combination of BMH-21 and Rapamycin resulted in a slight additive effect (synergy score: -8.99), an antagonistic relation between the two compounds was observed in PSN1 cells (synergy score: -12.15) (Figure 3-20 B). Particularly, the inhibitory effect of BMH-21 on cell

viability of PSN1 cells was moderately reduced in the presence of Rapamycin (Figure 3-20 B), suggesting that inhibition of mTORC1 limits the cellular sensitivity toward RNA Pol I inhibition via BMH-21 in this cell line.

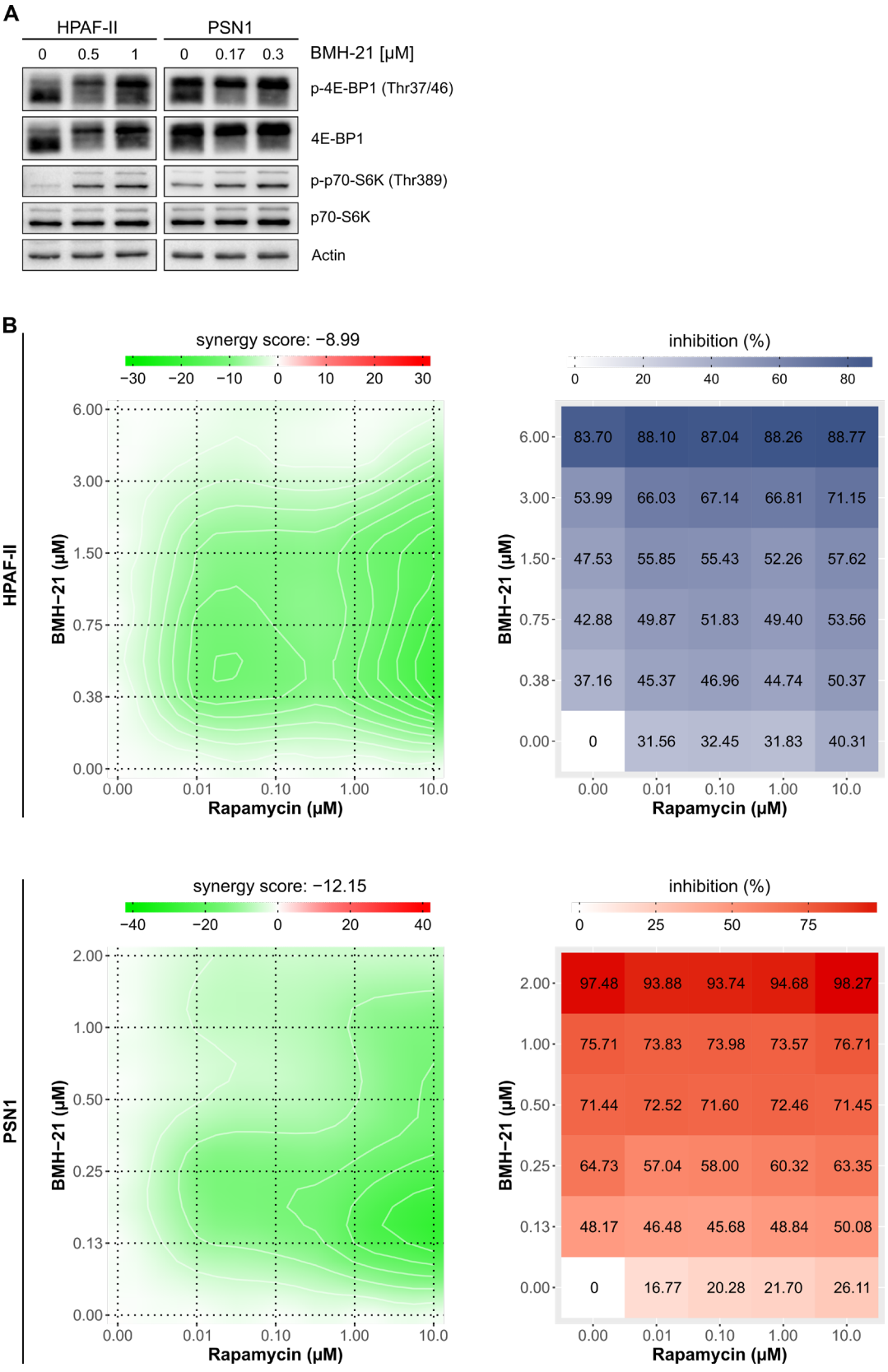

Figure 3-20 Continued

Figure 3-20 RNA Pol I inhibition causes deregulation of mTORC1 activity

(A) Western blot for the mTORC1 downstream targets (phospho-)4E-BP1 and (phospho-)p70-S6K in HPAF-II and PSN1 cells treated with BMH-21 at indicated concentrations for 48 h. **(B)** Multi-drug analysis for HPAF-II and PSN1 cells treated with BMH-21 and Rapamycin at the indicated concentrations for 72 h. The status of drug interaction was analyzed using the SynergyFinder web application (version 3.0, synergyfinder.fimm.fi) with the Bliss/Loewe consensus synergy scoring method. The synergy score (2D synergy plot) and fraction affected (heat map) are shown for one representative experiment (n = 3). Synergy score: < -10 = antagonism, -10 to 10 = additive effect, > 10 = synergism.

3.3.3 PDAC cells show metabolic reprogramming in response to BMH-21

The correlation between the PI3K-AKT-mTOR axis, RiBi, and translation further plays a pivotal role in the regulation of cellular energy metabolism. Previous studies demonstrated that translational- and metabolic rewiring, including upregulation of oxidative phosphorylation (OxPhos) and glycolysis, are key players in the cellular response and the development of treatment resistance upon RiBi-targeting therapies (Kusnadi et al., 2020).

GSEA for HPAF-II cells revealed a BMH-21-mediated transcriptional downregulation of various metabolic pathways (Figure 3-21 and Annexed Table 3), suggesting that PDAC cells undergo metabolic reprogramming in response to an impaired RiBi. Affected were, among others, glycolysis and OxPhos as the two major energy-providing pathways of the cell, as well as interconnected metabolic pathways such as the tricarboxylic acid (TCA) cycle, fatty acid oxidation, and the pentose phosphate pathway (Figure 3-21).

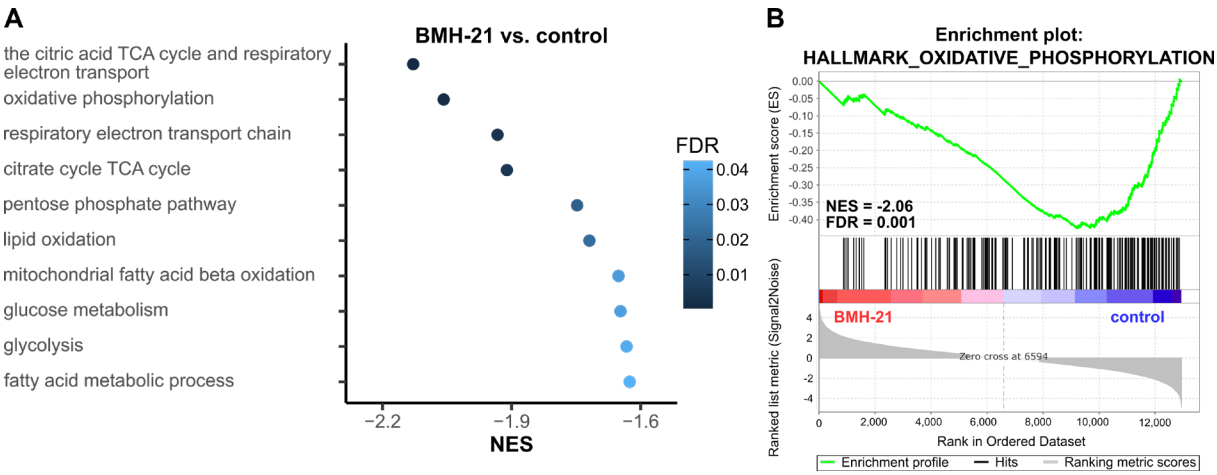

Figure 3-21 RNA Pol I inhibition leads to transcriptional downregulation of metabolic pathways

Gene set enrichment analysis of HPAF-II cells (BMH-21 vs. control). **(A)** Normalized enrichment scores (NES) and false discovery rates (FDR) are presented for a selection of metabolic pathways downregulated in BMH-21-treated cells. **(B)** Enrichment plot of one exemplary gene set (HALLMARK_OXIDATIVE_PHOSPHORYLATION) found to be significantly downregulated in response to BMH-21.

However, since the transcriptional profile does not always reflect the effective metabolic behavior, the influence of RNA Pol I inhibition on metabolic processes was also functionally investigated via seahorse metabolic flux analysis. By measuring the oxygen partial pressure and the pH of the medium in direct proximity to the cell layer, this method determines the oxygen consumption rate (OCR) and extracellular acidification rate (ECAR) as surrogate parameters for OxPhos and glycolysis, respectively. BMH-21 induced a substantial decrease in the ECAR for both HPAF-II and PSN1 cells (Figure 3-22 A), suggesting that, in accordance with the observed transcriptional alterations, glycolysis is functionally downregulated in response to treatment. The OCR was however upregulated in BMH-21-treated HPAF-II cells, resulting in a markedly increased OCR/ECAR ratio (Figure 3-22 A and B) which points to an enhanced metabolic dependency on OxPhos upon RNA Pol I inhibition. Similarly, a BMH-21-mediated increase in the OCR/ECAR ratio was detected for PSN1 cells, even though the OCR was slightly reduced upon treatment in this cell line (Figure 3-22 A and B).

In addition, the effect of RNA Pol I inhibition on the TCA cycle was evaluated by determining the activity of isocitrate dehydrogenase 3 (IDH3) for BMH-21-treated and respective control cells. IDH3 catalyzes the NAD^+-dependent oxidative decarboxylation of isocitrate into α-ketoglutarate, a rate-limiting step during the TCA cycle. However, BMH-21 did not significantly affect the IDH3 activity in HPAF-II or PSN1 cells (Figure 3-22 C). Thus, despite a transcriptional downregulation of various metabolic pathways in response to BMH-21 treatment, a considerable functional reduction was only observed for glycolysis, while the functionality of OxPhos and the TCA cycle appeared to be largely retained.

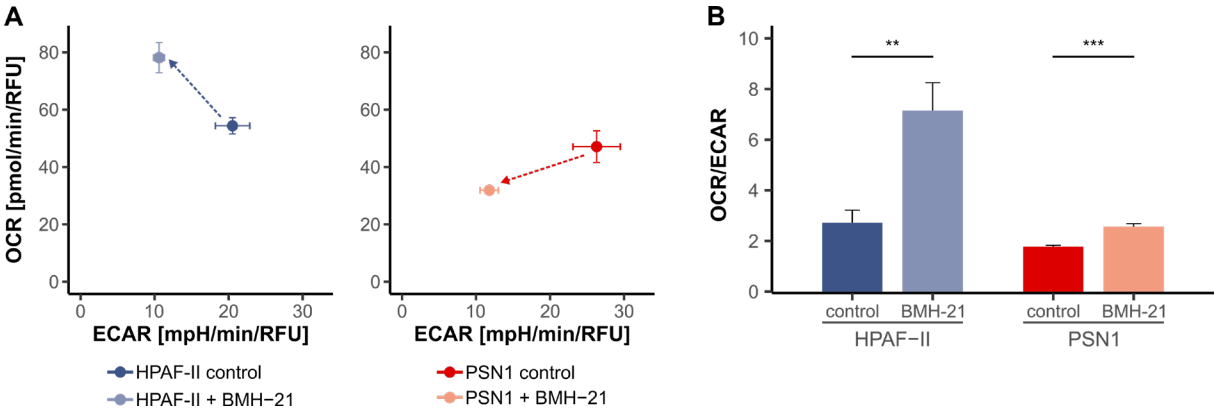

Figure 3-22 Continued

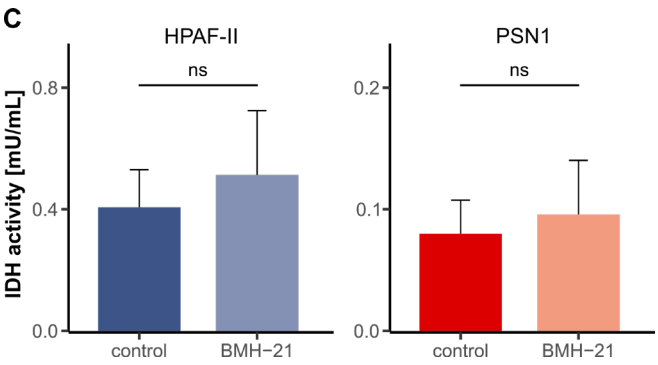

Figure 3-22 BMH-21 treatment causes alterations in cellular energy metabolism

(A, B) Seahorse metabolic flux analysis of HPAF-II and PSN1 cells after treatment with 0.5 µM (HPAF-II) or 0.17 µM (PSN1) BMH-21 for 72 h. **(A)** Energy maps for one representative experiment (n = 3). Extracellular acidification rates (ECAR) and oxygen consumption rates (OCR) were normalized to the DNA content determined by DAPI staining (scale factor: 10,000). Data represented as mean ± SD of five technical replicates. **(B)** OCR/ECAR ratios of BMH-21 treated and control cells. Data represented as mean + SD of three independent experiments. **(C)** Isocitrate dehydrogenase (IDH) 3 activity in HPAF-II and PSN1 cells after treatment with 0.5 µM (HPAF-II) or 0.17 µM (PSN1) BMH-21 for 72 h. Data represented as mean + SD of three independent experiments. ns not significant, ** $p < 0.01$, *** $p < 0.001$. RFU relative fluorescent unit.

4 Discussion

4.1 Ribosome Biogenesis is heterogeneous among PDAC models

RiBi is a tightly regulated process that requires the coordinated expression and interplay of different structural components (i.e., RPs, rRNAs) and several hundred RBFs (Dörner et al., 2023; Hurt et al., 2023). In a variety of cancer entities (e.g., cholangiocarcinoma, colon adenocarcinoma, and kidney renal clear cell carcinoma), the average expression of RPs and emerging paralogs was shown to be upregulated compared to corresponding normal tissue (Guimaraes & Zavolan, 2016). In the present work, analysis of publicly available array data from bulk tissue revealed no significant difference in the averaged expression of RPs between PDAC and normal pancreatic tissue. However, it must be considered that bulk tumor tissue is a heterogeneous collection of different cell types, including cancer cells, immune cells, and fibroblasts. Gene expression data of bulk tissue therefore reflect the contribution of all those individual cell types, making it difficult to obtain information about the role of RiBi specifically in cancer cells. Previous studies on bulk PDAC samples reported a decrease in the protein expression of RPs, as well as substantially lower rates of protein synthesis compared to the normal pancreas (van Dijk et al., 2019; Silwal-Pandit et al., 2022). However, in a different approach, Chan et al. specifically investigated cancer cells instead of bulk tumor tissue and observed that PDAC cells show increased levels of protein synthesis when directly compared to normal pancreatic ductal epithelial cells as the potential cell type-of-origin for PDAC (Chan et al., 2019). These opposed results are probably due to the striking differences in the cellular composition between PDAC and healthy pancreatic tissue that affect the comparative analysis of bulk material. In the normal pancreas, 85% of the organ's mass are acinar cells, which are responsible for the exocrine secretion of digestive enzymes and therefore exhibit high levels of protein synthesis (Case, 1978; van Dijk et al., 2019; Atkinson et al., 2020). On the other hand, acinar cells are rarely present in PDAC bulk tissue, which mainly comprises extracellular matrix, epithelial cancer cells, cancer-associated fibroblasts, and immune cells (Avsar & Pir, 2023). Consequently, when analyzing bulk tissue, differences in the RiBi- and protein synthesis rate between normal ductal epithelial cells and PDAC cells may be masked by the extremely high protein synthesis rates of acinar cells in the normal tissue.

Although the averaged expression of RPs was comparable between PDAC and normal pancreatic tissue samples, the analysis revealed that different groups of RPs exist,

which show comparatively increased (e.g., RPL39L, RPL10L) or reduced (e.g., RPL34, RPL32) expression in PDAC samples, respectively. This was in line with the findings of Guimaraes and Zavolan, who identified three distinct RP clusters that display either consistent upregulation (e.g., RPL36A, RPS2) or downregulation (e.g., RPL34, RPL9) across the tested cancer types, or presented with a rather variable dysregulation pattern (Guimaraes & Zavolan, 2016). Importantly, they also discovered that transcriptional up- or downregulation of individual RPs significantly correlated with the influence of respective RPs on the survival of melanoma cells (Shalem et al., 2014; Guimaraes & Zavolan, 2016). For instance, the knockdown of *RPL21*, which was shown to be downregulated in breast- and uterine cancer, caused a survival benefit in melanoma cells (Shalem et al., 2014; Guimaraes & Zavolan, 2016). These findings indicate that not only the overexpression of RPs and correspondingly increased RiBi activity but also the dysregulation of specific RPs and their partially extra-ribosomal functions may contribute to tumor development (Wool, 1996; Kang et al., 2021). RPL15, for example, is considered to act as a tumor suppressor in PDAC since low expression levels were associated with an increased invasive capacity of PDAC cells and poor overall survival in patient cohorts (Yan et al., 2015).

Furthermore, qualitative alterations in the RiBi- and translational machinery, i.e. changes in the composition or modification of ribosomal components, can lead to the formation of “onco-ribosomes” that drive a pro-oncogenic and growth-promoting translational pattern (Elhamamsy et al., 2022). Such alterations include loss of individual RPs, missense mutations that affect proper RP function, or exchange of RPs by respective paralogs (Pelletier et al., 2018). For instance, the here performed expression analysis of RP-encoding genes in PDAC and normal pancreatic tissue revealed higher expression levels of RPL39L in a subgroup of tumor samples compared to normal pancreatic tissue. RPL39L was originally described as a testis-specific protein but was found to be upregulated in various cancer types, including breast- and lung cancer (Nadano et al., 2002; Wong et al., 2014; Guimaraes & Zavolan, 2016). Recent studies indicate that the exchange of RPL39 by RPL39L in the peptide exit tunnel of the 80S ribosome can cause alterations in the co-translational protein folding, thus, affecting translational fidelity and proteome homeostasis (Gao & Wang, 2023). It should however be kept in mind that in the present work, only the mRNA expression of RPs was analyzed, which may differ from the respective protein levels. In breast cancer, for example, a relatively low correlation between mRNA- and protein

levels has been observed for RPs (Johansson et al., 2019) and it is therefore conceivable that significant differences between the gene expression and protein level of RPs are also present in PDAC. Thus, a comprehensive analysis of RPs at the proteome level is necessary to shed light on whether the heterogeneous dysregulation of RPs has a role in PDAC tumorigenesis.

It is well known that both oncogenes and tumor suppressors play an important role in the regulation of RiBi as they influence the transcription and function of ribosomal components and RBFs (Ruggero & Pandolfi, 2003; Pelletier et al., 2018). Here, analysis of PDAC patient samples revealed that MYC^{high} samples are enriched for the expression of RiBi- and translation-associated gene sets, suggesting that oncogenic deregulation of MYC has an impact on ribosome production in PDAC. MYC is considered one of the most important positive regulators of RiBi as it promotes the activity of all three RNA polymerases (RNA Pol I-III) as well as the translational capacity, resulting in enhanced availability of rRNAs, RPs, and RBFs (van Riggelen et al., 2010; Jiao et al., 2023). Furthermore, MYC supports RiBi by specifically promoting the expression of multiple factors involved in rRNA synthesis and -processing, including Fibrillarin, Nucleolin, Nucleophosmin, UBF-1, and TIF-IA (van Riggelen et al., 2010; Campbell & White, 2014). Deregulation of various RBFs, also resulting from deregulation of oncogenes and tumor suppressors, was observed in different cancer types and is often associated with poor prognosis (Marcel et al., 2013; Tafforeau et al., 2013; Cangelosi et al., 2022). Correspondingly, the here performed analysis of publicly available datasets revealed that high expression levels of Fibrillarin, Nucleolin, Nucleophosmin, and TIF-IA correlated with reduced overall survival of PDAC patients. On the other hand, for UBF-1 and RPA194, high expression levels were intriguingly associated with a better prognosis. It should however be noted that the function of the RiBi apparatus and especially the RNA Pol I machinery is not only regulated at the transcriptional level but also by post-translational modifications. These modifications play an important role in the dynamic adjustment of RiBi in response to alterations in cellular homeostasis or oncogenic signaling (Zhai & Comai, 2000; Stefanovsky et al., 2001; Zhao et al., 2003; Azman et al., 2023).

The sensitivity of cancer cells to RNA Pol I inhibition is thought to partially depend on their rate of RiBi. Thus, given the pronounced heterogeneity of PDAC, it was further addressed whether differences in the molecular subtype are associated with variations in RiBi regulation. The expression of RiBi-associated genes and 45S pre-rRNA, as well

as the nucleolar morphology, were analyzed in conventional PDAC cell lines and PDCs, which were transcriptionally characterized as classical or QM in prior studies (Collisson et al., 2011; Daemen et al., 2015; Heid et al., 2022). In conventional PDAC cell lines, the QM subtype was associated with an enrichment of RiBi-related gene sets and higher expression levels of 45S pre-rRNA, concurrent with faster proliferation rates. An increased rDNA transcription was previously shown to be essential for the induction of EMT, suggesting that RiBi plays an important role in the establishment of the more aggressive mesenchymal cell state and during cancer progression (Prakash et al., 2019). Together, these findings indicated that the level of RiBi may characterize different PDAC cell states in terms of molecular features, proliferative capacity, and aggressiveness.

The level of rRNA synthesis influences the nucleolar appearance, as nascent rRNA molecules are considered to function as a seed for the LLPS-driven nucleoli formation (Derenzini et al., 2009; Lafontaine et al., 2021). Among conventional PDAC cell lines, QM cells with comparatively higher RNA Pol I activity mainly displayed compact macronucleoli, whereas classical cell lines with lower rRNA expression levels presented a rather scattered nucleolar pattern. Thus, the difference in the nucleolar morphology between QM and classical PDAC cell lines is potentially a consequence of differences in the rRNA synthesis level. Importantly, the organization of nucleolar marker proteins was also preserved in orthotopic and subcutaneous xenografts of the respective PDAC cell lines, demonstrating that the subtype-specificity in the nucleolar morphology is maintained in an *in vivo* setting as well. Similar to the observation that PDAC cell lines present with a different nucleolar organization depending on their molecular subtype, Nicolle et al. described a correlation between the nucleolar appearance, the level of differentiation, and the transcriptional profile in PDAC PDXs (Nicolle et al., 2020). Well-differentiated tumors with high expression of classical genes had no histologically visible nucleolus, while poorly differentiated tumors were associated with a basal-like transcriptional profile and more prominent nucleoli (Nicolle et al., 2020). However, it should be noted that these findings are based on histological examination only and not on nucleolus-specific staining methods. Interestingly, results of previous studies suggest that epigenetic modulation of the rDNA chromatin state, which represents one of the two major mechanisms regulating the rRNA synthesis rate, has an impact on the nucleolar organization (Meshorer & Misteli, 2006; Grummt, 2010). In pluripotent embryonic stem cells, characterized by high levels of rRNA synthesis, an

open chromatin state of rDNA loci was linked with the appearance of a single large nucleolus (Meshorer & Misteli, 2006; Savic et al., 2014). On the other hand, differentiated cell states were associated with an increased abundance of repressive histone marks at rDNA regions, decreased levels of rRNA synthesis, and multiple smaller nucleoli that are surrounded by clusters of compact heterochromatin (Meshorer & Misteli, 2006; Savic et al., 2014). Additionally, Prakash et al. discovered that in breast cancer cells, upregulation of RiBi during EMT correlates with NoRC release from rDNA, accompanied by reduced methylation of rDNA promoter regions as well as induction of the activating epigenetic modifications H3K4Me3 and H3K27Ac (Prakash et al., 2019). Thus, epigenetic modulation of the rRNA gene loci may contribute to the observed differences in the rRNA synthesis rate and the nucleolar pattern between QM and classical PDAC cell lines, although validation of this theory requires further investigation.

For primary PDCs, comparable levels of RP expression and 45S rRNA synthesis, as well as similar proliferation rates were observed in almost all tested cell lines. One exception was the cell line PDC3, which had a substantially lower proliferation rate, yet did not differ greatly from the other cell lines regarding the RiBi activity. In brief, subtype-specific differences in RiBi as they were observed in conventional cell lines (i.e., higher levels of RiBi in QM compared to classical cells), were not present in PDCs. It should however be taken into account that, in tumors, the classification into classical and QM follows a gradual pattern. The conventional cell lines used in the present study represent the extremes of the classical or QM subtype and thus show strong expression of the respective molecular characteristics (Daemen et al., 2015). In turn, primary PDCs generally show a less clear manifestation of the classical- and QM-specific characteristics, which is potentially due to polyclonality and the presence of hybrid-state cells in primary cultures. While the conventional cell lines have been in culture for several decades and therefore probably underwent clonal selection, which resulted in rather uniform cell populations, PDCs are in relatively early passages (< 30) and therefore probably still contain different cell clones. This could be, in part, responsible for the lack of subtype-specific differences in RiBi activity in this model system. Moreover, both compact and dispersed nucleoli were present in different cells of one PDC population, supporting the idea that polyclonality exists in the primary cell cultures.

Tumors of CKP mice present as moderately to poorly differentiated and rich in stromal components, thus, representing human PDAC histology relatively well (Bardeesy et al., 2006; Trajkovic-Arsic et al., 2017). In the present work, staining for different nucleolar markers revealed that the tumors are characterized by regional variation in the nucleolar organization throughout the tissue, with both scattered and compact nucleoli being observed. On the one hand, this variation could be attributed to the presence of different cell types (e.g., fibroblasts, immune cells, etc.) in the tumor. Nevertheless, both scattered and compact nucleoli were also detected when only pan-CK-positive cancer cells were considered, suggesting that both nucleolar structure types are present in cancer cells. Such nucleolar heterogeneity among cancer cells was previously described as a common phenomenon in tumor tissue, for example, in breast cancer specimens (Derenzini et al., 2009; Weeks et al., 2021). This heterogeneity reflects differences in the proliferation rate and cell doubling time between cancer cells, two parameters that are strongly linked to the level of RiBi and nucleolar size (Derenzini et al., 2009). Especially in highly dynamic tumor tissues, different factors, such as nutrient and oxygen availability, can influence the RiBi activity of cancer cells and thus their nucleolar appearance (Boulon et al., 2010).

4.2 Ribosome biogenesis inhibition has anticancer effects in PDAC

RNA Pol I-mediated transcription is the first and rate-limiting step of RiBi and its normally strict regulation is lost in cancer cells due to dysregulation of oncogenes and tumor suppressors (Sharifi & Bierhoff, 2018). Therefore, it is considered a promising target to specifically address highly proliferative cancer cells that present with hyperactive RiBi. Non-malignant cells, in turn, are thought to remain largely unaffected by RiBi-targeting approaches as they exhibit lower dependency on ribosome production, potentially due to the relatively long half-life of cytoplasmic ribosomes (Peltonen et al., 2014; Penzo et al., 2019). Multiple small-molecule inhibitors like CX-3543, CX-5461, and BMH-21 have been developed to impede RNA Pol I activity. CX-5461 and CX-3543 were originally described to inhibit rDNA transcription initiation or elongation, respectively, and showed promising effects in (pre-)clinical studies for different cancer entities, including hematologic malignancies, melanoma, breast-, prostate-, and pancreatic cancer (Drygin et al., 2009; Drygin et al., 2011; Rebello et al., 2016; El Hassouni et al., 2019; Khot et al., 2019; Hilton et al., 2022). In the present work, CX-5461 effectively inhibited the cell viability of all eight conventional PDAC cell lines tested, whereby the sensitivity correlated with the level of rRNA synthesis but did

not significantly differ between classical and QM cells. However, recent studies suggested that CX-3543 and CX-5461 exert their cytotoxic effect on cancer cells primarily by inducing replication-dependent DNA damage as a consequence of G4 stabilization (Xu et al., 2017). Therefore, alterations in the homologous repair pathway were proposed to cause synthetic lethality upon treatment with CX-5461, and consistently, an antitumor effect of CX-5461 was observed primarily in solid tumor patients with homologous repair deficiencies (Hilton et al., 2022).

To circumvent these extra-ribosomal effects, the present study focused on the small-molecule inhibitor BMH-21, which was shown to affect RNA Pol I-mediated transcription without activation of DNA damage sensing- and repair mechanisms (Colis et al., 2014). BMH-21 intercalates into GC-rich DNA regions, which are highly abundant in rRNA genes, thereby hindering RNA Pol I-mediated transcription at the level of initiation, promotor escape, and elongation. In the present study, BMH-21 treatment reduced the 45S rRNA expression in HPAF-II and PSN1 cells in a time- and dose-dependent manner and led to a strong reduction of cell viability in all conventional PDAC cell lines and PDCs tested. Importantly, Peltonen et al. previously showed that BMH-21 exerts low toxicity in non-malignant cells, although the treatment caused nucleolar stress in normal human fibroblasts (Peltonen et al., 2014). Similarly, ongoing studies from Ahmad et al. show that BMH-21 does not cause any cytotoxic effect in normal pancreatic ductal epithelial cells at twice the effective dose that was determined in respective PDAC cell lines (Ahmad et al., 2022).

Although originally identified as a p53 activator, the anticancer effect of BMH-21 was shown to be independent of the p53 status (Peltonen et al., 2014). This is essential in the context of PDAC therapy since p53 is mutated and thus non-functional in more than 70% of all PDAC cases (Waddell et al., 2015). The observed inhibitory effect of BMH-21 in PDAC cell lines was independent of the cellular p53 status as the treatment response of HPAC and KP-4 cells, characterized as p53-wild-type (Bairoch, 2018), was comparable to the response of the remaining conventional cell lines, all characterized as p53-mutant (Bairoch, 2018). Among conventional cell lines, stronger sensitivity toward BMH-21 was observed in QM compared to classical cells. This corresponded well with higher expression levels of RiBi-associated genes and 47S pre-rRNA as well as a higher proliferative capacity being detected for the QM subtype. For PDCs, on the other hand, treatment sensitivity did not correlate with the molecular subtype, which was in line with the more heterogeneous and subtype-

independent levels of RiBi activity observed in this model system. Importantly, PDC3 showed a certain resistance toward BMH-21 treatment potentially due to its comparatively low proliferation rate and correspondingly lower dependence on RiBi. Nevertheless, it can be concluded that, despite the observed differences in rRNA expression rates, BMH-21 treatment is efficient in both phenotypic states.

In addition to pharmacologic RNA Pol I inhibition via CX-5461 and BMH-21, siRNA-mediated knockdown was performed for the RNA Pol I catalytic subunit RPA194 (*POLR1A*). Although RPA194 was downregulated at the mRNA- and protein level, the knockdown was not sufficient to reliably inhibit rRNA transcription. Especially in HPAF-II cells, 45S pre-rRNA expression was nearly unaffected by POLR1A-knockdown. This suggests that either the remaining RPA194 is sufficient to maintain the normal cellular rRNA synthesis rate or the cells can compensate for the decreased RPA194 protein level. In PSN1 cells, one of the tested siRNAs caused a reduction of the 45S rRNA abundance but no restriction of cell viability, potentially because the remaining rRNA transcription is sufficient to maintain a normal cellular proliferation rate. Another possible reason is that alterations in the translational efficiency of proliferation-promoting mRNAs allow the cells to preserve an unaffected proliferation rate upon reduced 45S rRNA expression (Priyadarshini et al., 2023). Taken together, in contrast to the almost total withdrawal of RNA Pol I activity by pharmacologic targeting, incomplete inhibition of 45S rRNA transcription via partial elimination of the RNA Pol I catalytic subunit RPA194, is not sufficient to effectively restrict cell viability of PDAC cells. However, further research is required to understand the functional mechanisms leading to these results.

The nucleolus is considered a central stress response hub that changes its morphology in response to different environmental factors, especially when associated with reduced rRNA expression (Derenzini et al., 2009). This is because, according to the LLPS model, nascent pre-rRNA is an essential factor for the proper arrangement of RBFs and consequently for nucleolus formation (Lafontaine et al., 2021). Correspondingly, nucleolar disruption concurrent with the translocation of Fibrillarin, Nucleolin, Nucleophosmin, and UBF-1, was observed upon CX-5461- or BMH-21-mediated RNA Pol I inhibition in different cancer entities, including lymphoma, colorectal cancer, and melanoma (Bywater et al., 2013; Peltonen et al., 2014; Otto et al., 2022). Similarly, in the present study, loss of nucleolar integrity was observed in BMH-21-treated PDAC cell lines, as indicated by translocation or downregulation of

the nucleolar proteins Fibrillarin, Nucleolin, UBF-1, and RPA194, respectively. Given that the decrease in RPA194 was present at the protein- yet not at the mRNA level, post-transcriptional or post-translational regulation mechanisms can be suggested, especially since BMH-21 is known to induce proteasomal degradation of RPA194 (Peltonen et al., 2014). Additionally, a mild downregulation of UBF-1 at the mRNA- and protein level was present in BMH-21-treated PDAC cells. Such changes were, however, not observed in previous studies by Peltonen et al. who described a BMH-21-induced translocation of UBF-1 without alterations in the overall protein expression (Peltonen et al., 2014). Importantly, while in the present work, cells were analyzed after 48 and 72 h of BMH-21 treatment, the observations described by Peltonen et al. were made after a maximum of three hours. Thus, downregulation of UBF-1 may be a rather long-term treatment effect of BMH-21.

Nucleolar stress activates various downstream signaling pathways that can act in a p53-dependent or -independent manner and are primarily triggered by nucleolar proteins and RPs, including RPL3, RPL5, RPL11, RPS14, RPL23, Nucleophosmin, and ARF, once the association with the nucleolus is lost (Maehama et al., 2023). A well-described mechanism of p53 activation in response to RNA Pol I inhibition is the formation of the IRBC-complex that comprises 5S rRNA, RPL5, and RPL11 and binds to HDM2. This binding prevents the HDM2-mediated ubiquitylation of p53, resulting in reduced degradation and subsequent accumulation of p53 (Bursac et al., 2012; Donati et al., 2013). Other nucleolar proteins that contribute to an accumulation of p53 by binding HDM2 are RPL23, ARF, and Nucleophosmin, although Nucleophosmin was also shown to stabilize p53 via direct binding (Colombo et al., 2002; Jin et al., 2004; Kurki et al., 2004; Gjerset & Bandyopadhyay, 2006). Increased p53 levels consequently result in the activation of cell cycle arrest and cell death. However, given that various cancer types, including PDAC, are characterized by loss of p53 function (Waddell et al., 2015; Kastenhuber & Lowe, 2017) and that RNA Pol I inhibitors were shown to act independently of the cellular p53 status (Drygin et al., 2011; Peltonen et al., 2014), it was proposed that other mechanisms exist to modulate the nucleolar stress response in a p53-independent manner.

Initially, transcriptional analysis of BMH-21-treated HPAF-II cells revealed a substantial downregulation of various gene sets associated with MYC signaling, RiBi, and translation. These findings are in line with a previous study determining a suppression of RiBi- and translation-related genes upon BMH-21 treatment in glioma cells (Zisi et

al., 2023). Given that several components of the RiBi- and translation machinery are transcriptional targets of MYC (Ruggero, 2009), it is conceivable that the observed alterations in the expression pattern may be functionally related. Previous studies revealed that, in turn, multiple RPs (e.g., RPL5, RPL11, RPS14) can inhibit the expression or transcriptional activity of MYC, respectively (Zhou et al., 2013; Liao et al., 2014). This autoregulatory feedback mechanism is thought to sense abnormal RiBi in normal cells and exert a corresponding negative effect on ribosome production and proliferation to prevent tumor development (Dai et al., 2007; Liao et al., 2014). Consequently, MYC is considered a key factor in the nucleolar stress response since its downregulation in response to RiBi inhibition and the concomitant translocation of RPs is associated with cell cycle arrest, apoptosis, and senescence (van Riggelen et al., 2010; Maehama et al., 2023).

In the present study, apoptosis and an impaired cell cycle progression were identified as two mechanisms contributing to the BMH-21-mediated restriction of cell viability in PDAC cell lines. The HALLMARK “E2F targets” gene set was the most downregulated gene set in BMH-21-treated HPAF-II cells and cell cycle-associated genes were most represented among the top downregulated genes. At the functional level, FACS-based cell cycle analysis revealed a treatment-induced arrest in the G2/M phase, and simultaneously, increased protein levels of cleaved PARP and cleaved caspase-3 pointed to a BMH-21-mediated induction of apoptotic cell death. As modulators of cell cycle progression and apoptosis, E2F-1 and p21 are considered to play key roles in the p53-independent nucleolar stress response (Maehama et al., 2023). While under normal conditions, E2F-1 is protected from proteasomal degradation by its binding to HDM2, the binding of RPL5 and RPL11 to HDM2 inhibits this protective effect and results in E2F-1 downregulation (Zhang et al., 2005; Donati et al., 2011). Furthermore, RPL3 was described to cause an upregulation of p21 by transcriptional activation and direct protein stabilization, respectively (Russo et al., 2013; Russo et al., 2016). Thus, increased p21 activity and reduced E2F-1 signaling are considered two routes leading to induction of cell death and cell cycle arrest upon RNA Pol I inhibition (Maehama et al., 2023).

In this work, BMH-21 further caused an increase in the autophagic activity in PDAC cell lines, as indicated by elevated levels of autophagosome formation together with an enhanced autophagic flux. Various studies have previously described a link between nucleolar stress and autophagy, although the exact mechanisms are still

poorly understood (Pfister, 2019; Pfister, 2023). In cervical cancer- and osteosarcoma cell lines, for example, CX-5461-mediated nucleolar stress caused an increase in the expression of various autophagy core regulators, including *ATG7* and *ATG16L1* (Dannheisig et al., 2021). However, in the present study, BMH-21 treatment also led to an upregulation of mTORC1 activity, as shown by increased phosphorylation levels of p70-S6K and 4E-BP1. Simultaneous activation of autophagy and mTORC1 appear contradictory given that active mTORC1 is a well-described negative regulator of autophagy (Saxton & Sabatini, 2017). Nevertheless, in breast cancer cells, the nucleolar stress-related translocation of Nucleophosmin into the nucleoplasm was shown to induce a non-canonical autophagy pathway that was independent of starvation-associated autophagy (Katagiri et al., 2015). These findings demonstrate that in the context of nucleolar stress, autophagy can be induced via an mTORC1-independent mechanism, potentially explaining why autophagy induction and mTORC1 activation can occur simultaneously in BMH-21-treated PDAC cell lines.

To further investigate the functional role of autophagy in the cellular response to impaired RiBi, combinational treatment with BMH-21 and the autophagy inhibitor 3-MA was performed. More specifically, 3-MA functions as a PI3K inhibitor and hinders autophagosome formation by blocking the required PI3K complex activity (Petiot et al., 2000). In both HuP-T4 and PSN1 cells, an antagonistic relation between the two compounds was observed, indicating that autophagy exerts a pro-death function in response to an impaired rRNA synthesis in the present setting. Initially, autophagy induction upon nucleolar stress was considered a compensatory mechanism to recycle endogenous material, thereby exerting a pro-survival effect (Pfister, 2019). However, autophagy induction and cell death activation can also occur simultaneously, either in the context of apoptotic cell death or, more commonly, when autophagy supports the induction of apoptotic or necrotic cell death programs (Marino et al., 2014). Similar to the observations of the present study, nucleolar stress was indeed associated with pro-death autophagy in different settings. For example, treatment with the RNA Pol I inhibitors CX-5461 and Actinomycin D caused cell death-inducing autophagy in osteosarcoma-, cervical cancer-, and neuroblastoma cells, respectively (Drygin et al., 2011; Cortes et al., 2016; Duo et al., 2018). Furthermore, overexpression of the RNA Pol I-inhibiting nucleolar factor PICT-1 was associated with pro-death autophagy in glioblastoma- and breast cancer cells (Chen et al., 2016). Importantly, the PICT-1-mediated autophagy was independent of nucleolar disruption and requires inhibition of

mTORC1/p70-S6K signaling (Chen et al., 2016), suggesting that different mechanisms exist that trigger autophagy in response to RNA Pol I inhibition. It should however be noted that in the present work, the antiproliferative effect of BMH-21 was only partially reduced upon the addition of 3-MA, suggesting that autophagy is not the primary cell death-inducing mechanism activated upon RNA Pol I inhibition in PDAC cells.

4.3 Impairment of ribosome biogenesis affects other cellular processes

EMT is considered one of the key drivers of PDAC progression and the development of treatment resistance and is therefore associated with poor prognosis (Palamaris et al., 2021). Among conventional PDAC cell lines, those assigned to the QM subtype displayed greater RP- and 45S pre-rRNA expression as well as stronger sensitivity toward BMH-21. This suggests a higher dependency on RiBi in QM compared to classical cells. Previous studies discovered that, in breast cancer cells, EMT induction is accompanied by an upregulation of rDNA transcription and that inhibition of RNA Pol I activity halts the execution of the EMT process (Prakash et al., 2019). Furthermore, it was found that the incorporation of additional ribosomes, purified from *Escherichia coli* cultures, into breast cancer cells causes the induction of an EMT-like phenotype (Kudo et al., 2022). These findings suggested that upregulation of RiBi is essential to implement the metabolic plasticity needed for EMT completion and that modulations of rRNA synthesis can cause a shift in the phenotypic state of cancer cells (Elhamamsy et al., 2022). Therefore, it was investigated whether BMH-21-mediated inhibition of RNA Pol I activity affects the phenotypic state of classical and QM PDAC cell lines.

Intriguingly, RNA sequencing analysis showed an enrichment of EMT-related genes in BMH-21-treated HPAF-II cells. These results were validated by qPCR and western blot analysis showing a BMH-21-mediated upregulation of the mesenchymal marker Vimentin and the EMT-associated transcription factor Zeb1 at the mRNA and/or protein level. In PSN1 cells, on the other hand, no upregulation of Vimentin or Zeb1 was observed in response to BMH-21, potentially because PSN1 cells, given their QM character, exhibit a generally high expression of mesenchymal markers. However, in both HPAF-II and PSN1 cells, expression of the epithelial marker E-cadherin was preserved upon treatment, with mRNA levels being even moderately increased at higher concentrations of BMH-21. The observed BMH-21-induced upregulation of EMT-associated genes was surprising given that RNA Pol I-inhibition was previously described to impede the execution of the EMT program (Prakash et al., 2019). It should

however be noted that the experimental settings of the studies were significantly different. Prakash et al. used a concentration of CX-5461 that inhibits rDNA transcription in cells undergoing EMT but not in proliferating cells (Prakash et al., 2019). In contrast, the BMH-21 concentrations used in the present study resulted in strongly decreased levels of rRNA expression in the tested PDAC cell lines. Furthermore, a recent study revealed that upregulation of RiBi is not only required for the execution of an EMT program but also for the reverse process of MET (Ban et al., 2023). Therefore, it can be speculated that upon BMH-21-mediated RNA Pol I inhibition, the cells do not exhibit the metabolic plasticity required for the completion of an EMT or MET program, respectively. Consequently, the simultaneous upregulation of epithelial and mesenchymal markers in BMH-21-treated PDAC cells may be stress-induced deregulation rather than a switch in the phenotypic cell state. Nevertheless, it should be further elucidated whether the observed alterations are accompanied by functional consequences such as changes in the migratory capacity.

RiBi is considered one of the most energy-demanding processes of the cell and is therefore tightly connected to cellular metabolism and translation (Warner, 1999; Grummt, 2010; Orsolic et al., 2016). Given the role of mTOR in the complex regulation of these processes (Gentilella et al., 2015; Saxton & Sabatini, 2017), the influence of RNA Pol I inhibition on mTORC1 activity was investigated in PDAC cell lines. In BMH-21-treated HPAF-II and PSN1 cells, upregulation of mTORC1 signaling was observed, which may function as a compensatory mechanism upon impaired rRNA synthesis. Similarly, Liu et al. showed that alterations in the PES1-BOP1-WDR12-complex, which is involved in rRNA processing, led to increased activity of mTORC1 in human embryonic kidney cells (Liu et al., 2014). Therefore, they postulated that upon RiBi inhibition, cells upregulate mTORC1 signaling, aiming to overcome the limited ribosome capacity by increasing the translation efficiency (Liu et al., 2014). To further investigate the connection between RiBi inhibition and upregulation of mTORC1, PDAC cell lines were simultaneously treated with BMH-21 and the mTOR inhibitor Rapamycin. Intriguingly, the combination approach revealed an antagonistic interaction between the two inhibitors in PSN1 cells, with Rapamycin mildly reducing the BMH-21-mediated decrease in cell viability. This observation was in line with ongoing research by Fan et al. who describe Torin 1-mediated inhibition of mTORC1 as an inducer of resistance toward BMH-21 treatment in colorectal cancer, associated with an elevated translation of RP-encoding mRNAs (Fan et al., 2022). Conversely,

upon acute inhibition of RNA Pol I via CX-5461 in B-cell lymphoma, additional treatment with the mTOR inhibitor Everolimus led to a reduced translation of mRNAs encoding for translational regulators and concomitantly increased the treatment effect of CX-5461 (Devlin et al., 2016; Kusnadi et al., 2020). Nevertheless, similar to the mechanism described by Fan et al., long-term treatment with CX-5461 and Everolimus resulted in the development of treatment resistance, with an elevated translation of mRNAs encoding for various RPs as well as factors involved in translation initiation and -elongation (Kusnadi et al., 2020).

Proteome profiling would be necessary to assess whether the antagonistic interaction between BMH-21 and Rapamycin, observed in PSN1 cells, is due to alterations in the translation efficiency of RiBi- and translation-associated mRNAs. Additionally, it should be noted that the antagonistic effect between the inhibitors is moderately pronounced in PSN1 cells but absent in HPAF-II cells. This suggests that the related mechanism relies on cellular characteristics that require further investigation, with cellular mTOR dependency representing a potential investigative approach (Utomo et al., 2014). Nevertheless, since translational reprogramming in response to mTOR inhibition appears to follow different dynamics depending on the tumor model (Devlin et al., 2016; Kusnadi et al., 2020; Fan et al., 2022), caution needs to be taken when considering the combination of mTOR- and RiBi-targeting strategies.

Importantly, Kusnadi et al. further observed considerable metabolic alterations upon inhibition of RiBi and translation. While acute treatment with CX-5461 and Everolimus caused a decrease in the translation efficiency of metabolism-related mRNAs, acquired resistance toward CX-5461 alone or in combination with Everolimus was associated with functional upregulation of metabolic pathways (Kusnadi et al., 2020). These findings suggested that metabolic reprogramming plays an important role in the development of treatment resistance in the context of RiBi-targeting approaches. The present study showed that BMH-21 treatment caused a strong transcriptional downregulation of various metabolic pathways, including glycolysis, OxPhos, and the TCA cycle. Nonetheless, this decrease in the expression of metabolic genes did not fully match the functional metabolic alterations observed upon BMH-21 treatment. Seahorse metabolic flux analysis revealed a BMH-21-induced decrease in the ECAR in both HPAF-II and PSN1 cells, which could point to reduced glycolysis upon RNA Pol I inhibition. On the other hand, the OCR was only marginally affected by BMH-21 in PSN1 cells and even slightly increased in HPAF-II cells. Together with the

observation that the activity of IDH3, a rate-limiting enzyme in the TCA cycle, remained unaltered upon BMH-21 treatment, this indicated that the functionality of OxPhos and the TCA cycle is largely maintained. Thus, RNA Pol I inhibition potentially causes a shift in metabolic dependency toward OxPhos. Although similar metabolic alterations, i.e. reduced glycolysis and increased oxygen consumption, were previously described in the context of nucleolar stress, the underlying mechanisms were p53-dependent (Deisenroth & Zhang, 2011). Conversely, p53-independent mechanisms behind the interdependency between RNA Pol I inhibition and deregulations in cellular energy metabolism have so far been little investigated.

However, caution needs to be taken when drawing conclusions regarding glycolytic flux and OxPhos based on alterations in ECAR and OCR. Especially for the ECAR, previous publications pointed out that a) not all the lactate produced during glycolysis is necessarily effluxed but can also be oxidized in the mitochondria and b) extracellular acidification can also result from alternative anion/H^+ exchange mechanisms or carbon dioxide, derived from respiration (Schmidt et al., 2021). The observed BMH-21-mediated decrease in ECAR may therefore result from increased oxidation of glycolysis-derived pyruvate/lactate in the mitochondria rather than general downregulation of glycolysis. Metabolite profiling and isotype-labeling studies could provide further information about which metabolic changes occur in the course of RiBi inhibition. Nevertheless, together with previous findings, the observations from the present study suggest that combinational therapies, addressing the interplay between an impaired RiBi and metabolic alterations, are potentially a promising strategy for improving treatment outcomes (Kusnadi et al., 2020).

5 Conclusion and Outlook

Although previous studies suggested an important role of RiBi in PDAC, the effect of RNA Pol I inhibition in this cancer entity has been scarcely explored so far. The results of the present work further support the notion that oncogenic dysregulation may contribute to an increased RiBi activity in PDAC. Furthermore, BMH-21 exhibited notable efficacy in all conventional PDAC cell lines and PDCs tested, despite remarkable heterogeneity in RNA Pol I activity and nucleolar organization being present across the PDAC model systems. These findings consider RNA Pol I inhibition a promising approach for PDAC therapy. Additionally, the observed deregulation in mTORC1 signaling and metabolic pathways upon BMH-21 treatment presents an attractive base for investigating combinational treatment strategies.

Conclusions of the present work are limited by the fact that the implications of RNA Pol I inhibition were mainly investigated at the transcriptional level. Given that prior studies describe substantial alterations in the translational efficiency in response to RiBi-targeting therapies, effort should be dedicated to investigating how BMH-21 affects the ribosomal function in PDAC. In addition, it should be further explored which individual gene functions or pathways interact with RiBi or are affected in response to impaired RiBi. On the one hand, this would help to determine resistance mechanisms that allow cancer cells to circumvent the inhibitory effect of RiBi inhibition. Consequently, this knowledge could be used to override corresponding resistance mechanisms through the application of suitable combinational treatment approaches. On the other hand, it would also help to identify specific mutations or characteristics that render cells sensitive toward inhibition of RiBi, thereby supporting patient stratification and allowing the application of the respective treatment with the highest possible benefit. Furthermore, in the present work, the consequences of BMH-21 treatment were exclusively assessed based on *in vitro* models. Therefore, potential side effects and toxicity need to be further investigated *in vivo*, especially when considering that healthy pancreatic tissue is characterized by high levels of protein synthesis. In this context, it would be worthwhile to put effort into the development of novel compounds to improve specificity for RNA Pol I or to target RiBi via different mechanisms (e.g. RNA Pol III activity, ribosome assembly). Another future approach to facilitate selective targeting of cancer cells would be to use small molecules that specifically address alterations of ribosomes occurring in a tumor context.

References

Ahmad, M., Perez, C., Massey, A., Kashyap, V., Chauhan, N., Ahsan, H., . . . Hafeez, B. (2022). Abstract B035: Targeting ribosome biogenesis addition is a novel strategy for pancreatic cancer therapy. *Cancer Research, 82*(22_Supplement), B035-B035. doi:10.1158/1538-7445.Panca22-b035

Aiello, N. M., Maddipati, R., Norgard, R. J., Balli, D., Li, J., Yuan, S., . . . Stanger, B. Z. (2018). EMT Subtype Influences Epithelial Plasticity and Mode of Cell Migration. *Dev Cell, 45*(6), 681-695 e684. doi:10.1016/j.devcel.2018.05.027

Anger, A. M., Armache, J. P., Berninghausen, O., Habeck, M., Subklewe, M., Wilson, D. N., & Beckmann, R. (2013). Structures of the human and Drosophila 80S ribosome. *Nature, 497*(7447), 80-85. doi:10.1038/nature12104

Assenov, Y., Ramirez, F., Schelhorn, S. E., Lengauer, T., & Albrecht, M. (2008). Computing topological parameters of biological networks. *Bioinformatics, 24*(2), 282-284. doi:10.1093/bioinformatics/btm554

Atkinson, M. A., Campbell-Thompson, M., Kusmartseva, I., & Kaestner, K. H. (2020). Organisation of the human pancreas in health and in diabetes. *Diabetologia, 63*(10), 1966-1973. doi:10.1007/s00125-020-05203-7

Aung, K. L., Fischer, S. E., Denroche, R. E., Jang, G. H., Dodd, A., Creighton, S., . . . Knox, J. J. (2018). Genomics-Driven Precision Medicine for Advanced Pancreatic Cancer: Early Results from the COMPASS Trial. *Clin Cancer Res, 24*(6), 1344-1354. doi:10.1158/1078-0432.CCR-17-2994

Avsar, G., & Pir, P. (2023). An integrated study to decipher immunosuppressive cellular communication in the PDAC environment. *NPJ Syst Biol Appl, 9*(1), 56. doi:10.1038/s41540-023-00320-6

Azman, M. S., Alard, E. L., Dodel, M., Capraro, F., Faraway, R., Dermit, M., . . . Mardakheh, F. K. (2023). An ERK1/2-driven RNA-binding switch in nucleolin drives ribosome biogenesis and pancreatic tumorigenesis downstream of RAS oncogene. *EMBO J, 42*(11), e110902. doi:10.15252/embj.2022110902

Bailey, P., Chang, D. K., Nones, K., Johns, A. L., Patch, A. M., Gingras, M. C., . . . Grimmond, S. M. (2016). Genomic analyses identify molecular subtypes of pancreatic cancer. *Nature, 531*(7592), 47-52. doi:10.1038/nature16965

Bairoch, A. (2018). The Cellosaurus, a Cell-Line Knowledge Resource. *J Biomol Tech, 29*(2), 25-38. doi:10.7171/jbt.18-2902-002

Ban, Y., Zou, Y., Lee, S. B., R, B. B., Sheng, J., Cao, Y., . . . Gao, D. (2023). Targeting Ribosome Biogenesis as a Novel Therapeutic Approach to Overcome EMT-related Chemoresistance in Breast Cancer. *bioRxiv*. doi:10.1101/2023.06.28.546927

Bardeesy, N., Aguirre, A. J., Chu, G. C., Cheng, K. H., Lopez, L. V., Hezel, A. F., . . . Depinho, R. A. (2006). Both p16(Ink4a) and the p19(Arf)-p53 pathway constrain progression of pancreatic adenocarcinoma in the mouse. *Proc Natl Acad Sci U S A, 103*(15), 5947-5952. doi:10.1073/pnas.0601273103

Bardeesy, N., & DePinho, R. A. (2002). Pancreatic cancer biology and genetics. *Nat Rev Cancer, 2*(12), 897-909. doi:10.1038/nrc949

Bastide, A., & David, A. (2018). The ribosome, (slow) beating heart of cancer (stem) cell. *Oncogenesis, 7*(4), 34. doi:10.1038/s41389-018-0044-8

Bell, S. P., Learned, R. M., Jantzen, H. M., & Tjian, R. (1988). Functional cooperativity between transcription factors UBF1 and SL1 mediates human ribosomal RNA synthesis. *Science, 241*(4870), 1192-1197. doi:10.1126/science.3413483

Biggiogera, M., Burki, K., Kaufmann, S. H., Shaper, J. H., Gas, N., Amalric, F., & Fakan, S. (1990). Nucleolar distribution of proteins B23 and nucleolin in mouse

preimplantation embryos as visualized by immunoelectron microscopy. *Development, 110*(4), 1263-1270. doi:10.1242/dev.110.4.1263

Boisvert, F. M., van Koningsbruggen, S., Navascues, J., & Lamond, A. I. (2007). The multifunctional nucleolus. *Nat Rev Mol Cell Biol, 8*(7), 574-585. doi:10.1038/nrm2184

Boroughs, L. K., & DeBerardinis, R. J. (2015). Metabolic pathways promoting cancer cell survival and growth. *Nat Cell Biol, 17*(4), 351-359. doi:10.1038/ncb3124

Boulon, S., Westman, B. J., Hutten, S., Boisvert, F. M., & Lamond, A. I. (2010). The nucleolus under stress. *Mol Cell, 40*(2), 216-227. doi:10.1016/j.molcel.2010.09.024

Bouvet, P., Diaz, J. J., Kindbeiter, K., Madjar, J. J., & Amalric, F. (1998). Nucleolin interacts with several ribosomal proteins through its RGG domain. *J Biol Chem, 273*(30), 19025-19029. doi:10.1074/jbc.273.30.19025

Bronsert, P., Kohler, I., Timme, S., Kiefer, S., Werner, M., Schilling, O., . . . Wellner, U. F. (2014). Prognostic significance of Zinc finger E-box binding homeobox 1 (ZEB1) expression in cancer cells and cancer-associated fibroblasts in pancreatic head cancer. *Surgery, 156*(1), 97-108. doi:10.1016/j.surg.2014.02.018

Bruno, P. M., Lu, M., Dennis, K. A., Inam, H., Moore, C. J., Sheehe, J., . . . Pritchard, J. R. (2020). The primary mechanism of cytotoxicity of the chemotherapeutic agent CX-5461 is topoisomerase II poisoning. *Proc Natl Acad Sci U S A, 117*(8), 4053-4060. doi:10.1073/pnas.1921649117

Burger, K., Muhl, B., Harasim, T., Rohrmoser, M., Malamoussi, A., Orban, M., . . . Eick, D. (2010). Chemotherapeutic drugs inhibit ribosome biogenesis at various levels. *J Biol Chem, 285*(16), 12416-12425. doi:10.1074/jbc.M109.074211

Bursac, S., Brdovcak, M. C., Pfannkuchen, M., Orsolic, I., Golomb, L., Zhu, Y., . . . Volarevic, S. (2012). Mutual protection of ribosomal proteins L5 and L11 from degradation is essential for p53 activation upon ribosomal biogenesis stress. *Proc Natl Acad Sci U S A, 109*(50), 20467-20472. doi:10.1073/pnas.1218535109

Bywater, M. J., Pearson, R. B., McArthur, G. A., & Hannan, R. D. (2013). Dysregulation of the basal RNA polymerase transcription apparatus in cancer. *Nat Rev Cancer, 13*(5), 299-314. doi:10.1038/nrc3496

Campbell, K. J., & White, R. J. (2014). MYC regulation of cell growth through control of transcription by RNA polymerases I and III. *Cold Spring Harb Perspect Med, 4*(5). doi:10.1101/cshperspect.a018408

Cancer Genome Atlas Research Network. (2017). Integrated Genomic Characterization of Pancreatic Ductal Adenocarcinoma. *Cancer Cell, 32*(2), 185-203 e113. doi:10.1016/j.ccell.2017.07.007

Cangelosi, D., Brignole, C., Bensa, V., Tamma, R., Malaguti, F., Carlini, B., . . . Pastorino, F. (2022). Nucleolin expression has prognostic value in neuroblastoma patients. *EBioMedicine, 85*, 104300. doi:10.1016/j.ebiom.2022.104300

Case, R. M. (1978). Synthesis, intracellular transport and discharge of exportable proteins in the pancreatic acinar cell and other cells. *Biol Rev Camb Philos Soc, 53*(2), 211-354. doi:10.1111/j.1469-185x.1978.tb01437.x

Chaker-Margot, M., & Klinge, S. (2019). Assembly and early maturation of large subunit precursors. *RNA, 25*(4), 465-471. doi:10.1261/rna.069799.118

Chan-Seng-Yue, M., Kim, J. C., Wilson, G. W., Ng, K., Figueroa, E. F., O'Kane, G. M., . . . Notta, F. (2020). Transcription phenotypes of pancreatic cancer are driven by genomic events during tumor evolution. *Nat Genet, 52*(2), 231-240. doi:10.1038/s41588-019-0566-9

Chan, K., Robert, F., Oertlin, C., Kapeller-Libermann, D., Avizonis, D., Gutierrez, J., . . . Chio, I. I. C. (2019). eIF4A supports an oncogenic translation program in pancreatic ductal adenocarcinoma. *Nat Commun, 10*(1), 5151. doi:10.1038/s41467-019-13086-5

Chandra, R., & Liddle, R. A. (2009). Neural and hormonal regulation of pancreatic secretion. *Curr Opin Gastroenterol, 25*(5), 441-446. doi:10.1097/MOG.0b013e32832e9c41

Chen, H., Duo, Y., Hu, B., Wang, Z., Zhang, F., Tsai, H., . . . Huang, L. (2016). PICT-1 triggers a pro-death autophagy through inhibiting rRNA transcription and AKT/mTOR/p70S6K signaling pathway. *Oncotarget, 7*(48), 78747-78763. doi:10.18632/oncotarget.12288

Cheung, P. F., Yang, J., Fang, R., Borgers, A., Krengel, K., Stoffel, A., . . . Siveke, J. T. (2022). Progranulin mediates immune evasion of pancreatic ductal adenocarcinoma through regulation of MHCI expression. *Nat Commun, 13*(1), 156. doi:10.1038/s41467-021-27088-9

Ciganda, M., & Williams, N. (2011). Eukaryotic 5S rRNA biogenesis. *Wiley Interdiscip Rev RNA, 2*(4), 523-533. doi:10.1002/wrna.74

Colis, L., Peltonen, K., Sirajuddin, P., Liu, H., Sanders, S., Ernst, G., . . . Laiho, M. (2014). DNA intercalator BMH-21 inhibits RNA polymerase I independent of DNA damage response. *Oncotarget, 5*(12), 4361-4369. doi:10.18632/oncotarget.2020

Collisson, E. A., Sadanandam, A., Olson, P., Gibb, W. J., Truitt, M., Gu, S., . . . Gray, J. W. (2011). Subtypes of pancreatic ductal adenocarcinoma and their differing responses to therapy. *Nat Med, 17*(4), 500-503. doi:10.1038/nm.2344

Colombo, E., Marine, J. C., Danovi, D., Falini, B., & Pelicci, P. G. (2002). Nucleophosmin regulates the stability and transcriptional activity of p53. *Nat Cell Biol, 4*(7), 529-533. doi:10.1038/ncb814

Cong, R., Das, S., Ugrinova, I., Kumar, S., Mongelard, F., Wong, J., & Bouvet, P. (2012). Interaction of nucleolin with ribosomal RNA genes and its role in RNA polymerase I transcription. *Nucleic Acids Res, 40*(19), 9441-9454. doi:10.1093/nar/gks720

Connor, A. A., & Gallinger, S. (2022). Pancreatic cancer evolution and heterogeneity: integrating omics and clinical data. *Nat Rev Cancer, 22*(3), 131-142. doi:10.1038/s41568-021-00418-1

Conroy, T., Desseigne, F., Ychou, M., Bouche, O., Guimbaud, R., Becouarn, Y., . . . Intergroup, P. (2011). FOLFIRINOX versus gemcitabine for metastatic pancreatic cancer. *N Engl J Med, 364*(19), 1817-1825. doi:10.1056/NEJMoa1011923

Cortes, C. L., Veiga, S. R., Almacellas, E., Hernandez-Losa, J., Ferreres, J. C., Kozma, S. C., . . . Tauler, A. (2016). Effect of low doses of actinomycin D on neuroblastoma cell lines. *Mol Cancer, 15*, 1. doi:10.1186/s12943-015-0489-8

Daemen, A., Peterson, D., Sahu, N., McCord, R., Du, X., Liu, B., . . . Evangelista, M. (2015). Metabolite profiling stratifies pancreatic ductal adenocarcinomas into subtypes with distinct sensitivities to metabolic inhibitors. *Proc Natl Acad Sci U S A, 112*(32), E4410-4417. doi:10.1073/pnas.1501605112

Dai, M. S., Sears, R., & Lu, H. (2007). Feedback regulation of c-Myc by ribosomal protein L11. *Cell Cycle, 6*(22), 2735-2741. doi:10.4161/cc.6.22.4895

Dannheisig, D. P., Schimansky, A., Donow, C., & Pfister, A. S. (2021). Nucleolar Stress Functions Upstream to Stimulate Expression of Autophagy Regulators. *Cancers (Basel), 13*(24). doi:10.3390/cancers13246220

DeBerardinis, R. J., & Chandel, N. S. (2016). Fundamentals of cancer metabolism. *Sci Adv, 2*(5), e1600200. doi:10.1126/sciadv.1600200

DeBerardinis, R. J., Lum, J. J., Hatzivassiliou, G., & Thompson, C. B. (2008). The biology of cancer: metabolic reprogramming fuels cell growth and proliferation. *Cell Metab, 7*(1), 11-20. doi:10.1016/j.cmet.2007.10.002

Deisenroth, C., & Zhang, Y. (2011). The Ribosomal Protein-Mdm2-p53 Pathway and Energy Metabolism: Bridging the Gap between Feast and Famine. *Genes Cancer, 2*(4), 392-403. doi:10.1177/1947601911409737

Derenzini, M., Montanaro, L., & Trere, D. (2009). What the nucleolus says to a tumour pathologist. *Histopathology, 54*(6), 753-762. doi:10.1111/j.1365-2559.2008.03168.x

Devlin, J. R., Hannan, K. M., Hein, N., Cullinane, C., Kusnadi, E., Ng, P. Y., . . . Pearson, R. B. (2016). Combination Therapy Targeting Ribosome Biogenesis and mRNA Translation Synergistically Extends Survival in MYC-Driven Lymphoma. *Cancer Discov, 6*(1), 59-70. doi:10.1158/2159-8290.CD-14-0673

Dobin, A., Davis, C. A., Schlesinger, F., Drenkow, J., Zaleski, C., Jha, S., . . . Gingeras, T. R. (2013). STAR: ultrafast universal RNA-seq aligner. *Bioinformatics, 29*(1), 15-21. doi:10.1093/bioinformatics/bts635

Donati, G., Brighenti, E., Vici, M., Mazzini, G., Trere, D., Montanaro, L., & Derenzini, M. (2011). Selective inhibition of rRNA transcription downregulates E2F-1: a new p53-independent mechanism linking cell growth to cell proliferation. *J Cell Sci, 124*(Pt 17), 3017-3028. doi:10.1242/jcs.086074

Donati, G., Peddigari, S., Mercer, C. A., & Thomas, G. (2013). 5S ribosomal RNA is an essential component of a nascent ribosomal precursor complex that regulates the Hdm2-p53 checkpoint. *Cell Rep, 4*(1), 87-98. doi:10.1016/j.celrep.2013.05.045

Doncheva, N. T., Morris, J. H., Gorodkin, J., & Jensen, L. J. (2019). Cytoscape StringApp: Network Analysis and Visualization of Proteomics Data. *J Proteome Res, 18*(2), 623-632. doi:10.1021/acs.jproteome.8b00702

Dörner, K., Ruggeri, C., Zemp, I., & Kutay, U. (2023). Ribosome biogenesis factors-from names to functions. *EMBO J, 42*(7), e112699. doi:10.15252/embj.2022112699

Drygin, D., Lin, A., Bliesath, J., Ho, C. B., O'Brien, S. E., Proffitt, C., . . . Rice, W. G. (2011). Targeting RNA polymerase I with an oral small molecule CX-5461 inhibits ribosomal RNA synthesis and solid tumor growth. *Cancer Res, 71*(4), 1418-1430. doi:10.1158/0008-5472.CAN-10-1728

Drygin, D., Siddiqui-Jain, A., O'Brien, S., Schwaebe, M., Lin, A., Bliesath, J., . . . Rice, W. G. (2009). Anticancer activity of CX-3543: a direct inhibitor of rRNA biogenesis. *Cancer Res, 69*(19), 7653-7661. doi:10.1158/0008-5472.CAN-09-1304

Duo, Y., Yang, M., Du, Z., Feng, C., Xing, C., Wu, Y., . . . Chen, H. (2018). CX-5461-loaded nucleolus-targeting nanoplatform for cancer therapy through induction of pro-death autophagy. *Acta Biomater, 79*, 317-330. doi:10.1016/j.actbio.2018.08.035

El Hassouni, B., Sarkisjan, D., Vos, J. C., Giovannetti, E., & Peters, G. J. (2019). Targeting the Ribosome Biogenesis Key Molecule Fibrillarin to Avoid Chemoresistance. *Curr Med Chem, 26*(33), 6020-6032. doi:10.2174/0929867326666181203133332

Elhamamsy, A. R., Metge, B. J., Alsheikh, H. A., Shevde, L. A., & Samant, R. S. (2022). Ribosome Biogenesis: A Central Player in Cancer Metastasis and Therapeutic Resistance. *Cancer Res, 82*(13), 2344-2353. doi:10.1158/0008-5472.CAN-21-4087

Encarnacion-Rosado, J., & Kimmelman, A. C. (2021). Harnessing metabolic dependencies in pancreatic cancers. *Nat Rev Gastroenterol Hepatol, 18*(7), 482-492. doi:10.1038/s41575-021-00431-7

Espiau-Romera, P., Courtois, S., Parejo-Alonso, B., & Sancho, P. (2020). Molecular and Metabolic Subtypes Correspondence for Pancreatic Ductal Adenocarcinoma Classification. *J Clin Med, 9*(12). doi:10.3390/jcm9124128

Espinet, E., Klein, L., Pure, E., & Singh, S. K. (2022). Mechanisms of PDAC subtype heterogeneity and therapy response. *Trends Cancer, 8*(12), 1060-1071. doi:10.1016/j.trecan.2022.08.005

Evan, T., Wang, V. M., & Behrens, A. (2022). The roles of intratumour heterogeneity in the biology and treatment of pancreatic ductal adenocarcinoma. *Oncogene, 41*(42), 4686-4695. doi:10.1038/s41388-022-02448-x

Falahati, H., Pelham-Webb, B., Blythe, S., & Wieschaus, E. (2016). Nucleation by rRNA Dictates the Precision of Nucleolus Assembly. *Curr Biol, 26*(3), 277-285. doi:10.1016/j.cub.2015.11.065

Fan, W., Liu, H., Pitts, S., Ford, B., Rajeshkumar, N., & Laiho, M. (2022). Abstract 3247: Functional CRISPR-Cas9 screens identify master regulators of resistance to chemical targeting of RNA polymerase I. *Cancer Research, 82*(12_Supplement), 3247-3247. doi:10.1158/1538-7445.Am2022-3247

Fatica, A., Galardi, S., Altieri, F., & Bozzoni, I. (2000). Fibrillarin binds directly and specifically to U16 box C/D snoRNA. *RNA, 6*(1), 88-95. doi:10.1017/s1355838200991623

FC, M., Davis, T., & authors, g. (2022). ggpattern: 'ggplot2' Pattern Geoms. R package version 1.0.0. Retrieved from https://CRAN.R-project.org/package=ggpattern

Fell, J. B., Fischer, J. P., Baer, B. R., Blake, J. F., Bouhana, K., Briere, D. M., . . . Marx, M. A. (2020). Identification of the Clinical Development Candidate MRTX849, a Covalent KRAS(G12C) Inhibitor for the Treatment of Cancer. *J Med Chem, 63*(13), 6679-6693. doi:10.1021/acs.jmedchem.9b02052

Ferguson, A., Wang, L., Altman, R. B., Terry, D. S., Juette, M. F., Burnett, B. J., . . . Blanchard, S. C. (2015). Functional Dynamics within the Human Ribosome Regulate the Rate of Active Protein Synthesis. *Mol Cell, 60*(3), 475-486. doi:10.1016/j.molcel.2015.09.013

Feric, M., Vaidya, N., Harmon, T. S., Mitrea, D. M., Zhu, L., Richardson, T. M., . . . Brangwynne, C. P. (2016). Coexisting Liquid Phases Underlie Nucleolar Subcompartments. *Cell, 165*(7), 1686-1697. doi:10.1016/j.cell.2016.04.047

Fujikura, K., Hosoda, W., Felsenstein, M., Song, Q., Reiter, J. G., Zheng, L., . . . Wood, L. D. (2021). Multiregion whole-exome sequencing of intraductal papillary mucinous neoplasms reveals frequent somatic KLF4 mutations predominantly in low-grade regions. *Gut, 70*(5), 928-939. doi:10.1136/gutjnl-2020-321217

Galili, T. (2015). dendextend: an R package for visualizing, adjusting and comparing trees of hierarchical clustering. *Bioinformatics, 31*(22), 3718-3720. doi:10.1093/bioinformatics/btv428

Gao, Y., & Wang, H. (2023). Ribosome Heterogeneity in Development and Disease. *bioRxiv*, 2023.2007.2025.550527. doi:10.1101/2023.07.25.550527

Gentilella, A., Kozma, S. C., & Thomas, G. (2015). A liaison between mTOR signaling, ribosome biogenesis and cancer. *Biochim Biophys Acta, 1849*(7), 812-820. doi:10.1016/j.bbagrm.2015.02.005

Ginisty, H., Amalric, F., & Bouvet, P. (1998). Nucleolin functions in the first step of ribosomal RNA processing. *EMBO J, 17*(5), 1476-1486. doi:10.1093/emboj/17.5.1476

Ginisty, H., Sicard, H., Roger, B., & Bouvet, P. (1999). Structure and functions of nucleolin. *J Cell Sci, 112 (Pt 6)*, 761-772. doi:10.1242/jcs.112.6.761

Gjerset, R. A., & Bandyopadhyay, K. (2006). Regulation of p14ARF through subnuclear compartmentalization. *Cell Cycle, 5*(7), 686-690. doi:10.4161/cc.5.7.2623

Golan, T., Hammel, P., Reni, M., Van Cutsem, E., Macarulla, T., Hall, M. J., . . . Kindler, H. L. (2019). Maintenance Olaparib for Germline BRCA-Mutated Metastatic Pancreatic Cancer. *N Engl J Med, 381*(4), 317-327. doi:10.1056/NEJMoa1903387

Groot, V. P., Gemenetzis, G., Blair, A. B., Ding, D., Javed, A. A., Burkhart, R. A., . . . He, J. (2018). Implications of the Pattern of Disease Recurrence on Survival Following Pancreatectomy for Pancreatic Ductal Adenocarcinoma. *Ann Surg Oncol, 25*(8), 2475-2483. doi:10.1245/s10434-018-6558-7

Grossberg, A. J., Chu, L. C., Deig, C. R., Fishman, E. K., Hwang, W. L., Maitra, A., . . . Thomas, C. R., Jr. (2020). Multidisciplinary standards of care and recent progress in pancreatic ductal adenocarcinoma. *CA Cancer J Clin, 70*(5), 375-403. doi:10.3322/caac.21626

Grummt, I. (2010). Wisely chosen paths--regulation of rRNA synthesis: delivered on 30 June 2010 at the 35th FEBS Congress in Gothenburg, Sweden. *FEBS J, 277*(22), 4626-4639. doi:10.1111/j.1742-4658.2010.07892.x

Grummt, I., & Langst, G. (2013). Epigenetic control of RNA polymerase I transcription in mammalian cells. *Biochim Biophys Acta, 1829*(3-4), 393-404. doi:10.1016/j.bbagrm.2012.10.004

Guetg, C., Lienemann, P., Sirri, V., Grummt, I., Hernandez-Verdun, D., Hottiger, M. O., . . . Santoro, R. (2010). The NoRC complex mediates the heterochromatin formation and stability of silent rRNA genes and centromeric repeats. *EMBO J, 29*(13), 2135-2146. doi:10.1038/emboj.2010.17

Guimaraes, J. C., & Zavolan, M. (2016). Patterns of ribosomal protein expression specify normal and malignant human cells. *Genome Biol, 17*(1), 236. doi:10.1186/s13059-016-1104-z

Halbrook, C. J., Lyssiotis, C. A., Pasca di Magliano, M., & Maitra, A. (2023). Pancreatic cancer: Advances and challenges. *Cell, 186*(8), 1729-1754. doi:10.1016/j.cell.2023.02.014

Hanahan, D., & Weinberg, R. A. (2011). Hallmarks of cancer: the next generation. *Cell, 144*(5), 646-674. doi:10.1016/j.cell.2011.02.013

Hannan, K. M., Brandenburger, Y., Jenkins, A., Sharkey, K., Cavanaugh, A., Rothblum, L., . . . Hannan, R. D. (2003). mTOR-dependent regulation of ribosomal gene transcription requires S6K1 and is mediated by phosphorylation of the carboxy-terminal activation domain of the nucleolar transcription factor UBF. *Mol Cell Biol, 23*(23), 8862-8877. doi:10.1128/MCB.23.23.8862-8877.2003

Hayashi, A., Fan, J., Chen, R., Ho, Y. J., Makohon-Moore, A. P., Lecomte, N., . . . Iacobuzio-Donahue, C. A. (2020). A unifying paradigm for transcriptional heterogeneity and squamous features in pancreatic ductal adenocarcinoma. *Nat Cancer, 1*(1), 59-74. doi:10.1038/s43018-019-0010-1

Hegedus, L., Szucs, K. D., Kudla, M., Heidenreich, J., Jendrossek, V., Pena-Llopis, S., . . . Hegedus, B. (2022). Nintedanib and Dasatinib Treatments Induce Protective Autophagy as a Potential Resistance Mechanism in MPM Cells. *Front Cell Dev Biol, 10*, 852812. doi:10.3389/fcell.2022.852812

Heid, I., Münch, C., Karakaya, S., Lueong, S. S., Winkelkotte, A. M., Liffers, S. T., . . . Siveke, J. T. (2022). Functional noninvasive detection of glycolytic pancreatic ductal adenocarcinoma. *Cancer Metab, 10*(1), 24. doi:10.1186/s40170-022-00298-5

Henras, A. K., Plisson-Chastang, C., O'Donohue, M. F., Chakraborty, A., & Gleizes, P. E. (2015). An overview of pre-ribosomal RNA processing in eukaryotes. *Wiley Interdiscip Rev RNA, 6*(2), 225-242. doi:10.1002/wrna.1269

Henras, A. K., Soudet, J., Gerus, M., Lebaron, S., Caizergues-Ferrer, M., Mougin, A., & Henry, Y. (2008). The post-transcriptional steps of eukaryotic ribosome biogenesis. *Cell Mol Life Sci, 65*(15), 2334-2359. doi:10.1007/s00018-008-8027-0

Hilton, J., Gelmon, K., Bedard, P. L., Tu, D., Xu, H., Tinker, A. V., . . . Cescon, D. W. (2022). Results of the phase I CCTG IND.231 trial of CX-5461 in patients with advanced solid tumors enriched for DNA-repair deficiencies. *Nat Commun, 13*(1), 3607. doi:10.1038/s41467-022-31199-2

Hoppe, S., Bierhoff, H., Cado, I., Weber, A., Tiebe, M., Grummt, I., & Voit, R. (2009). AMP-activated protein kinase adapts rRNA synthesis to cellular energy supply. *Proc Natl Acad Sci U S A, 106*(42), 17781-17786. doi:10.1073/pnas.0909873106

Hurt, E., Cheng, J., Babetaler, J., Iwasa, J., & Beckmann, R. (2023). SnapShot: Eukaryotic ribosome biogenesis I. *Cell, 186*(10), 2282-2282 e2281. doi:10.1016/j.cell.2023.04.030

Ianevski, A., Giri, A. K., & Aittokallio, T. (2022). SynergyFinder 3.0: an interactive analysis and consensus interpretation of multi-drug synergies across multiple samples. *Nucleic Acids Res, 50*(W1), W739-W743. doi:10.1093/nar/gkac382

Iguchi, E., Safgren, S. L., Marks, D. L., Olson, R. L., & Fernandez-Zapico, M. E. (2016). Pancreatic Cancer, A Mis-interpreter of the Epigenetic Language. *Yale J Biol Med, 89*(4), 575-590. Retrieved from https://www.ncbi.nlm.nih.gov/pubmed/28018146

Jacobs, R. Q., Huffines, A. K., Laiho, M., & Schneider, D. A. (2022). The small-molecule BMH-21 directly inhibits transcription elongation and DNA occupancy of RNA polymerase I in vivo and in vitro. *J Biol Chem, 298*(1), 101450. doi:10.1016/j.jbc.2021.101450

James, A., Wang, Y., Raje, H., Rosby, R., & DiMario, P. (2014). Nucleolar stress with and without p53. *Nucleus, 5*(5), 402-426. doi:10.4161/nucl.32235

Jefferies, H. B., Fumagalli, S., Dennis, P. B., Reinhard, C., Pearson, R. B., & Thomas, G. (1997). Rapamycin suppresses 5'TOP mRNA translation through inhibition of p70s6k. *EMBO J, 16*(12), 3693-3704. doi:10.1093/emboj/16.12.3693

Jiao, L., Liu, Y., Yu, X. Y., Pan, X., Zhang, Y., Tu, J., . . . Li, Y. (2023). Ribosome biogenesis in disease: new players and therapeutic targets. *Signal Transduct Target Ther, 8*(1), 15. doi:10.1038/s41392-022-01285-4

Jin, A., Itahana, K., O'Keefe, K., & Zhang, Y. (2004). Inhibition of HDM2 and activation of p53 by ribosomal protein L23. *Mol Cell Biol, 24*(17), 7669-7680. doi:10.1128/MCB.24.17.7669-7680.2004

Johansson, H. J., Socciarelli, F., Vacanti, N. M., Haugen, M. H., Zhu, Y., Siavelis, I., . . . Lehtio, J. (2019). Breast cancer quantitative proteome and proteogenomic landscape. *Nat Commun, 10*(1), 1600. doi:10.1038/s41467-019-09018-y

Johnson, A. W., Lund, E., & Dahlberg, J. (2002). Nuclear export of ribosomal subunits. *Trends Biochem Sci, 27*(11), 580-585. doi:10.1016/s0968-0004(02)02208-9

Juiz, N., Elkaoutari, A., Bigonnet, M., Gayet, O., Roques, J., Nicolle, R., . . . Dusetti, N. (2020). Basal-like and classical cells coexist in pancreatic cancer revealed by single-cell analysis on biopsy-derived pancreatic cancer organoids from the classical subtype. *FASEB J, 34*(9), 12214-12228. doi:10.1096/fj.202000363RR

Kanda, M., Matthaei, H., Wu, J., Hong, S. M., Yu, J., Borges, M., . . . Goggins, M. (2012). Presence of somatic mutations in most early-stage pancreatic

intraepithelial neoplasia. *Gastroenterology, 142*(4), 730-733 e739. doi:10.1053/j.gastro.2011.12.042

Kang, J., Brajanovski, N., Chan, K. T., Xuan, J., Pearson, R. B., & Sanij, E. (2021). Ribosomal proteins and human diseases: molecular mechanisms and targeted therapy. *Signal Transduct Target Ther, 6*(1), 323. doi:10.1038/s41392-021-00728-8

Kantidakis, T., Ramsbottom, B. A., Birch, J. L., Dowding, S. N., & White, R. J. (2010). mTOR associates with TFIIIC, is found at tRNA and 5S rRNA genes, and targets their repressor Maf1. *Proc Natl Acad Sci U S A, 107*(26), 11823-11828. doi:10.1073/pnas.1005188107

Karakaya, S. (2020). *Metabolic subtyping and targeting of pancreatic ductal adenocarcinoma.* Retrieved from https://doi.org/10.17185/duepublico/73673

Karasinska, J. M., Topham, J. T., Kalloger, S. E., Jang, G. H., Denroche, R. E., Culibrk, L., . . . Schaeffer, D. F. (2020). Altered Gene Expression along the Glycolysis-Cholesterol Synthesis Axis Is Associated with Outcome in Pancreatic Cancer. *Clin Cancer Res, 26*(1), 135-146. doi:10.1158/1078-0432.CCR-19-1543

Karpinska, M., & Czauderna, M. (2022). Pancreas-Its Functions, Disorders, and Physiological Impact on the Mammals' Organism. *Front Physiol, 13*, 807632. doi:10.3389/fphys.2022.807632

Kassambara, A., Kosinski, M., & Biecek, P. (2021). _survminer: Drawing Survival Curves using 'ggplot2'_. R package version 0.4.9. Retrieved from https://CRAN.R-project.org/package=survminer

Kastenhuber, E. R., & Lowe, S. W. (2017). Putting p53 in Context. *Cell, 170*(6), 1062-1078. doi:10.1016/j.cell.2017.08.028

Katagiri, N., Kuroda, T., Kishimoto, H., Hayashi, Y., Kumazawa, T., & Kimura, K. (2015). The nucleolar protein nucleophosmin is essential for autophagy induced by inhibiting Pol I transcription. *Sci Rep, 5*, 8903. doi:10.1038/srep08903

Khot, A., Brajanovski, N., Cameron, D. P., Hein, N., Maclachlan, K. H., Sanij, E., . . . Harrison, S. J. (2019). First-in-Human RNA Polymerase I Transcription Inhibitor CX-5461 in Patients with Advanced Hematologic Cancers: Results of a Phase I Dose-Escalation Study. *Cancer Discov, 9*(8), 1036-1049. doi:10.1158/2159-8290.CD-18-1455

Klimstra, D. S. (2007). Nonductal neoplasms of the pancreas. *Mod Pathol, 20 Suppl 1*, S94-112. doi:10.1038/modpathol.3800686

Kramer, G., Boehringer, D., Ban, N., & Bukau, B. (2009). The ribosome as a platform for co-translational processing, folding and targeting of newly synthesized proteins. *Nat Struct Mol Biol, 16*(6), 589-597. doi:10.1038/nsmb.1614

Kudo, M., Anam, M. B., Istiaq, A., Ahmad, S. A. I., Ito, N., & Ohta, K. (2022). Ribosome Incorporation Induces EMT-like Phenomenon with Cell Cycle Arrest in Human Breast Cancer Cell. *Cells Tissues Organs, 211*(2), 212-221. doi:10.1159/000513908

Kurki, S., Peltonen, K., Latonen, L., Kiviharju, T. M., Ojala, P. M., Meek, D., & Laiho, M. (2004). Nucleolar protein NPM interacts with HDM2 and protects tumor suppressor protein p53 from HDM2-mediated degradation. *Cancer Cell, 5*(5), 465-475. doi:10.1016/s1535-6108(04)00110-2

Kusnadi, E. P., Trigos, A. S., Cullinane, C., Goode, D. L., Larsson, O., Devlin, J. R., . . . Pearson, R. B. (2020). Reprogrammed mRNA translation drives resistance to therapeutic targeting of ribosome biogenesis. *EMBO J, 39*(21), e105111. doi:10.15252/embj.2020105111

Laferte, A., Favry, E., Sentenac, A., Riva, M., Carles, C., & Chedin, S. (2006). The transcriptional activity of RNA polymerase I is a key determinant for the level of

all ribosome components. *Genes Dev, 20*(15), 2030-2040. doi:10.1101/gad.386106

Lafontaine, D. L., Bousquet-Antonelli, C., Henry, Y., Caizergues-Ferrer, M., & Tollervey, D. (1998). The box H + ACA snoRNAs carry Cbf5p, the putative rRNA pseudouridine synthase. *Genes Dev, 12*(4), 527-537. doi:10.1101/gad.12.4.527

Lafontaine, D. L. J., Riback, J. A., Bascetin, R., & Brangwynne, C. P. (2021). The nucleolus as a multiphase liquid condensate. *Nat Rev Mol Cell Biol, 22*(3), 165-182. doi:10.1038/s41580-020-0272-6

Lanman, B. A., Allen, J. R., Allen, J. G., Amegadzie, A. K., Ashton, K. S., Booker, S. K., . . . Cee, V. J. (2020). Discovery of a Covalent Inhibitor of KRAS(G12C) (AMG 510) for the Treatment of Solid Tumors. *J Med Chem, 63*(1), 52-65. doi:10.1021/acs.jmedchem.9b01180

Leek, J. T., Johnson, W. E., Parker, H. S., Jaffe, A. E., & Storey, J. D. (2012). The sva package for removing batch effects and other unwanted variation in high-throughput experiments. *Bioinformatics, 28*(6), 882-883. doi:10.1093/bioinformatics/bts034

Levy, S., Avni, D., Hariharan, N., Perry, R. P., & Meyuhas, O. (1991). Oligopyrimidine tract at the 5' end of mammalian ribosomal protein mRNAs is required for their translational control. *Proc Natl Acad Sci U S A, 88*(8), 3319-3323. doi:10.1073/pnas.88.8.3319

Li, D., & Wang, J. (2020). Ribosome heterogeneity in stem cells and development. *J Cell Biol, 219*(6). doi:10.1083/jcb.202001108

Liao, J. M., Zhou, X., Gatignol, A., & Lu, H. (2014). Ribosomal proteins L5 and L11 co-operatively inactivate c-Myc via RNA-induced silencing complex. *Oncogene, 33*(41), 4916-4923. doi:10.1038/onc.2013.430

Liu, R., Iadevaia, V., Averous, J., Taylor, P. M., Zhang, Z., & Proud, C. G. (2014). Impairing the production of ribosomal RNA activates mammalian target of rapamycin complex 1 signalling and downstream translation factors. *Nucleic Acids Res, 42*(8), 5083-5096. doi:10.1093/nar/gku130

Livak, K. J., & Schmittgen, T. D. (2001). Analysis of relative gene expression data using real-time quantitative PCR and the 2(-Delta Delta C(T)) Method. *Methods, 25*(4), 402-408. doi:10.1006/meth.2001.1262

Logsdon, C. D. (2004). Pancreatic Enzyme Secretion (Physiology). In L. R. Johnson (Ed.), *Encyclopedia of Gastroenterology* (pp. Pages 68-75): Elsevier.

Love, M. I., Huber, W., & Anders, S. (2014). Moderated estimation of fold change and dispersion for RNA-seq data with DESeq2. *Genome Biol, 15*(12), 550. doi:10.1186/s13059-014-0550-8

Luo, J. (2021). KRAS mutation in pancreatic cancer. *Semin Oncol, 48*(1), 10-18. doi:10.1053/j.seminoncol.2021.02.003

Luo, W., Yang, G., Qiu, J., Luan, J., Zhang, Y., You, L., . . . Zhao, Y. (2019). Novel discoveries targeting gemcitabine-based chemoresistance and new therapies in pancreatic cancer: How far are we from the destination? *Cancer Med, 8*(14), 6403-6413. doi:10.1002/cam4.2384

Maehama, T., Nishio, M., Otani, J., Mak, T. W., & Suzuki, A. (2023). Nucleolar stress: Molecular mechanisms and related human diseases. *Cancer Sci, 114*(5), 2078-2086. doi:10.1111/cas.15755

Marcel, V., Ghayad, S. E., Belin, S., Therizols, G., Morel, A. P., Solano-Gonzalez, E., . . . Diaz, J. J. (2013). p53 acts as a safeguard of translational control by regulating fibrillarin and rRNA methylation in cancer. *Cancer Cell, 24*(3), 318-330. doi:10.1016/j.ccr.2013.08.013

Marino, G., Niso-Santano, M., Baehrecke, E. H., & Kroemer, G. (2014). Self-consumption: the interplay of autophagy and apoptosis. *Nat Rev Mol Cell Biol, 15*(2), 81-94. doi:10.1038/nrm3735

Mayer, C., Bierhoff, H., & Grummt, I. (2005). The nucleolus as a stress sensor: JNK2 inactivates the transcription factor TIF-IA and down-regulates rRNA synthesis. *Genes Dev, 19*(8), 933-941. doi:10.1101/gad.333205

Mayer, C., Zhao, J., Yuan, X., & Grummt, I. (2004). mTOR-dependent activation of the transcription factor TIF-IA links rRNA synthesis to nutrient availability. *Genes Dev, 18*(4), 423-434. doi:10.1101/gad.285504

Mazur, P. K., Herner, A., Mello, S. S., Wirth, M., Hausmann, S., Sanchez-Rivera, F. J., . . . Siveke, J. T. (2015). Combined inhibition of BET family proteins and histone deacetylases as a potential epigenetics-based therapy for pancreatic ductal adenocarcinoma. *Nat Med, 21*(10), 1163-1171. doi:10.1038/nm.3952

McGuigan, A., Kelly, P., Turkington, R. C., Jones, C., Coleman, H. G., & McCain, R. S. (2018). Pancreatic cancer: A review of clinical diagnosis, epidemiology, treatment and outcomes. *World J Gastroenterol, 24*(43), 4846-4861. doi:10.3748/wjg.v24.i43.4846

Meshorer, E., & Misteli, T. (2006). Chromatin in pluripotent embryonic stem cells and differentiation. *Nat Rev Mol Cell Biol, 7*(7), 540-546. doi:10.1038/nrm1938

Metge, B. J., Kammerud, S. C., Pruitt, H. C., Shevde, L. A., & Samant, R. S. (2021). Hypoxia re-programs 2'-O-Me modifications on ribosomal RNA. *iScience, 24*(1), 102010. doi:10.1016/j.isci.2020.102010

Metz, D. C., & Jensen, R. T. (2008). Gastrointestinal neuroendocrine tumors: pancreatic endocrine tumors. *Gastroenterology, 135*(5), 1469-1492. doi:10.1053/j.gastro.2008.05.047

Miller, G., Panov, K. I., Friedrich, J. K., Trinkle-Mulcahy, L., Lamond, A. I., & Zomerdijk, J. C. (2001). hRRN3 is essential in the SL1-mediated recruitment of RNA Polymerase I to rRNA gene promoters. *EMBO J, 20*(6), 1373-1382. doi:10.1093/emboj/20.6.1373

Moffitt, R. A., Marayati, R., Flate, E. L., Volmar, K. E., Loeza, S. G., Hoadley, K. A., . . . Yeh, J. J. (2015). Virtual microdissection identifies distinct tumor- and stroma-specific subtypes of pancreatic ductal adenocarcinoma. *Nat Genet, 47*(10), 1168-1178. doi:10.1038/ng.3398

Mootha, V. K., Lindgren, C. M., Eriksson, K. F., Subramanian, A., Sihag, S., Lehar, J., . . . Groop, L. C. (2003). PGC-1alpha-responsive genes involved in oxidative phosphorylation are coordinately downregulated in human diabetes. *Nat Genet, 34*(3), 267-273. doi:10.1038/ng1180

Morris, J. H., Kuchinsky, A., Ferrin, T. E., & Pico, A. R. (2014). enhancedGraphics: a Cytoscape app for enhanced node graphics. *F1000Res, 3*, 147. doi:10.12688/f1000research.4460.1

Murayama, A., Ohmori, K., Fujimura, A., Minami, H., Yasuzawa-Tanaka, K., Kuroda, T., . . . Yanagisawa, J. (2008). Epigenetic control of rDNA loci in response to intracellular energy status. *Cell, 133*(4), 627-639. doi:10.1016/j.cell.2008.03.030

Nadano, D., Notsu, T., Matsuda, T., & Sato, T. (2002). A human gene encoding a protein homologous to ribosomal protein L39 is normally expressed in the testis and derepressed in multiple cancer cells. *Biochim Biophys Acta, 1577*(3), 430-436. doi:10.1016/s0167-4781(02)00445-1

Neuwirth, E. (2022). RColorBrewer: ColorBrewer Palettes. R package version 1.1-3. Retrieved from https://CRAN.R-project.org/package=RColorBrewer

Nicolle, R., Blum, Y., Duconseil, P., Vanbrugghe, C., Brandone, N., Poizat, F., . . . Dusetti, N. (2020). Establishment of a pancreatic adenocarcinoma molecular

gradient (PAMG) that predicts the clinical outcome of pancreatic cancer. *EBioMedicine, 57*, 102858. doi:10.1016/j.ebiom.2020.102858

Norris, K., Hopes, T., & Aspden, J. L. (2021). Ribosome heterogeneity and specialization in development. *Wiley Interdiscip Rev RNA, 12*(4), e1644. doi:10.1002/wrna.1644

Orsolic, I., Jurada, D., Pullen, N., Oren, M., Eliopoulos, A. G., & Volarevic, S. (2016). The relationship between the nucleolus and cancer: Current evidence and emerging paradigms. *Semin Cancer Biol, 37-38*, 36-50. doi:10.1016/j.semcancer.2015.12.004

Orth, M., Metzger, P., Gerum, S., Mayerle, J., Schneider, G., Belka, C., . . . Lauber, K. (2019). Pancreatic ductal adenocarcinoma: biological hallmarks, current status, and future perspectives of combined modality treatment approaches. *Radiat Oncol, 14*(1), 141. doi:10.1186/s13014-019-1345-6

Otto, C., Kastner, C., Schmidt, S., Uttinger, K., Baluapuri, A., Denk, S., . . . Wiegering, A. (2022). RNA polymerase I inhibition induces terminal differentiation, growth arrest, and vulnerability to senolytics in colorectal cancer cells. *Mol Oncol, 16*(15), 2788-2809. doi:10.1002/1878-0261.13265

Palamaris, K., Felekouras, E., & Sakellariou, S. (2021). Epithelial to Mesenchymal Transition: Key Regulator of Pancreatic Ductal Adenocarcinoma Progression and Chemoresistance. *Cancers (Basel), 13*(21). doi:10.3390/cancers13215532

Pelletier, J., Thomas, G., & Volarevic, S. (2018). Ribosome biogenesis in cancer: new players and therapeutic avenues. *Nat Rev Cancer, 18*(1), 51-63. doi:10.1038/nrc.2017.104

Peltonen, K., Colis, L., Liu, H., Jaamaa, S., Moore, H. M., Enback, J., . . . Laiho, M. (2010). Identification of novel p53 pathway activating small-molecule compounds reveals unexpected similarities with known therapeutic agents. *PLoS One, 5*(9), e12996. doi:10.1371/journal.pone.0012996

Peltonen, K., Colis, L., Liu, H., Trivedi, R., Moubarek, M. S., Moore, H. M., . . . Laiho, M. (2014). A targeting modality for destruction of RNA polymerase I that possesses anticancer activity. *Cancer Cell, 25*(1), 77-90. doi:10.1016/j.ccr.2013.12.009

Penzo, M., Montanaro, L., Trere, D., & Derenzini, M. (2019). The Ribosome Biogenesis-Cancer Connection. *Cells, 8*(1). doi:10.3390/cells8010055

Pereira, S. P., Oldfield, L., Ney, A., Hart, P. A., Keane, M. G., Pandol, S. J., . . . Costello, E. (2020). Early detection of pancreatic cancer. *Lancet Gastroenterol Hepatol, 5*(7), 698-710. doi:10.1016/S2468-1253(19)30416-9

Petiot, A., Ogier-Denis, E., Blommaart, E. F., Meijer, A. J., & Codogno, P. (2000). Distinct classes of phosphatidylinositol 3'-kinases are involved in signaling pathways that control macroautophagy in HT-29 cells. *J Biol Chem, 275*(2), 992-998. doi:10.1074/jbc.275.2.992

Pfister, A. S. (2019). Emerging Role of the Nucleolar Stress Response in Autophagy. *Front Cell Neurosci, 13*, 156. doi:10.3389/fncel.2019.00156

Pfister, A. S. (2023). An Update on Nucleolar Stress: The Transcriptional Control of Autophagy. *Cells, 12*(16). doi:10.3390/cells12162071

Pianese, G. (1896). Beitraege zur Histologie und Aetiologie der Carconoms.[Contributions to the histology and etiology of carcinomas.]. *Beitr Pathol Anat Allgem Pathol, 142*, 1-193.

Prakash, V., Carson, B. B., Feenstra, J. M., Dass, R. A., Sekyrova, P., Hoshino, A., . . . Vincent, C. T. (2019). Ribosome biogenesis during cell cycle arrest fuels EMT in development and disease. *Nat Commun, 10*(1), 2110. doi:10.1038/s41467-019-10100-8

Principe, D. R., Underwood, P. W., Korc, M., Trevino, J. G., Munshi, H. G., & Rana, A. (2021). The Current Treatment Paradigm for Pancreatic Ductal Adenocarcinoma and Barriers to Therapeutic Efficacy. *Front Oncol, 11*, 688377. doi:10.3389/fonc.2021.688377

Priyadarshini, N., Venkatarama Puppala, N., Jayaprakash, J. P., Khandelia, P., Sharma, V., & Mohannath, G. (2023). Downregulation of ribosomal RNA (rRNA) genes in human head and neck squamous cell carcinoma (HNSCC) cells correlates with rDNA promoter hypermethylation. *Gene, 888*, 147793. doi:10.1016/j.gene.2023.147793

Qian, Z. R., Rubinson, D. A., Nowak, J. A., Morales-Oyarvide, V., Dunne, R. F., Kozak, M. M., . . . Wolpin, B. M. (2018). Association of Alterations in Main Driver Genes With Outcomes of Patients With Resected Pancreatic Ductal Adenocarcinoma. *JAMA Oncol, 4*(3), e173420. doi:10.1001/jamaoncol.2017.3420

R Core Team. (2022). R: A language and environment for statistical computing. R Foundation for Statistical Computing. Vienna, Austria. . Retrieved from https://www.R-project.org/

Rahib, L., Smith, B. D., Aizenberg, R., Rosenzweig, A. B., Fleshman, J. M., & Matrisian, L. M. (2014). Projecting cancer incidence and deaths to 2030: the unexpected burden of thyroid, liver, and pancreas cancers in the United States. *Cancer Res, 74*(11), 2913-2921. doi:10.1158/0008-5472.CAN-14-0155

Ramakrishnan, V. (2002). Ribosome structure and the mechanism of translation. *Cell, 108*(4), 557-572. doi:10.1016/s0092-8674(02)00619-0

Raska, I., Shaw, P. J., & Cmarko, D. (2006). New insights into nucleolar architecture and activity. *Int Rev Cytol, 255*, 177-235. doi:10.1016/S0074-7696(06)55004-1

Raudvere, U., Kolberg, L., Kuzmin, I., Arak, T., Adler, P., Peterson, H., & Vilo, J. (2019). g:Profiler: a web server for functional enrichment analysis and conversions of gene lists (2019 update). *Nucleic Acids Res, 47*(W1), W191-W198. doi:10.1093/nar/gkz369

Rebello, R. J., Kusnadi, E., Cameron, D. P., Pearson, H. B., Lesmana, A., Devlin, J. R., . . . Furic, L. (2016). The Dual Inhibition of RNA Pol I Transcription and PIM Kinase as a New Therapeutic Approach to Treat Advanced Prostate Cancer. *Clin Cancer Res, 22*(22), 5539-5552. doi:10.1158/1078-0432.CCR-16-0124

Ritz, C., Baty, F., Streibig, J. C., & Gerhard, D. (2015). Dose-Response Analysis Using R. *PLoS One, 10*(12), e0146021. doi:10.1371/journal.pone.0146021

Röder, P. V., Wu, B., Liu, Y., & Han, W. (2016). Pancreatic regulation of glucose homeostasis. *Exp Mol Med, 48*(3), e219. doi:10.1038/emm.2016.6

RStudio Team. (2022). RStudio: Integrated Development Environment for R. . RStudio, PBC, Boston, MA. . Retrieved from http://www.rstudio.com/

Ruggero, D. (2009). The role of Myc-induced protein synthesis in cancer. *Cancer Res, 69*(23), 8839-8843. doi:10.1158/0008-5472.CAN-09-1970

Ruggero, D. (2013). Translational control in cancer etiology. *Cold Spring Harb Perspect Biol, 5*(2). doi:10.1101/cshperspect.a012336

Ruggero, D., & Pandolfi, P. P. (2003). Does the ribosome translate cancer? *Nat Rev Cancer, 3*(3), 179-192. doi:10.1038/nrc1015

Russo, A., Esposito, D., Catillo, M., Pietropaolo, C., Crescenzi, E., & Russo, G. (2013). Human rpL3 induces G(1)/S arrest or apoptosis by modulating p21 (waf1/cip1) levels in a p53-independent manner. *Cell Cycle, 12*(1), 76-87. doi:10.4161/cc.22963

Russo, A., Pagliara, V., Albano, F., Esposito, D., Sagar, V., Loreni, F., . . . Russo, G. (2016). Regulatory role of rpL3 in cell response to nucleolar stress induced by Act D in tumor cells lacking functional p53. *Cell Cycle, 15*(1), 41-51. doi:10.1080/15384101.2015.1120926

Russo, A., & Russo, G. (2017). Ribosomal Proteins Control or Bypass p53 during Nucleolar Stress. *Int J Mol Sci, 18*(1). doi:10.3390/ijms18010140

Sally, A., McGowan, R., Finn, K., & Moran, B. M. (2022). Current and Future Therapies for Pancreatic Ductal Adenocarcinoma. *Cancers (Basel), 14*(10). doi:10.3390/cancers14102417

Santoro, R., Li, J., & Grummt, I. (2002). The nucleolar remodeling complex NoRC mediates heterochromatin formation and silencing of ribosomal gene transcription. *Nat Genet, 32*(3), 393-396. doi:10.1038/ng1010

Savic, N., Bar, D., Leone, S., Frommel, S. C., Weber, F. A., Vollenweider, E., . . . Santoro, R. (2014). lncRNA maturation to initiate heterochromatin formation in the nucleolus is required for exit from pluripotency in ESCs. *Cell Stem Cell, 15*(6), 720-734. doi:10.1016/j.stem.2014.10.005

Saxton, R. A., & Sabatini, D. M. (2017). mTOR Signaling in Growth, Metabolism, and Disease. *Cell, 169*(2), 361-371. doi:10.1016/j.cell.2017.03.035

Schiff, P. B., & Horwitz, S. B. (1980). Taxol stabilizes microtubules in mouse fibroblast cells. *Proc Natl Acad Sci U S A, 77*(3), 1561-1565. doi:10.1073/pnas.77.3.1561

Schmidt, C. A., Fisher-Wellman, K. H., & Neufer, P. D. (2021). From OCR and ECAR to energy: Perspectives on the design and interpretation of bioenergetics studies. *J Biol Chem, 297*(4), 101140. doi:10.1016/j.jbc.2021.101140

Schneider, G., Wirth, M., Keller, U., & Saur, D. (2021). Rationale for MYC imaging and targeting in pancreatic cancer. *EJNMMI Res, 11*(1), 104. doi:10.1186/s13550-021-00843-1

Shalem, O., Sanjana, N. E., Hartenian, E., Shi, X., Scott, D. A., Mikkelson, T., . . . Zhang, F. (2014). Genome-scale CRISPR-Cas9 knockout screening in human cells. *Science, 343*(6166), 84-87. doi:10.1126/science.1247005

Shannon, P., Markiel, A., Ozier, O., Baliga, N. S., Wang, J. T., Ramage, D., . . . Ideker, T. (2003). Cytoscape: a software environment for integrated models of biomolecular interaction networks. *Genome Res, 13*(11), 2498-2504. doi:10.1101/gr.1239303

Sharifi, S., & Bierhoff, H. (2018). Regulation of RNA Polymerase I Transcription in Development, Disease, and Aging. *Annu Rev Biochem, 87*, 51-73. doi:10.1146/annurev-biochem-062917-012612

Sherman, M. H., & Beatty, G. L. (2023). Tumor Microenvironment in Pancreatic Cancer Pathogenesis and Therapeutic Resistance. *Annu Rev Pathol, 18*, 123-148. doi:10.1146/annurev-pathmechdis-031621-024600

Shi, Z., Fujii, K., Kovary, K. M., Genuth, N. R., Rost, H. L., Teruel, M. N., & Barna, M. (2017). Heterogeneous Ribosomes Preferentially Translate Distinct Subpools of mRNAs Genome-wide. *Mol Cell, 67*(1), 71-83 e77. doi:10.1016/j.molcel.2017.05.021

Shih, H. P., Wang, A., & Sander, M. (2013). Pancreas organogenesis: from lineage determination to morphogenesis. *Annu Rev Cell Dev Biol, 29*, 81-105. doi:10.1146/annurev-cellbio-101512-122405

Shor, B., Wu, J., Shakey, Q., Toral-Barza, L., Shi, C., Follettie, M., & Yu, K. (2010). Requirement of the mTOR kinase for the regulation of Maf1 phosphorylation and control of RNA polymerase III-dependent transcription in cancer cells. *J Biol Chem, 285*(20), 15380-15392. doi:10.1074/jbc.M109.071639

Siegel, R. L., Miller, K. D., Wagle, N. S., & Jemal, A. (2023). Cancer statistics, 2023. *CA Cancer J Clin, 73*(1), 17-48. doi:10.3322/caac.21763

Silwal-Pandit, L., Stalberg, S. M., Johansson, H. J., Mermelekas, G., Lothe, I. M. B., Skrede, M. L., . . . Kure, E. H. (2022). Proteome Analysis of Pancreatic Tumors Implicates Extracellular Matrix in Patient Outcome. *Cancer Res Commun, 2*(6), 434-446. doi:10.1158/2767-9764.CRC-21-0100

Sonenberg, N., & Hinnebusch, A. G. (2009). Regulation of translation initiation in eukaryotes: mechanisms and biological targets. *Cell, 136*(4), 731-745. doi:10.1016/j.cell.2009.01.042

Spahn, C. M., Beckmann, R., Eswar, N., Penczek, P. A., Sali, A., Blobel, G., & Frank, J. (2001). Structure of the 80S ribosome from Saccharomyces cerevisiae--tRNA-ribosome and subunit-subunit interactions. *Cell, 107*(3), 373-386. doi:10.1016/s0092-8674(01)00539-6

Stefanovsky, V. Y., Pelletier, G., Hannan, R., Gagnon-Kugler, T., Rothblum, L. I., & Moss, T. (2001). An immediate response of ribosomal transcription to growth factor stimulation in mammals is mediated by ERK phosphorylation of UBF. *Mol Cell, 8*(5), 1063-1073. doi:10.1016/s1097-2765(01)00384-7

Strickler, J. H., Satake, H., George, T. J., Yaeger, R., Hollebecque, A., Garrido-Laguna, I., . . . Hong, D. S. (2023). Sotorasib in KRAS p.G12C-Mutated Advanced Pancreatic Cancer. *N Engl J Med, 388*(1), 33-43. doi:10.1056/NEJMoa2208470

Subramanian, A., Tamayo, P., Mootha, V. K., Mukherjee, S., Ebert, B. L., Gillette, M. A., . . . Mesirov, J. P. (2005). Gene set enrichment analysis: a knowledge-based approach for interpreting genome-wide expression profiles. *Proc Natl Acad Sci U S A, 102*(43), 15545-15550. doi:10.1073/pnas.0506580102

Sung, H., Ferlay, J., Siegel, R. L., Laversanne, M., Soerjomataram, I., Jemal, A., & Bray, F. (2021). Global Cancer Statistics 2020: GLOBOCAN Estimates of Incidence and Mortality Worldwide for 36 Cancers in 185 Countries. *CA Cancer J Clin, 71*(3), 209-249. doi:10.3322/caac.21660

Tafforeau, L., Zorbas, C., Langhendries, J. L., Mullineux, S. T., Stamatopoulou, V., Mullier, R., . . . Lafontaine, D. L. (2013). The complexity of human ribosome biogenesis revealed by systematic nucleolar screening of Pre-rRNA processing factors. *Mol Cell, 51*(4), 539-551. doi:10.1016/j.molcel.2013.08.011

Therneau, T. (2022). A Package for Survival Analysis in R. R package version 3.4-0. Retrieved from https://CRAN.R-project.org/package=survival

Trajkovic-Arsic, M., Heid, I., Steiger, K., Gupta, A., Fingerle, A., Worner, C., . . . Siveke, J. T. (2017). Apparent Diffusion Coefficient (ADC) predicts therapy response in pancreatic ductal adenocarcinoma. *Sci Rep, 7*(1), 17038. doi:10.1038/s41598-017-16826-z

Tschochner, H., & Hurt, E. (2003). Pre-ribosomes on the road from the nucleolus to the cytoplasm. *Trends Cell Biol, 13*(5), 255-263. doi:10.1016/s0962-8924(03)00054-0

Uhlen, M., Zhang, C., Lee, S., Sjostedt, E., Fagerberg, L., Bidkhori, G., . . . Ponten, F. (2017). A pathology atlas of the human cancer transcriptome. *Science, 357*(6352). doi:10.1126/science.aan2507

Utomo, W. K., Narayanan, V., Biermann, K., van Eijck, C. H., Bruno, M. J., Peppelenbosch, M. P., & Braat, H. (2014). mTOR is a promising therapeutical target in a subpopulation of pancreatic adenocarcinoma. *Cancer Lett, 346*(2), 309-317. doi:10.1016/j.canlet.2014.01.014

van Dijk, D. P. J., Horstman, A. M. H., Smeets, J. S. J., den Dulk, M., Grabsch, H. I., Dejong, C. H. C., . . . van Loon, L. J. C. (2019). Tumour-specific and organ-specific protein synthesis rates in patients with pancreatic cancer. *J Cachexia Sarcopenia Muscle, 10*(3), 549-556. doi:10.1002/jcsm.12419

van Riggelen, J., Yetil, A., & Felsher, D. W. (2010). MYC as a regulator of ribosome biogenesis and protein synthesis. *Nat Rev Cancer, 10*(4), 301-309. doi:10.1038/nrc2819

Vega-Rubin-de-Celis, S., Zou, Z., Fernandez, A. F., Ci, B., Kim, M., Xiao, G., . . . Levine, B. (2018). Increased autophagy blocks HER2-mediated breast

tumorigenesis. *Proc Natl Acad Sci U S A, 115*(16), 4176-4181. doi:10.1073/pnas.1717800115

Von Hoff, D. D., Ervin, T., Arena, F. P., Chiorean, E. G., Infante, J., Moore, M., . . . Renschler, M. F. (2013). Increased survival in pancreatic cancer with nab-paclitaxel plus gemcitabine. *N Engl J Med, 369*(18), 1691-1703. doi:10.1056/NEJMoa1304369

Waddell, N., Pajic, M., Patch, A. M., Chang, D. K., Kassahn, K. S., Bailey, P., . . . Grimmond, S. M. (2015). Whole genomes redefine the mutational landscape of pancreatic cancer. *Nature, 518*(7540), 495-501. doi:10.1038/nature14169

Wang, X., Allen, S., Blake, J. F., Bowcut, V., Briere, D. M., Calinisan, A., . . . Marx, M. A. (2022). Identification of MRTX1133, a Noncovalent, Potent, and Selective KRAS(G12D) Inhibitor. *J Med Chem, 65*(4), 3123-3133. doi:10.1021/acs.jmedchem.1c01688

Warner, J. R. (1999). The economics of ribosome biosynthesis in yeast. *Trends Biochem Sci, 24*(11), 437-440. doi:10.1016/s0968-0004(99)01460-7

Warnes, G., Bolker, B., Bonebakker, L., Gentleman, R., Huber, W., Liaw, A., . . . Venables, B. (2022). gplots: Various R Programming Tools for Plotting Data. R package version 3.1.3. Retrieved from https://CRAN.R-project.org/package=gplots

Weeks, S. E., Kammerud, S. C., Metge, B. J., AlSheikh, H. A., Schneider, D. A., Chen, D., . . . Samant, R. S. (2021). Inhibiting beta-catenin disables nucleolar functions in triple-negative breast cancer. *Cell Death Dis, 12*(3), 242. doi:10.1038/s41419-021-03531-z

Werle, S. D., Ikonomi, N., Lausser, L., Kestler, A., Weidner, F. M., Schwab, J. D., . . . Kestler, H. A. (2023). A systems biology approach to define mechanisms, phenotypes, and drivers in PanNETs with a personalized perspective. *NPJ Syst Biol Appl, 9*(1), 22. doi:10.1038/s41540-023-00283-8

Wickham, H., Averick, M., Bryan, J., Chang, W., McGowan, L. D., François, R., . . . Yutani, H. (2019). Welcome to the tidyverse. *Journal of Open Source Software, *4*(43), 1686.* doi:10.21105/joss.01686.

Will, R., Bauer, K., Kudla, M., Montero-Vergara, J., Wiemann, S., Jendrossek, V., . . . Vega-Rubin-de-Celis, S. (2022). A Dual HiBiT-GFP-LC3 Lentiviral Reporter for Autophagy Flux Assessment. *Methods Mol Biol, 2445*, 75-98. doi:10.1007/978-1-0716-2071-7_6

Wong, M. C. S., Jiang, J. Y., Liang, M., Fang, Y., Yeung, M. S., & Sung, J. J. Y. (2017). Global temporal patterns of pancreatic cancer and association with socioeconomic development. *Sci Rep, 7*(1), 3165. doi:10.1038/s41598-017-02997-2

Wong, Q. W., Li, J., Ng, S. R., Lim, S. G., Yang, H., & Vardy, L. A. (2014). RPL39L is an example of a recently evolved ribosomal protein paralog that shows highly specific tissue expression patterns and is upregulated in ESCs and HCC tumors. *RNA Biol, 11*(1), 33-41. doi:10.4161/rna.27427

Wool, I. G. (1996). Extraribosomal functions of ribosomal proteins. *Trends Biochem Sci, 21*(5), 164-165. Retrieved from https://www.ncbi.nlm.nih.gov/pubmed/8871397

Xu, H., Di Antonio, M., McKinney, S., Mathew, V., Ho, B., O'Neil, N. J., . . . Aparicio, S. (2017). CX-5461 is a DNA G-quadruplex stabilizer with selective lethality in BRCA1/2 deficient tumours. *Nat Commun, 8*, 14432. doi:10.1038/ncomms14432

Xue, S., & Barna, M. (2012). Specialized ribosomes: a new frontier in gene regulation and organismal biology. *Nat Rev Mol Cell Biol, 13*(6), 355-369. doi:10.1038/nrm3359

Yan, T. T., Fu, X. L., Li, J., Bian, Y. N., Liu, D. J., Hua, R., . . . Hong, J. (2015). Downregulation of RPL15 may predict poor survival and associate with tumor progression in pancreatic ductal adenocarcinoma. *Oncotarget, 6*(35), 37028-37042. doi:10.18632/oncotarget.5939

Yang, K., Yang, J., & Yi, J. (2018). Nucleolar Stress: hallmarks, sensing mechanism and diseases. *Cell Stress, 2*(6), 125-140. doi:10.15698/cst2018.06.139

Yao, R. W., Xu, G., Wang, Y., Shan, L., Luan, P. F., Wang, Y., . . . Chen, L. L. (2019). Nascent Pre-rRNA Sorting via Phase Separation Drives the Assembly of Dense Fibrillar Components in the Human Nucleolus. *Mol Cell, 76*(5), 767-783 e711. doi:10.1016/j.molcel.2019.08.014

Ye, J., Coulouris, G., Zaretskaya, I., Cutcutache, I., Rozen, S., & Madden, T. L. (2012). Primer-BLAST: a tool to design target-specific primers for polymerase chain reaction. *BMC Bioinformatics, 13*, 134. doi:10.1186/1471-2105-13-134

Yuan, X., Feng, W., Imhof, A., Grummt, I., & Zhou, Y. (2007). Activation of RNA polymerase I transcription by cockayne syndrome group B protein and histone methyltransferase G9a. *Mol Cell, 27*(4), 585-595. doi:10.1016/j.molcel.2007.06.021

Zhai, W., & Comai, L. (2000). Repression of RNA polymerase I transcription by the tumor suppressor p53. *Mol Cell Biol, 20*(16), 5930-5938. doi:10.1128/MCB.20.16.5930-5938.2000

Zhang, Z., Wang, H., Li, M., Rayburn, E. R., Agrawal, S., & Zhang, R. (2005). Stabilization of E2F1 protein by MDM2 through the E2F1 ubiquitination pathway. *Oncogene, 24*(48), 7238-7247. doi:10.1038/sj.onc.1208814

Zhao, J., Yuan, X., Frodin, M., & Grummt, I. (2003). ERK-dependent phosphorylation of the transcription initiation factor TIF-IA is required for RNA polymerase I transcription and cell growth. *Mol Cell, 11*(2), 405-413. doi:10.1016/s1097-2765(03)00036-4

Zhen, D. B., Rabe, K. G., Gallinger, S., Syngal, S., Schwartz, A. G., Goggins, M. G., . . . Petersen, G. M. (2015). BRCA1, BRCA2, PALB2, and CDKN2A mutations in familial pancreatic cancer: a PACGENE study. *Genet Med, 17*(7), 569-577. doi:10.1038/gim.2014.153

Zhou, X., Hao, Q., Liao, J. M., Liao, P., & Lu, H. (2013). Ribosomal protein S14 negatively regulates c-Myc activity. *J Biol Chem, 288*(30), 21793-21801. doi:10.1074/jbc.M112.445122

Zhou, Y., Schmitz, K. M., Mayer, C., Yuan, X., Akhtar, A., & Grummt, I. (2009). Reversible acetylation of the chromatin remodelling complex NoRC is required for non-coding RNA-dependent silencing. *Nat Cell Biol, 11*(8), 1010-1016. doi:10.1038/ncb1914

Zisi, A., Kanellis, D. C., Moussaud, S., Karlsson, I., Caren, H., Brautigam, L., . . . Lindstrom, M. S. (2023). Small molecule-mediated disruption of ribosome biogenesis synergizes with FGFR inhibitors to suppress glioma cell growth. *Neuro Oncol, 25*(6), 1058-1072. doi:10.1093/neuonc/noac286

Appendix

List of Abbreviations

Abbreviation	*Description*
%	Percent
% v/v	Volume percent
% w/v	Weight percent
°C	Degree celsius
µL	Microliter
µM	Micromolar
5-FU	5-Fluorouracil
BCA	Bicinchoninic acid
BPE	Bovine pituitary extract
BSA	Bovine serum albumin
cDNA	Complementary DNA
DAPI	4′,6-diamidino-2-phenylindole
DFC	Dense fibrillar component
DMEM	Dulbecco’s Modified Eagle Medium
DMSO	Dimethyl sulfoxide
DNA	Deoxyribonucleic acid
ECAR	Extracellular acidification rate
EDTA	Ethylenediaminetetraacetic acid
EMT	Epithelial-mesenchymal transition
ETS	External transcribed spacer
FBS	Fetal bovine serum
FC	Fibrillar center
FDR	False discovery rate
FFPE	Formalin-fixed, paraffin-embedded
Fwd	Forward

Abbreviation	*Description*
G4	G-quadruplex
GC	Granular component
GFP	Green fluorescent protein
GSEA	Gene set enrichment analysis
h	Hour
hEGF	Human epidermal growth factor
HRP	Horseradish peroxidase
IC_{50}	Half maximal inhibitory concentration
IF	Immunofluorescence
IHC	Immunohistochemistry
IPMN	Intraductal papillary mucinous neoplasm
IRBC	Impaired ribosome biogenesis checkpoint
IRES	Internal ribosome entry site
ITS	Internal transcribed spacer
LLPS	Liquid-liquid phase separation
MET	Mesenchymal-epithelial transition
min	Minute
mL	Milliliter
mM	Millimolar
mRNA	Messenger RNA
Nab-paclitaxel	Nanoparticle albumin-bound paclitaxel
NC	Negative control
NES	Normalized enrichment score
ng	Nanogram
NGS	Normal goat serum
nM	Nanomolar
NoRC	Nucleolar chromatin remodeling complex
OCR	Oxygen consumption rate

Abbreviation	*Description*
OxPhos	Oxidative phosphorylation
PanIN	Pancreatic intraepithelial neoplasia
PanNET	Pancreatic neuroendocrine tumor
PBS	Phosphate-buffered saline
PBS-T	PBS + 0.05% Triton X-100
PDAC	Pancreatic ductal adenocarcinoma
PDC	Patient-derived cells
PDX	Patient-derived xenografts
PFA	Paraformaldehyde
QM	Quasi-mesenchymal
q(RT-)PCR	Quantitative (real-time) polymerase chain reaction
RBF	Ribosome biogenesis factor
rDNA	Ribosomal DNA
RFU	Relative fluorescent unit
RiBi	Ribosome biogenesis
RNA	Ribonucleic acid
RNA Pol	RNA polymerase
RP	Ribosomal protein
RPL	Ribosomal protein (large subunit)
RPMI	Roswell Park Memorial Institute
RPS	Ribosomal protein (small subunit)
rRNA	Ribosomal RNA
RT	Room temperature
Rvs	Reverse
S	Svedberg unit
s	Second
SD	Standard deviation

Abbreviation	*Description*
siRNA	Small interfering RNA
snoRNP	Small nucleolar ribonucleoprotein complex
SNP	Single nucleotide polymorphism
TBS	Tris-buffered saline
TCA	Tricarboxylic acid
TCGA	The Cancer Genome Atlas
tRNA	Transfer RNA
5’ TOP	5’ Terminal Oligopyrimidine tract

List of Figures

List of Tables

Annexed Figures

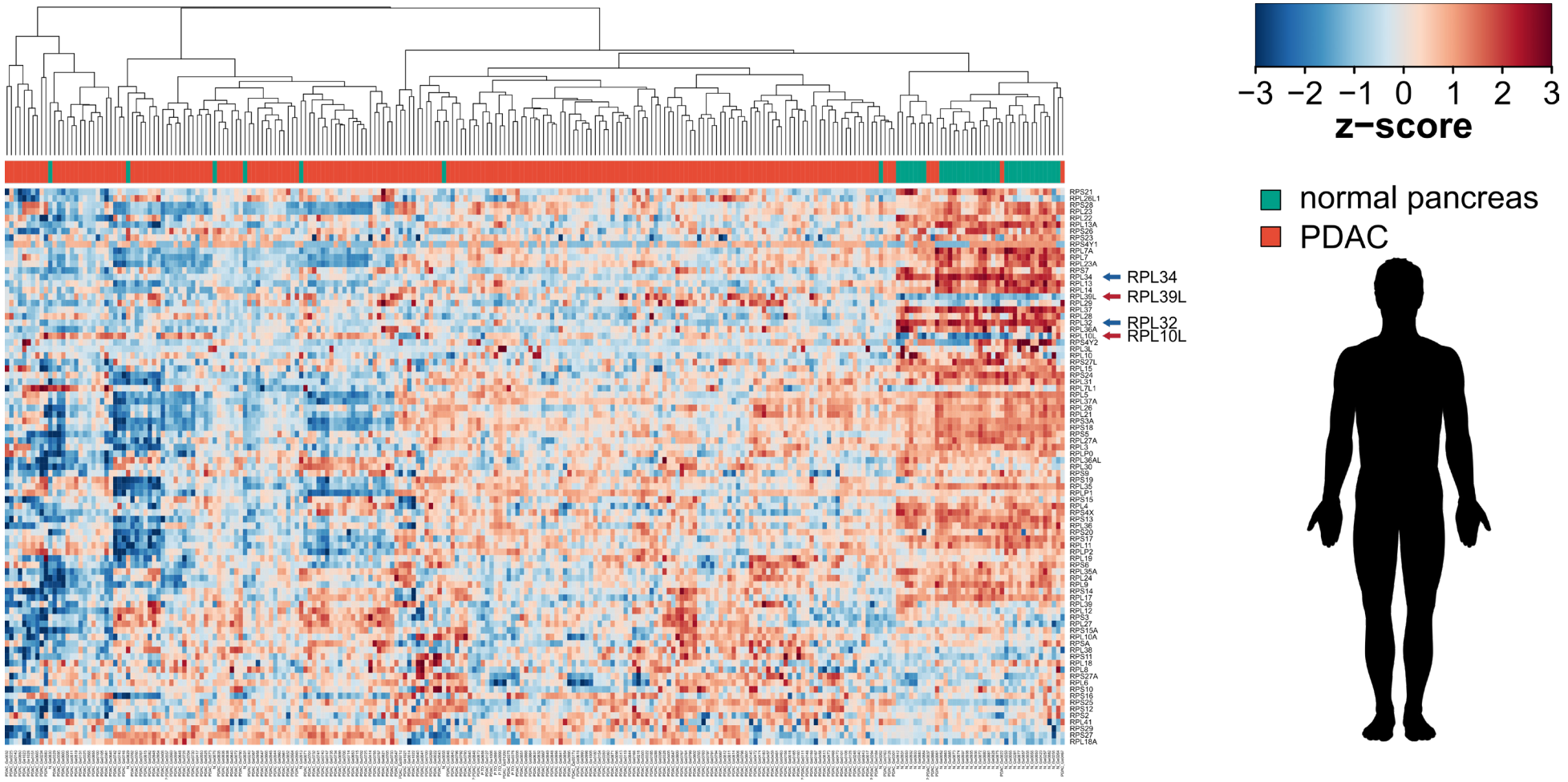

Annexed Figure 1: Related to Figure 3-1

Enlarged image of the heatmap for ribosomal protein (RP) gene expression in PDAC patient samples and normal pancreatic tissue (E-MTAB-1791) shown in Figure 3-1. Multiple RPs, for example, RPL34 and RPL32 (dark blue arrows) tend to show higher expression levels in normal pancreatic tissue compared to PDAC samples. Other RPs, including RPL10L and RPL39L (dark red arrows), show in turn higher expression levels in a subset of PDAC samples compared to normal pancreatic tissue.

Annexed Tables

Annexed Table 1: GSEA – Selection of ribosome biogenesis- and translation-associated gene sets enriched in PDAC patient samples classified as MYC^{high}

Database	*Gene set*	*Size*	*Normalized Enrichment Score*	*False discovery rate*
HALLMARK	MYC_TARGETS_V1	199	2.46	0.00E+00
GOBP	CYTOPLASMIC_TRANSLATION	152	2.41	0.00E+00
REACTOME	EUKARYOTIC_TRANSLATION_INITIATION	117	2.37	0.00E+00
REACTOME	RRNA_PROCESSING	196	2.35	0.00E+00
KEGG	RIBOSOME	85	2.32	0.00E+00
REACTOME	EUKARYOTIC_TRANSLATION_ELONGATION	92	2.17	2.72E-04
GOBP	RIBOSOMAL_LARGE_SUBUNIT_BIOGENESIS	63	2.16	2.37E-04
GOBP	RIBOSOME_BIOGENESIS	270	2.02	2.85E-03
REACTOME	TRANSLATION	289	2.00	3.92E-03
GOBP	RIBONUCLEOPROTEIN_COMPLEX_BIOGENESIS	406	2.00	4.06E-03
HALLMARK	MYC_TARGETS_V2	56	1.95	6.85E-03
GOBP	RRNA_PROCESSING	194	1.93	9.11E-03
GOBP	REGULATION_OF_RRNA_PROCESSING	15	1.84	2.15E-02
GOBP	TRANSLATIONAL_INITIATION	117	1.82	2.72E-02
GOBP	MATURATION_OF_SSU_RRNA	45	1.81	2.86E-02
GOBP	MATURATION_OF_LSU_RRNA	20	1.76	4.50E-02
REACTOME	TRNA_PROCESSING	101	1.76	4.56E-02
REACTOME	RRNA_MODIFICATION_IN_THE_NUCLEUS_AND_CYTOSOL	55	1.75	4.60E-02
GOBP	RIBOSOMAL_SMALL_SUBUNIT_BIOGENESIS	68	1.75	4.62E-02

Annexed Table 2: GSEA – Selection of ribosome biogenesis- and translation-associated gene sets enriched in PDAC cell lines of the QM subtype

Database	*Gene set*	*Size*	*Normalized Enrichment Score*	*False discovery rate*
GOBP	RRNA_PROCESSING	195	2.96	0.00E+00
GOBP	RIBONUCLEOPROTEIN_COMPLEX_BIOGENESIS	437	2.90	0.00E+00
GOBP	RIBOSOME_BIOGENESIS	297	2.86	0.00E+00
GOBP	CYTOPLASMIC_TRANSLATION	155	2.76	0.00E+00
GOBP	RRNA_METABOLIC_PROCESS	258	2.67	0.00E+00
GOBP	EUKARYOTIC_TRANSLATION_INITIATION	115	2.66	0.00E+00
GOBP	RIBOSOMAL_LARGE_SUBUNIT_BIOGENESIS	73	2.63	0.00E+00
GOBP	RIBOSOME	83	2.61	0.00E+00
GOBP	RIBONUCLEOPROTEIN_COMPLEX_SUBUNIT_ORGANIZATION	199	2.54	0.00E+00
GOBP	TRANSLATION	285	2.53	0.00E+00
GOBP	RIBOSOMAL_SMALL_SUBUNIT_BIOGENESIS	74	2.53	0.00E+00
GOBP	RRNA_MODIFICATION_IN_THE_NUCLEUS_AND_CYTOSOL	59	2.44	0.00E+00
GOBP	MATURATION_OF_SSU_RRNA	52	2.42	0.00E+00
GOBP	MATURATION_OF_SSU_RRNA_FROM_TRICISTRONIC_RRNA_TRANSCRIPT_SSU_RRNA_5_8S_RRNA_LSU_RRNA	37	2.33	9.55E-05
GOBP	RIBOSOME_ASSEMBLY	57	2.31	8.81E-05
GOBP	MATURATION_OF_LSU_RRNA	26	2.28	1.23E-04
GOBP	AMINOACYL_TRNA_BIOSYNTHESIS	41	2.26	1.57E-04
GOBP	TRNA_METABOLIC_PROCESS	190	2.14	5.70E-04
GOBP	CLEAVAGE_INVOLVED_IN_RRNA_PROCESSING	27	2.12	6.57E-04
GOBP	RIBOSOMAL_LARGE_SUBUNIT_ASSEMBLY	24	2.09	1.01E-03

Database	*Gene set*	*Size*	*Normalized Enrichment Score*	*False discovery rate*
GOBP	RNA_POLYMERASE_I_TRANSCRIPTION_INITIATION	45	2.06	1.42E-03
GOBP	MATURATION_OF_5_8S_RRNA	35	2.06	1.45E-03
GOBP	PROTEIN_FOLDING	185	2.06	1.55E-03
GOBP	RIBOSOMAL_SUBUNIT_EXPORT_FROM_NUCLEUS	15	2.03	2.00E-03
GOBP	POSITIVE_REGULATION_OF_TRANSCRIPTION_BY_RNA_POLYMERASE_I	31	2.02	2.22E-03
GOBP	REGULATION_OF_RRNA_PROCESSING	16	1.98	3.59E-03
GOBP	TRANSCRIPTION_BY_RNA_POLYMERASE_I	58	1.98	3.60E-03
GOBP	CYTOPLASMIC_TRANSLATIONAL_INITIATION	40	1.97	4.09E-03
KEGG	REGULATION_OF_TRANSCRIPTION_BY_RNA_POLYMERASE_I	41	1.96	4.56E-03
REACTOME	RNA_POLYMERASE_I_TRANSCRIPTION_TERMINATION	29	1.95	4.91E-03
REACTOME	MATURATION_OF_5_8S_RRNA_FROM_TRICISTRONIC_RRNA_TRANSCRIPT_SSU_RRNA_5_8S_RRNA_LSU_RRNA	24	1.92	6.98E-03
REACTOME	TRNA_PROCESSING	129	1.90	8.44E-03
REACTOME	TRANSCRIPTION_BY_RNA_POLYMERASE_III	51	1.86	1.12E-02
REACTOME	RRNA_TRANSCRIPTION	36	1.85	1.22E-02
REACTOME	NUCLEOLUS_ORGANIZATION	18	1.83	1.44E-02
REACTOME	RNA_POLYMERASE_III_TRANSCRIPTION	41	1.79	1.98E-02
REACTOME	RNA_POLYMERASE_III_TRANSCRIPTION_TERMINATION	23	1.77	2.28E-02
REACTOME	TRANSLATIONAL_INITIATION	110	1.72	3.08E-02
REACTOME	RNA_POLYMERASE_I_TRANSCRIPTION	65	1.70	3.82E-02
REACTOME	POSITIVE_REGULATION_OF_TRANSLATION	123	1.68	4.10E-02
REACTOME	FORMATION_OF_CYTOPLASMIC_TRANSLATION_INITIATION_COMPLEX	16	1.66	4.55E-02

Annexed Table 3: GSEA – Selection of gene sets downregulated in response to RNA polymerase I inhibition in HPAF-II cells

Database	*Gene set*	*Size*	*Normalized Enrichment Score*	*False discovery rate*
	Ribosome biogenesis and translation			
HALLMARK	MYC_TARGETS_V1	199	-2.85	0.00E+00
HALLMARK	MYC_TARGETS_V2	57	-2.46	0.00E+00
KEGG	RIBOSOME	82	-2.44	0.00E+00
REACTOME	TRANSLATION	281	-2.43	0.00E+00
GOBP	CYTOPLASMIC_TRANSLATION	149	-2.33	0.00E+00
REACTOME	EUKARYOTIC_TRANSLATION_INITIATION	112	-2.26	3.77E-05
REACTOME	RRNA_PROCESSING	193	-2.24	7.17E-05
GOBP	RIBONUCLEOPROTEIN_COMPLEX_BIOGENESIS	435	-2.01	1.63E-03
GOBP	TRNA_METABOLIC_PROCESS	189	-2.00	1.87E-03
GOBP	RIBONUCLEOPROTEIN_COMPLEX_SUBUNIT_ORGANIZATION	196	-1.94	3.55E-03
GOBP	TRNA_PROCESSING	129	-1.91	4.43E-03
GOBP	POSITIVE_REGULATION_OF_TRANSCRIPTION_BY_RNA_POLYMERASE_I	29	-1.87	6.90E-03
GOBP	CYTOPLASMIC_TRANSLATIONAL_INITIATION	38	-1.83	9.53E-03
REACTOME	RRNA_MODIFICATION_IN_THE_NUCLEUS_AND_CYTOSOL	57	-1.83	9.54E-03
GOBP	RIBOSOME_BIOGENESIS	297	-1.82	1.07E-02
GOBP	RIBOSOMAL_LARGE_SUBUNIT_BIOGENESIS	73	-1.71	2.40E-02
GOBP	RIBOSOMAL_SMALL_SUBUNIT_BIOGENESIS	76	-1.68	3.00E-02
GOBP	RRNA_METABOLIC_PROCESS	258	-1.67	3.17E-02
GOBP	TRNA_MODIFICATION	91	-1.64	3.81E-02
GOBP	MATURATION_OF_5_8S_RRNA	36	-1.62	4.38E-02
GOBP	NUCLEOLAR_LARGE_RRNA_TRANSCRIPTION_BY_RNA_POLYMERASE_I	21	-1.61	4.68E-02

Database	*Gene set*	*Size*	*Normalized Enrichment Score*	*False discovery rate*
	Cell cycle regulation			
HALLMARK	E2F_TARGETS	199	-3.46	0.00E+00
HALLMARK	G2M_CHECKPOINT	196	-3.13	0.00E+00
GOBP	CHROMOSOME_SEGREGATION	312	-2.94	0.00E+00
GOBP	REGULATION_OF_CHROMOSOME_SEGREGATION	113	-2.92	0.00E+00
GOBP	METAPHASE_ANAPHASE_TRANSITION_OF_CELL_CYCLE	86	-2.85	0.00E+00
REACTOME	CELL_CYCLE_CHECKPOINTS	257	-2.81	0.00E+00
REACTOME	CELL_CYCLE_MITOTIC	493	-2.80	0.00E+00
GOBP	REGULATION_OF_MITOTIC_SISTER_CHROMATID_SEGREGATION	50	-2.79	0.00E+00
REACTOME	S_PHASE	155	-2.71	0.00E+00
REACTOME	MITOTIC_G1_PHASE_AND_G1_S_TRANSITION	144	-2.70	0.00E+00
KEGG	CELL_CYCLE	113	-2.64	0.00E+00
GOBP	REGULATION_OF_CELL_CYCLE_CHECKPOINT	44	-2.61	0.00E+00
GOBP	POSITIVE_REGULATION_OF_CELL_CYCLE_PHASE_TRANSITION	93	-2.59	0.00E+00
REACTOME	G2_M_CHECKPOINTS	140	-2.54	0.00E+00
REACTOME	M_PHASE	355	-2.48	0.00E+00
GOBP	REGULATION_OF_CELL_CYCLE_PHASE_TRANSITION	364	-2.47	0.00E+00
REACTOME	G0_AND_EARLY_G1	25	-2.46	0.00E+00
GOBP	POSITIVE_REGULATION_OF_CELL_CYCLE_PROCESS	198	-2.45	0.00E+00
GOBP	CELL_CYCLE_CHECKPOINT_SIGNALING	173	-2.43	0.00E+00
GOBP	CELL_CYCLE_PHASE_TRANSITION	467	-2.41	0.00E+00
GOBP	REGULATION_OF_MITOTIC_CELL_CYCLE_PHASE_TRANSITION	282	-2.40	0.00E+00
GOBP	MITOTIC_CELL_CYCLE_PHASE_TRANSITION	382	-2.39	0.00E+00

Database	*Gene set*	*Size*	*Normalized Enrichment Score*	*False discovery rate*
GOBP	MITOTIC_CELL_CYCLE_CHECKPOINT_SIGNALING	130	-2.39	0.00E+00
GOBP	POSITIVE_REGULATION_OF_CELL_CYCLE	258	-2.35	0.00E+00
GOBP	CELL_CYCLE_G2_M_PHASE_TRANSITION	139	-2.34	0.00E+00
GOBP	POSITIVE_REGULATION_OF_MITOTIC_CELL_CYCLE	100	-2.31	0.00E+00
REACTOME	CYCLIN_A_B1_B2_ASSOCIATED_EVENTS_DURING_G2_M_TRANSITION	24	-2.29	8.33E-06
GOBP	NEGATIVE_REGULATION_OF_MITOTIC_CELL_CYCLE_PHASE_TRANSITION	154	-2.26	3.80E-05
GOBP	NEGATIVE_REGULATION_OF_CELL_CYCLE_PROCESS	260	-2.26	3.74E-05
GOBP	POSITIVE_REGULATION_OF_CELL_CYCLE_G2_M_PHASE_TRANSITION	28	-2.22	8.88E-05
GOBP	REGULATION_OF_MITOTIC_CELL_CYCLE	409	-2.22	8.69E-05
GOBP	POSITIVE_REGULATION_OF_CELL_CYCLE_CHECKPOINT	17	-2.16	2.70E-04
GOBP	REGULATION_OF_CELL_CYCLE_G2_M_PHASE_TRANSITION	98	-2.16	2.68E-04
REACTOME	G2_M_DNA_DAMAGE_CHECKPOINT	70	-2.11	5.23E-04
GOBP	NEGATIVE_REGULATION_OF_MITOTIC_CELL_CYCLE	194	-2.10	5.94E-04
GOBP	NEGATIVE_REGULATION_OF_CELL_CYCLE	321	-1.93	3.68E-03
GOBP	POSITIVE_REGULATION_OF_CELL_CYCLE_G1_S_PHASE_TRANSITION	43	-1.90	4.93E-03
REACTOME	MITOTIC_G2_G2_M_PHASES	182	-1.85	7.71E-03
GOBP	CELL_CYCLE_G1_S_PHASE_TRANSITION	205	-1.78	1.43E-02
GOBP	POSITIVE_REGULATION_OF_G1_S_TRANSITION_OF_MITOTIC_CELL_CYCLE	33	-1.75	1.81E-02
GOBP	MITOTIC_G2_DNA_DAMAGE_CHECKPOINT_SIGNALING	33	-1.72	2.26E-02
GOBP	MITOTIC_G2_M_TRANSITION_CHECKPOINT	48	-1.69	2.76E-02
GOBP	NEGATIVE_REGULATION_OF_CELL_CYCLE_G2_M_PHASE_TRANSITION	60	-1.62	4.44E-02
GOBP	REGULATION_OF_CELL_CYCLE_G1_S_PHASE_TRANSITION	149	-1.60	4.88E-02

Database	*Gene set*	*Size*	*Normalized Enrichment Score*	*False discovery rate*
	Cellular metabolism			
GOBP	THE_CITRIC_ACID_TCA_CYCLE_AND_RESPIRATORY_ELECTRON_TRANSPORT	167	-2.13	4.25E-04
GOBP	OXIDATIVE_PHOSPHORYLATION	197	-2.06	1.02E-03
GOBP	ELECTRON_TRANSPORT_CHAIN	149	-1.95	3.11E-03
GOBP	RESPIRATORY_ELECTRON_TRANSPORT_CHAIN	109	-1.93	3.67E-03
KEGG	CITRATE_CYCLE_TCA_CYCLE	27	-1.91	4.45E-03
GOBP	PYRUVATE_METABOLISM_AND_CITRIC_ACID_TCA_CYCLE	50	-1.90	5.17E-03
GOBP	TRICARBOXYLIC_ACID_CYCLE	28	-1.89	5.31E-03
GOBP	ATP_SYNTHESIS_COUPLED_ELECTRON_TRANSPORT	91	-1.87	6.48E-03
GOBP	CELLULAR_RESPIRATION	208	-1.85	7.72E-03
HALLMARK	MITOCHONDRIAL_RESPIRATORY_CHAIN_COMPLEX_ASSEMBLY	98	-1.82	1.07E-02
KEGG	ATP_BIOSYNTHETIC_PROCESS	95	-1.80	1.27E-02
REACTOME	RESPIRATORY_ELECTRON_TRANSPORT	101	-1.76	1.69E-02
REACTOME	ACETYL_COA_METABOLIC_PROCESS	27	-1.75	1.79E-02
REACTOME	PENTOSE_PHOSPHATE_PATHWAY	21	-1.75	1.82E-02
REACTOME	LIPID_OXIDATION	84	-1.72	2.25E-02
REACTOME	OXIDATIVE_PHOSPHORYLATION	113	-1.71	2.35E-02
REACTOME	FATTY_ACID_CATABOLIC_PROCESS	81	-1.69	2.73E-02
REACTOME	MITOCHONDRIAL_FATTY_ACID_BETA_OXIDATION	31	-1.65	3.64E-02
REACTOME	GLUCOSE_METABOLISM	78	-1.65	3.73E-02
REACTOME	GLYCOLYSIS	62	-1.63	4.07E-02
REACTOME	FATTY_ACID_METABOLIC_PROCESS	258	-1.63	4.24E-02

Annexed Table 4: STRING analysis – Pathways enriched in the top 150 genes downregulated in response to BMH-21 in HPAF-II cells

Database	*Gene set*	*Number of genes*	*False discovery rate*
GOBP	Cell cycle	38	4.10E-24
GOBP	Mitotic cell cycle	26	8.37E-18
GOBP	Cell cycle process	27	3.17E-16
GOBP	Mitotic cell cycle process	23	7.11E-16
GOBP	Regulation of cell cycle	29	1.38E-15
GOBP	Regulation of cell cycle process	23	2.13E-13
GOBP	Chromosome organization	23	9.83E-11
GOBP	Regulation of cell cycle phase transition	17	1.45E-10
GOBP	Regulation of mitotic cell cycle	17	1.04E-09
GOBP	Cell division	17	2.64E-09
GOBP	Nuclear division	14	6.65E-09
GOBP	Regulation of mitotic cell cycle phase transition	14	8.69E-09
GOBP	DNA metabolic process	19	1.06E-08
GOBP	Chromosome segregation	13	1.65E-08
GOBP	Organelle organization	36	1.65E-08
GOBP	Microtubule cytoskeleton organization	16	2.82E-08
GOBP	DNA repair	15	8.99E-08
GOBP	Negative regulation of cell cycle process	12	1.25E-07
GOBP	Negative regulation of cell cycle	13	1.97E-07
GOBP	Nuclear chromosome segregation	11	2.86E-07
GOBP	Mitotic nuclear division	10	3.70E-07
GOBP	Positive regulation of cell cycle process	11	6.37E-07
GOBP	DNA replication	10	1.28E-06

Database	*Gene set*	*Number of genes*	*False discovery rate*
GOBP	Cellular component organization	40	1.08E-05
GOBP	Cytoskeleton organization	18	3.20E-05
GOBP	Nucleic acid metabolic process	24	3.20E-05
GOBP	Cellular response to stress	20	4.62E-05
GOBP	Heterocycle metabolic process	26	2.80E-04
GOBP	Nucleobase-containing compound metabolic process	25	3.30E-04
GOBP	Cellular aromatic compound metabolic process	26	3.50E-04
GOBP	Cellular component assembly	23	7.10E-04
GOBP	Cellular macromolecule metabolic process	23	9.20E-04
GOBP	Organic cyclic compound metabolic process	26	1.30E-03
GOBP	Cellular nitrogen compound metabolic process	27	1.70E-03
GOBP	Regulation of DNA metabolic process	10	2.60E-03
GOBP	Macromolecule metabolic process	34	1.91E-02
GOBP	Regulation of organelle organization	13	2.07E-02
GOBP	Nitrogen compound metabolic process	37	2.30E-02
GOBP	Cellular process	61	4.39E-02
GOBP	Organelle assembly	10	4.42E-02
REACTOME	Cell Cycle	29	8.36E-22
REACTOME	Cell Cycle, Mitotic	26	1.48E-20
REACTOME	Cell Cycle Checkpoints	13	6.97E-09
REACTOME	M Phase	14	2.29E-08
REACTOME	Mitotic Anaphase	10	2.08E-06
REACTOME	Gene expression (Transcription)	14	1.93E-02
REACTOME	RNA Polymerase II Transcription	13	2.45E-02

Acknowledgments

First and foremost, I would like to express my sincere gratitude to Prof. Dr. Jens T. Siveke for granting me the opportunity to undertake my studies in his group and to be part of this interesting research project. I am thankful for the support over the past four years and for the chance to participate in many project-related as well as interdisciplinary training.

Moreover, I would like to offer my special thanks to Dr. Marija Trajkovic-Arsic for her exceptional guidance and supervision during my doctoral studies, for her patience and feedback, and for providing expertise and advice with every theoretical and practical question. Thank you also for carefully proofreading this thesis.

My gratitude further extends to Prof. Dr. Alexander Schramm and Prof. Dr. Björn Scheffler for being part of my Thesis Advisory Committee. Thank you for the valuable discussions, remarks, and suggestions that decisively shaped and improved my project.

I am also deeply grateful to Prof. Dr. Perihan Nalbant for agreeing to be the second examiner for my dissertation.

Special thanks also to Dr. Sven T. Liffers for analyzing the RNA sequencing data generated in the course of the present work, and for providing the corresponding method section.

Moreover, I very much appreciate the support from PD Dr. Smiths S. Lueong who provided the gene expression data of conventional cell lines and PDCs.

I am also very thankful to Dr. Silvia Vega-Rubín-de-Celis who generously shared her knowledge and expertise on the topic of autophagy. I would like to thank her as well as Matthias Kudla for performing the Autophagy LC3 HiBiT reporter assay and the GFP LC3 assay, and also for providing the respective method sections.

Furthermore, I would like to thank Dr. Kristina Althoff, Rui Fang, Konstantinos Savvatakis, and Vuk Dinovic for their indispensable organizational and technical support in conducting the animal experiments and tissue preparation. Special thanks to Dr. Kristina Althoff also for providing the corresponding method section.

I would further like to gratefully mention the team at Life & Brain GmbH who performed RNA sequencing of our samples.

Additionally, I would like to express my deepest appreciation to all current and former members of our group for their professional and moral support. Thank you for the enjoyable activities outside the laboratory and for making the past four years such an inspiring and memorable time.

Finally, I wish to extend my heartfelt gratitude to my family and friends for their unconditional love and faith, for their patience and understanding, as well as for their support and encouragement throughout my PhD studies.

Curriculum Vitae

Der Lebenslauf ist in der Online-Version aus Gründen des Datenschutzes nicht enthalten.

Der Lebenslauf ist in der Online-Version aus Gründen des Datenschutzes nicht enthalten.

Declarations

In accordance with § 6 (para. 2, clause g) of the Regulations Governing the Doctoral Proceedings of the Faculty of Biology for awarding the doctoral degree Dr. rer. nat., I hereby declare that I represent the field to which the topic “Characterization and targeting of ribosome biogenesis in cellular and tissue subtypes of pancreatic ductal adenocarcinoma” is assigned in research and teaching and that I support the application of Corinna Münch.

Essen, 15.02.2024 _____

Prof. Dr. Jens T. Siveke

In accordance with § 7 (para. 2, clause d and f) of the Regulations Governing the Doctoral Proceedings of the Faculty of Biology for awarding the doctoral degree Dr. rer. nat., I hereby declare that I have written the herewith submitted dissertation independently using only the materials listed, and have cited all sources taken over verbatim or in content as such.

Essen, 15.02.2024 _____

Corinna Münch

In accordance with § 7 (para. 2, clause e and g) of the Regulations Governing the Doctoral Proceedings of the Faculty of Biology for awarding the doctoral degree Dr. rer. nat., I hereby declare that I have undertaken no previous attempts to attain a doctoral degree, that the current work has not been rejected by any other faculty, and that I am submitting the dissertation only in this procedure.

Essen, 15.02.2024 _____

Corinna Münch